Dimensional Reduction for Identical Kuramoto Oscillators: A Geometric Perspective

Author: Bolun Chen

Boston College Electronic Thesis or Dissertation, 2017

Boston College

The Graduate School of the Morrissey College of Arts and Sciences

Department of Physics

Dimensional Reduction for Identical Kuramoto Oscillators: A Geometric Perspective

a dissertation

by

Bolun Chen

submitted in partial fulfillment of the requirements

for the degree of

Doctor of Philosophy

July 2017

Dimensional Reduction for Identical Kuramoto Oscillators: A Geometric Perspective

by

Bolun Chen

Dissertation Advisors: Jan Engelbrecht, Renato Mirollo

ABSTRACT

Many phenomena in nature that involve ordering in time can be understood as collective behavior of coupled oscillators. One paradigm for studying a population of self-sustained oscillators is the Kuramoto model, where each oscillator is described by a phase variable, and interacts with other oscillators through trigonometric functions of phase differences.

This dissertation studies N identical Kuramoto oscillators in a general form

$$\dot{\theta}_j = A + B\cos\theta_j + C\sin\theta_j \qquad j = 1, \ldots, N,$$

where coefficients A, B, and C are symmetric functions of all oscillators $(\theta_1, \ldots, \theta_N)$. Dynamics of this model live in group orbits of Möbius transformations, which are low-dimensional manifolds in the full state space.

When the system is a phase model (invariant under a global phase shift), trajectories in a group orbit can be identified as flows in the unit disk with an intrinsic hyperbolic metric. A simple criterion for such system to be a gradient flow is found, which leads to new classes of models that can be described by potential or Hamiltonian functions while exhibiting a large number of constants of motions.

A generalization to extended phase models with non-identical couplings gives rise to richer structures of fixed points and bifurcations. When the coupling weights sum to zero, the system is simultaneously gradient and Hamiltonian. The flows mimic field lines of a two-dimensional electrostatic system consisting of equal amounts of positive and negative charges. Bifurcations on a partially synchronized subspace are discussed as well.

To reduce is to gain; Sophistication leads to confusion.

Tao Te Ching, Chapter 22

ACKNOWLEDGEMENTS

First of all, I want to express my most sincere gratitude to my advisors: Jan Engelbrecht and Rennie Mirollo. This dissertation could not have been completed without their guidance and support. Through countless stimulating and encouraging discussions, I not only gained solid understanding of physics and math but also gradually developed my own taste for good research. I will always cherish the Eureka moment with Rennie when we realized the analogy between Kuramoto oscillators and 2D electrostatics. Likewise, I will always remember Jan's poetic interpretation on fixed points and beyond: "*Birth is a source; Death is a sink; Life is the saddles in between.*"

I am equally grateful to Andrzej Herczynski and Seth Fraden for being the committee members. Andrzej's insightful comments and constructive suggestions tremendously improved this work. Enlightening conversations with Seth and his group members Ian and Mike opened a new door for future collaboration.

A special tribute must be made to Eric Schwartz at Boston University: Thank you so much, Eric, for your amazing lectures that introduced me to the world of computational neuroscience, and for the long-time support and encouragement!

I would like to thank faculty members at BC physics, especially Pradip Bakshi, Kevin Bedell, David Broido, Mike Graf, Kris Kempa, and Rein Uritam, whom I was fortunate to learn from, talk to or work with.

Special thanks to Scott Bortolotto, Jane Carter, Nancy Chervy, and Sile Power for being so helpful and making the physics department like a big family; also to Susan Shea at BC

OISS for her incredible kindness and professional advice.

Lots of friends at BC helped me in every possible way: Yitz Calm, Xiang Chen, Wenping Cui, Luke D'Imperio, Nawa Dahal, Victoria Gabriele, Matt Gochan, Huicong Hu, Jiaotao Kong, Te Lai and Evaline Lai, Hua Li, Kunyi Li, Nathan Nesbitt, Yun Peng and Tomasz Szatanek, Ruijun Qin and Chenyu Lin, Bryan Rachmilowitz, Aaron Rose and Amy Rose, Alex Shvonski, Luciano Silvestri and Stefano Silversti, Tianyi Sun and Ye Zhu, Xuanyuan Wu and Fan Ye, Mengliang Yao, Bing Ye, Qingyi Yu and Zhao Qin, Wei Zhang, Yi Zhang, He Zhao, Hongbo Zhao, and Wenwen Zhou. Thank you!

In the meantime, I wish to thank some old friends for many happy hours that we spent together: Xinglei Chai and Shuang Ci, Shen Chang and Ran Li, Xiaochuan Dai, Tiancheng Deng, Lin Du, Yaodi Fan, He Gao, Youyang Hou and Yang Li, Nianqiao Ju, Chaoyi Li, Yuqing Lin, Ying Liu, Zisu Peng, Song Sai, Likun Shi, Siyuan Wang and Lin Zhang, Xiaozhou Wang, Yangyang Wang, Yu Wang, Qianshi Wei, Wen Xie and Yusheng Qi, Chuanxi Yang and Xinyi Zhang, Hang Yu, Chongzhi Zang and Sha Yu, Mengyuan Zhang and Haohan Zhu, Tong Zhang, Sishuang Zhang and Zijian Shao, Wei Zhang, Xizhu Zhao, Yawei Zhao and Zhengjun Li, Kuangyu Zheng, and Yan Zhu.

I will not forget my teachers and collaborators in China: Qie Tang, Supeng Kou, Yunbo Zhang, Shu Chen, Biao Wu, Wenan Guo, Xiaobin Huang, Lanfeng Liu, Gaoyong Sun and Jing Yu. I learned a lot of physics from them. I really appreciate it.

This dissertation is dedicated to my family. I am deeply indebted to my parents for their unconditional love. I am also truly grateful to my uncle Qingping Chen and aunt Hongyan Xu, my cousins Yanke Liao and Weili Li, uncle Zhihong Cui and aunt Feng Jing, and especially, Ping Guo and Xueling Yu.

To Xiaoqing: I could not have finished my Ph.D. without you being at my side. No words can express how thankful I am, for your caring, patience and companionship over the years, and for making me a better person.

TABLE OF CONTENTS

ACKNOWLEDGEMENTS viii

LIST OF FIGURES xii

LIST OF TABLES xiii

CHAPTER

I. Introduction 1

1.1 Early work of Winfree and Kuramoto 3
1.2 Neutral Stability and Low-dimensional Dynamics 7
1.3 Motivation and Outlines 11

II. Formalism 13

2.1 Watanabe-Strogatz Transformation 13
2.2 Group Theoretic Approach 16
2.2.1 The Riccati Equation 16
2.2.2 Homogeneous Condition and Phase Models 18
2.2.3 Möbius Transformations 19
2.2.4 Möbius Group and Group Orbits (G-orbits) 23
2.2.5 Cross-ratios as Constants of Motion 25
2.2.6 Reduced Group Orbits 26
2.3 Connecting Möbius to Watanabe-Strogatz 31
2.4 Summary 33

III. Phase Models 35

3.1 Flows in Reduced Group Orbits 35
3.1.1 Fixed Points 35
3.1.2 Flows for $Z_q Z_{1-q}$ Models 43

3.2 Geometry of Reduced Group Orbits . . . 48
3.2.1 Poincaré Disk . . . 48
3.2.2 Gradient Condition . . . 51
3.3 Potentials for Phase Models . . . 60
3.3.1 Z_1 Model . . . 61
3.3.2 $Z_2 Z_{-1}$ Model . . . 64
3.4 Flows on $(N-1,1)$ Edges . . . 68
3.4.1 Bifurcation Diagrams . . . 68
3.4.2 New Fixed Points for $Z_p Z_{1-p}$ Models . . . 73
3.5 Summary . . . 77

IV. Extended Phase Models . . . 79

4.1 Extended Z_1 Phase Models . . . 80
4.1.1 Gradient-Hamiltonian Structures . . . 81
4.1.2 An Analogue with $2D$ Electrostatics . . . 87
4.1.3 Fixed Points and Stability . . . 90
4.1.4 Flows on $(N-1,1)$ Edges . . . 94
4.2 Extended $Z_2 Z_{-1}$ model . . . 95
4.3 Fixed Points on $(N-1,1)$ Edges . . . 99
4.4 Summary . . . 101

V. Conclusions . . . 103

BIBLIOGRAPHY . . . 105

LIST OF FIGURES

Figure

1.1	Synchronous fireflies	2
1.2	Limit cycle oscillators and phase variables	4
1.3	Synchronization transition in Kuramoto model	6
2.1	Möbius evolution	20
2.2	Examples of group orbits	24
2.3	Reduced group orbits	27
2.4	$\underset{\sim}{S^1}$, T^{N-1}, and the unit disk	28
2.5	$\widetilde{Gp}$ vs. Δ for $N = 4$	30
3.1	$\dot{w}$ flows for Z_1 model	38
3.2	$\dot{w}$ flows for Z_2Z_{-1} model	40
3.3	Radial component $f(r)$ for Z_2 model	43
3.4	Escher's Circle Limit I	50
3.5	Geodesics for Z_1 model	51
3.6	Rotated $\dot{w}$ flows for Z_1 model	55
3.7	Potentials for Z_1 model	65
3.8	Potentials for Z_2Z_{-1} model	68
3.9	Bifurcations on the $(N-1, 1)$ edge	71
3.10	Bifurcations on the $(N-1, 1)$ edge in limiting cases	72
4.1	Trajectories of $\mathrm{Im}F = \mathrm{const}$	86
4.2	Potentials for extended Z_1 model	87
4.3	Circular flows and $2D$ Dipole Field	89
4.4	Flows and potentials for extended Z_2Z_{-1} model	99

LIST OF TABLES

Table

2.1 A dictionary between the reduced G-orbit $\widetilde{Gp}$ and the unit disk Δ. 30
3.1 Zeros of Z_2 on the real axis ($\phi = 0$). 42
3.2 Zeros of Z_2 on the first symmetry axis ($\phi = \pi/N$). 42
3.3 A Table of $\Sigma_q(s)$ on the splay base point. 45
3.4 Zeros of Z_3 on the real axis ($\phi = 0$). 47
3.5 Zeros of Z_3 on the first symmetry axis ($\phi = \pi/N$). 48
4.1 Typical charge densities, electric fields and potentials in $2D$ electrostatics 88
4.2 An analog between extended Kuramoto phase models and $2D$ electrostatics 90
4.3 Fixed points and their stability of the extended Z_1 phase model. 94

CHAPTER I

Introduction

In a letter to his father in 1665, Dutch physicist Christiaan Huygens, who is now known for his work on vibrations and waves, wrote (*Pikovsky et al.*, 2003):

> While I was forced to stay in bed for a few days and made observations on my two clocks of the new workshop, I noticed a wonderful effect that nobody could have thought of before. The two clocks, while hanging [on the wall] side by side with a distance of one or two feet between, kept in pace relative to each other with a precision so high that the two pendulums always swung together, and never varied. While I admired this for some time, I finally found that this happened due to a sort of *sympathy*: when I made the pendulums swing at differing paces, I found that half an hour later, they always returned to synchronism and kept it constantly afterwards, ... [this sympathy] in my opinion, cannot be caused by anything other than the imperceptible stirring of the air due to the motion of the pendulums.

This is the first record of mutual synchrony in scientific literature. Interestingly, from the perspective of dynamical systems, Huygens' observation contains several key elements: a system of self-sustained oscillators (two pendulum clocks), a fixed point (the synchronism),

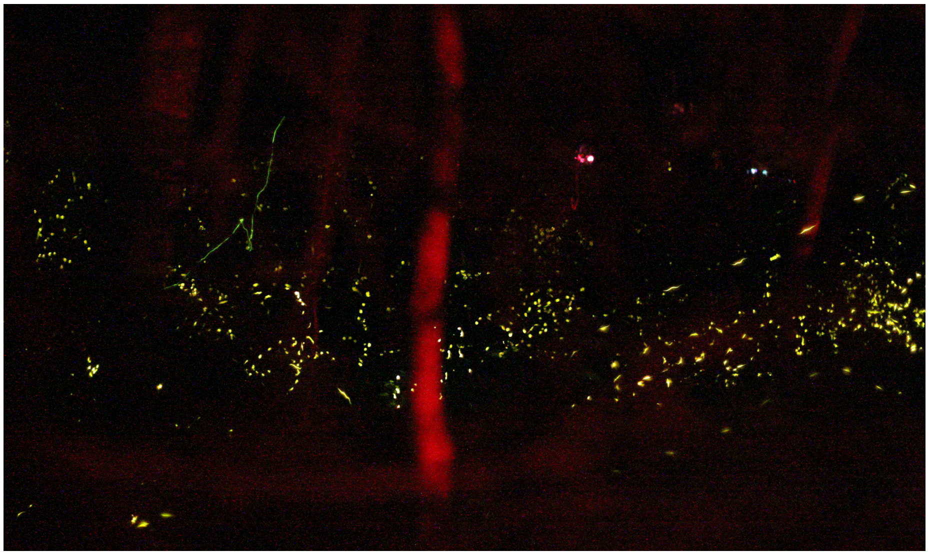

Figure 1.1: Synchronous flashing of fireflies at the Great Smoky Mountains National Park in June 2015 (taken by a friend of the author).

stability of the fixed point upon perturbations ("always returned to synchronism"), and a coupling mechanism (stirring of the air due to pendulums' motion).

Ever since the era of Huygens, European travelers to southeast Asia came home with colorful anecdotes about synchronous flashings of fireflies that stretch for miles along riverbanks (*Strogatz*, 2004). In fact, similar phenomena that involve self-organization and orderings in time are common in nature. Chirping crickets, bumping heart cells, bursting neurons, are just a few examples.

All of them, to some extent, can be thought of as collective behaviors of nonlinear oscillators, which exhibit independent oscillations (thus a well-defined phase, see Figure 1.2) when isolated and coherent dynamics when coupled together. The coupling can be pulsatile or continuous, depending on specific physical or biological mechanisms behind the signal transmission process. When the coupling is weak, each oscillator maintains its motion with adjusted phase and/or frequency. Loosely speaking, each self-sustained oscillator can be considered as a stable limit cycle in a state space. It is the freedom of the phase (i.e. the neutrality along the limit cycle) that makes mutual entrainment possible.

1.1 Early work of Winfree and Kuramoto

Although people have been intrigued by the rich patterns that show temporal ordering for centuries, the study of coupled self-sustained oscillators has a relatively short history. One decisive step along this direction came in 1967, when Arthur Winfree, then a graduate student at Princeton, proposed a phenomenological model for N coupled oscillators (*Winfree*, 1967). He treated each oscillator as a phase variable θ_j with a natural frequency ω_j drawn from some distribution $g(\omega)$. Oscillators evolve according to N coupled ordinary differential equations (ODEs),

$$\dot{\theta}_j = \omega_j + Z(\theta_j) \sum_{l=1}^{N} X(\theta_l), \quad j = 1, \ldots, N. \tag{1.1}$$

Here, the sum $\sum_l X(\theta_l)$ describes the influence from the whole population. The response of oscillator j depends on the sensitivity function $Z(\theta_j)$ on receiving the influence.

Winfree found a transition from an incoherent state where all oscillators move at their own pace to a coherent state where a subset of the population moves in unison. This transition results from a competition between the spread-out in the natural frequency and the coupling function. For a fixed coupling strength, as the system becomes more homogeneous, there is a threshold for the width of $g(\omega)$ above which oscillators start to synchronize.

Eight years later, inspired by Winfree's discovery, Yoshiki Kuramoto derived a more tractable model (*Kuramoto*, 1975). Using physical arguments and perturbative averaging method, Kuramoto showed that long-term dynamics for N weakly-coupled limit-cycle os-

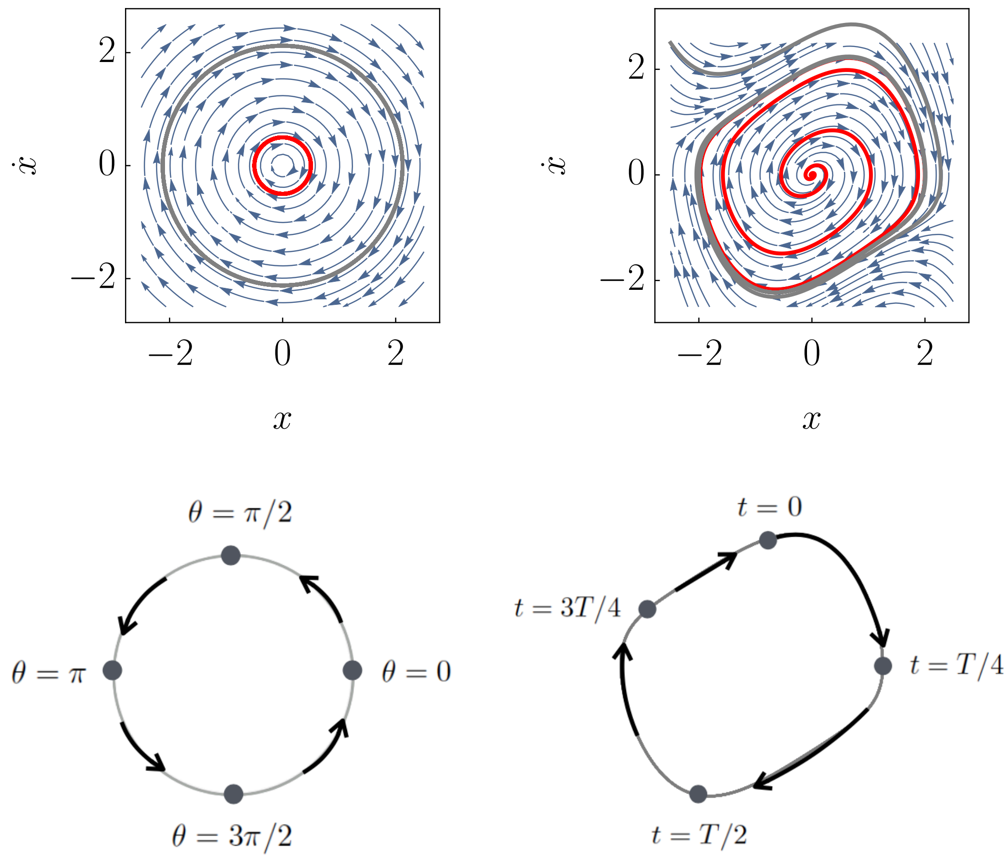

Figure 1.2: Upper left panel: The phase portrait for a simple harmonic oscillator $\ddot{x} = -\frac{k}{m}x \equiv -\tilde{\omega}^2 x$. Each closed orbit is characterized by mechanical energy $E = \frac{1}{2}m\dot{x}^2 + \frac{1}{2}kx^2$ (the constant of motion) and is neutrally stable.
Upper right panel: The phase portrait for a Van der Pol oscillator $\ddot{x} = -\tilde{\omega}^2 x + \beta(1 - x^2)\dot{x}$. A stable limit cycle attracts all initial conditions and corresponds to quasi-periodic oscillations with period T.
Lower panel: Defining a phase variable on a limit cycle: $\theta(t) = \frac{2\pi t}{T}$ as fractions of the period. A limit cycle oscillator is described by uniform flows $\dot{\theta} = \omega$ with natural frequency $\omega = \frac{2\pi}{T}$.

cillators are determined by their phase differences,

$$\dot{\theta}_j = \omega_j + \sum_{l=1}^{N} \Gamma_{jl}(\theta_l - \theta_j). \tag{1.2}$$

He then considered a solvable form for Γ_{jl}, $\Gamma_{jl}(\theta_l - \theta_j) = \frac{K}{N}\sin(\theta_l - \theta_j)$ with K denoting the coupling strength. Namely, the coupling function is assumed to be identical, all-to-all and sinusoidal,

$$\dot{\theta}_j = \omega_j + \frac{K}{N}\sum_{l=1}^{N} \sin(\theta_l - \theta_j). \tag{1.3}$$

This is the Kuramoto model, which has become a classic paradigm for studies of coupled oscillator systems.

Since the phase of an oscillator is between 0 and 2π, it can be visualized as a point on the unit circle and represented by a complex number $z_j = e^{i\theta_j}$. Now for a population of oscillators, a useful quantity that characterizes synchrony is the average of all z_j's,

$$Z_1(z) = \langle z \rangle = \frac{1}{N}\sum_{l=1}^{N} e^{i\theta_l} = \frac{1}{N}\sum_{l=1}^{N} z_l, \tag{1.4}$$

which is also known as the order parameter, or the first moment, or the center of mass of N points on the unit circle. Since Z_1 is a complex number, it can be written as $Z_1 = Re^{i\psi}$.

When all oscillators are synchronized, $\theta_j = \psi$, $\forall j$. The amplitude of Z_1 becomes the unity, $|Z_1| = \left|\frac{1}{N}\sum_{l=1}^{N} e^{i\psi}\right| = |e^{i\psi}| = 1$. When the population is completely incoherent, the average should sum up to zero, $|Z_1| = 0$. Therefore, a finite $|Z_1|$ indicates the onset of synchrony, as shown in Figure 1.3.

Since the coupling term can be reduced as

$$\frac{1}{N}\sum_{l=1}^{N} \sin(\theta_l - \theta_j) = R\sin(\psi - \theta_j),$$

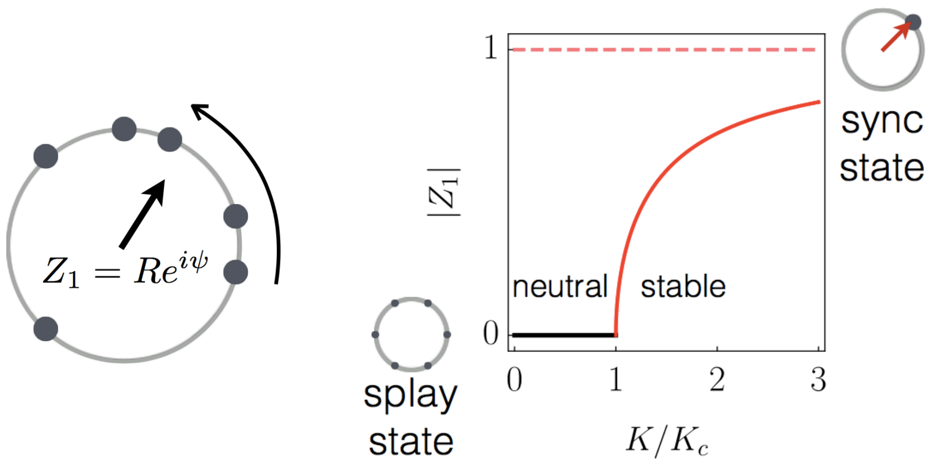

Figure 1.3: Left panel: An illustration of six Kuramoto oscillators (gray filled circles) moving counterclockwise on the unit circle. The order parameter $Z_1 = \frac{1}{6}\sum_{j=1}^{6} e^{i\theta_j}$ is denoted as a black straight arrow with an amplitude R and a phase ψ.
Right panel: The amplitude of the order parameter Z_1 of the Kuramoto model [Eq. (1.3)] as a function of the coupling strength K in the large N limit. The synchronization transition occurs at a critical value K_c. The upper right inset figure shows the fully synchronized state (the sync state) with $|Z_1| = 1$. The lower left inset figure shows an incoherent state (the splay state) with $|Z_1| = 0$. Note that entire incoherent branch has neutral stability.

the ODE for θ_j has a simpler form,

$$\dot{\theta}_j = \omega_j + KR\sin(\psi - \theta_j). \tag{1.5}$$

The amplitude R and the phase ψ of the order parameter Z_1 can be solved self-consistently for a given frequency distribution.

Kuramoto first did that calculation and found a critical value K_c for the synchronization transition (see Figure 1.3):

$$\begin{cases} |Z_1| > 0 & K \geq K_c \\ |Z_1| = 0 & K < K_c \end{cases}.$$

For a symmetric frequency distribution $g(\omega) = g(-\omega)$, Kuramoto found that K_c is determined by the central frequency, $K_c = \frac{2}{\pi g(0)}$. He also obtained the correct scaling for the amplitude $R(K) \sim (1 - K_c/K)^{1/2}$ for $K \geq K_c$ with a Lorenzian frequency distribution.

1.2 Neutral Stability and Low-dimensional Dynamics

After Kuramoto's original work, lots of effort (*Acebrón et al.*, 2005) have been made to understand his model. Researchers in the late 80s and early 90s were intrigued by the stability problem (*Strogatz*, 2000): It would be satisfactory to show the synchronization transition as a result of some bifurcation when K varies.

In the large N limit, one can use a time-dependent density $\rho_\omega(\theta, t)$ to describe the probability of finding oscillators with natural frequency ω in $[\theta, \theta + d\theta)$ on the unit circle at time t. The density satisfies the normalization condition, $\int_0^{2\pi} \rho_\omega(\theta, t) = 1$, and evolves according to the continuity equation,

$$\frac{\partial \rho}{\partial t} + \frac{\partial}{\partial \theta}(\rho v) = 0, \tag{1.6}$$

where v is the instantaneous velocity of oscillators at phase θ,

$$v(\theta, t) = \omega + KR\sin(\psi - \theta). \tag{1.7}$$

The order parameter then becomes the expectation value with the density $\rho_\omega(\theta, t)$ and the frequency distribution $g(\omega)$,

$$Z_1 = \langle z \rangle = \left\langle e^{i\theta} \right\rangle = \int_{-\infty}^{+\infty} d\omega g(\omega) \int_0^{2\pi} d\theta \rho_\omega(\theta, t) e^{i\theta}. \tag{1.8}$$

A linearization analysis (*Strogatz and Mirollo*, 1991) found that the incoherent, uniform state $\rho = \frac{1}{2\pi}$ has a continuous spectrum lying on the imaginary axis when $K < K_c$. A real, positive eigenvalue emerges at $K = K_c$, stabilizing the coherent (i.e. sync) state. This result confirms Kuramoto's heuristic mean-field argument when $K > K_c$. However, it shows that the incoherent state is neutrally stable when $K < K_c$. The origin of this neutral stability was unclear at that time.

Another well-studied system that sheds light on the Kuramoto model is superconducting Josephson junction arrays with a constant driving current and a purly resistive load. In the over-damped region, each junction can be described by a phase oscillator whose dynamics are governed by a dimensionless ODE driven by a first-order trigonometric function (*Tsang et al.*, 1991; *Marvel et al.*, 2009),

$$\dot{\theta}_j = \Omega - (b+1)\cos\theta_j + \frac{1}{N}\sum_{l=1}^{N}\cos\theta_l. \tag{1.9}$$

Here Ω is the natural frequency, b is determined by the resistance of the junction. This system can be mapped to the Kuramoto model under certain conditions.

In the early 90s, of particular interest was a highly symmetric configuration called the "splay state" (see the inset in Figure 1.3), where all oscillators are equally staggered in phase, $\theta_j(t) = \phi(t - jT/N)$ with $j = 1, \ldots, N$ and ϕ denoting a periodic function of period T. Since the order parameter is zero for the splay state, it is a finite-N version of the incoherent state of Kuramoto model. Similar neutral stability was found (*Mirollo*, 1994).

The first successful attempt of solving the neutral stability puzzle was made by Strogatz and Watanabe (*Watanabe and Strogatz*, 1993, 1994). They consider N identical globally-coupled phase oscillators under the evolution

$$\dot{\theta}_j = A + B\sin\theta_j + C\cos\theta_j \qquad j = 1, \ldots, N, \tag{1.10}$$

where coefficients A, B and C are real symmetric functions in $(\theta_1, \ldots, \theta_N)$ that are the same for all oscillators. Note that the Kuramoto model [Eq. (1.3)] and the Josephson junction arrays [Eq. (1.9)] are two special cases of this general form.

Through a nearly sixty pages calculation, Watanabe and Strogatz (WS) constructed $N-3$ independent constants of motion. The remaining three degrees of freedom define a three-dimensional manifold. The full state space (the N-dimensional torus T^N) is foliated into a family of $3D$ manifolds, each one characterized by $N-3$ constants of motion. Similar to equal-energy surfaces in a Hamiltonian system (Figure 1.2), these low-dimensional manifolds are neutrally stable.

WS further proved that there is at least one incoherent fixed point on each $3D$ manifold. Perturbation along the splay orbit is neutral (e.g. applying a global rotation), while perturbing in other $N-3$ directions leads to an orbit in a different $3D$ manifold, which does not go back to the original orbit. So there are $N-3+1=N-2$ neutral directions, which explained an earlier numerical observation (*Nichols and Wiesenfeld*, 1992).

The WS theory thus is recognized as one of the most important work in studies of identical Kuramoto systems. However, the origin of those constants of motion and low-dimensional manifolds awaits a lucid explanation.

On the continuous side ($N \to \infty$), a long-sought low-dimensional reduction scheme for the classical Kuramoto model was proposed by Ott and Antonsen (*Ott and Antonsen*, 2008, 2009; *Ott et al.*, 2011), also known as the Ott-Antonsen (OA) ansatz. They made two observations:

1. Existence of a $2D$ invariant manifold: A special class of densities $\rho_\omega(\theta; r, \varphi)$ are invariant under the evolution of Eqs. (1.6) and (1.7). For a given frequency ω, they have the form of a Poisson density,

$$\rho_\omega(\theta; r, \varphi) = \frac{1}{2\pi} \frac{1-r^2}{1-2r\cos(\theta-\varphi)+r^2}, \tag{1.11}$$

which is parameterized by two real numbers $r \in [0, 1]$ and $\varphi \in [0, 2\pi]$. The domain of r and φ is a closed disk. Every point in the disk corresponds to a density ρ. This essentially establishes a $2D$ invariant manifold for each frequency ω in the infinite-dimensional state space of the Kuramoto model.

2. Conditional low-dimensional dynamics of the order parameter: If the dependence of the Poisson density on the frequency satisfies certain analyticity conditions, the order parameter [Eq. (1.8)] has asymptotic dynamics on a low-dimensional invariant manifold (*Mirollo*, 2012).

The OA ansatz immediately received a lot of attention and has been generalized to various types of coupled oscillators (*Pikovsky and Rosenblum*, 2015).

To understand the genesis of the OA ansatz and its connection to the WS theory, Marvel et al.(*Marvel et al.*, 2009) pointed out that the key is group theory. We will explain this point in greater detail in Chapter 2. For now, here is a brief summary:

For systems in the form of Eq. (2.1), the time-evolution $\theta_j(t)$ is a unit-disk-preserving Möbius transformation on an initial condition (*Pikovsky and Rosenblum*, 2008; *Marvel et al.*, 2009), $\theta_j(t) = M_t\theta_j(0)$. Such Möbius transformations M form a three-dimensional group G (*Marvel et al.*, 2009). The group action on a base point $p = (\theta_1, \ldots, \theta_N) \in T^N$ generates a group orbit $Gp = \{Mp|M \in G\}$, which is a $3D$ manifold in T^N. The full state space T^N is then decomposed into different group orbits, which are all invariant under the flow of Eq. (2.1). On each group orbit there are $N - 3$ constants of motion identified as cross-ratios of oscillators' configuration (*Goebel*, 1995). Therefore, the neutral $3D$ manifolds found by WS are essentially group orbits of Möbius transformations. In addition, the Poisson density $\rho_\omega(\theta)$, which is of central importance in the OA ansatz [Eq. (1.11)], naturally emerges as the Jacobian of Möbius transformations on the unit circle.

This group-theory-based framework not only explains the neutral stability in the WS theory and low-dimensional dynamics in the OA ansatz (*Mirollo*, 2012), it also leads to a complete classification of attractors for Kuramoto network (*Engelbrecht and Mirollo*, 2014): For $N > 3$, the possible attractors are fixed points or limit cycles of either fully synchronized states or $(N-1, 1)$ states ($N-1$ oscillators are synced with one outlier).

1.3 Motivation and Outlines

Given the success of group theory analysis, there is a missing piece in interpreting the WS theory: They considered the effect of adding a phase shift δ to the sinusoidal coupling, or the "cosine" model,

$$\dot{\theta}_j = \omega + \frac{1}{N}\sum_{l=1}^{N}\cos(\theta_l - \theta_j - \delta). \tag{1.12}$$

The ODE is unchanged under a global phase shift, $\theta_j \to \theta_j + c$ for any real angle c. This additional symmetry further reduces the state space to a family of $2D$ manifolds. On each $2D$ manifold, WS constructed a function $\mathcal{H}$ with $\dot{\mathcal{H}} = |Z_1|\sin\delta$. It becomes a new constant of motion when $\delta = 0$, and can be interpreted as the Hamiltonian.

We have noted the fundamental role of the Möbius group in studies of Kuramoto oscillator network. It would be satisfactory to have a better understanding on 1) the Hamiltonian structure of the cosine model, and 2) dynamics in a group orbit from a more natural (geometric) perspective.

Inspired by the motivation, this dissertation revisits the general model considered in the WS thoery, i.e., N identical globally-coupled phase oscillators:

$$\dot{\theta}_j = A + B\cos\theta_j + C\sin\theta_j.$$

We will derive the reduced dynamics on the $3D$ manifold as the group orbit of Möbius transformations. In the presence of a global rotational invariance, the group orbit reduces to $2D$, which is equivalent to the Poincaré disk of hyperbolic geometry.

One of the main results of this dissertation is to show the cosine model [Eq. (2.7)] is a gradient flow with respect to the hyperbolic metric when $\delta = \pm\pi/2$. It becomes a Hamiltonian system when $\delta = 0$ with the $\mathcal{H}$ as the Hamiltonian. More importantly, we will demonstrate that Eq. (2.7) is merely one example with such a gradient/Hamiltonian structure. In fact, we will derive a general condition for a Kuramoto network to have this property, followed by more examples.

We then further extend our discussion to include non-identical couplings by introducing unequal weights in the order parameter. This extended model will be shown to exhibit a richer structure of bifurcations between fixed points. Of particular interest is a special case when all coupling weights sum up to zero, which has a nice analog as a $2D$ electrostatic problem.

The organization of this dissertation is as follows:

In Chapter 2, we review the WS paper in greater details and derive the explicit equations for the dynamics on the Möbius orbits. We also summarize some basic facts about the Möbius transformation, the Riccati equation, and the cross-ratio.

In Chapter 3, we turn to the phase model with the additional rotational symmetry. Trajectories in a reduced group orbit are equivalent to flows in the unit disk with hyperbolic geometry. We derive a general condition for a model to be a gradient flow. This enables us finding a potential function for the identical Kuramoto model, as well as new classes of phase models. Fixed points and bifurcations for these new models are discussed.

In Chapter 4, we consider extended phase models where oscillators contribute to the order parameter with different weights. Applying the gradient condition, we obtain the potentials and the Hamiltonians for new phase models. Stability of fixed points is also analyzed.

Finally, we conclude with a short summary in Chapter 5.

CHAPTER II

Formalism

In this chapter, we will briefly review the seminal work by Watabane and Strogatz (*Watanabe and Strogatz*, 1993, 1994), which can be understood from the perspective of group theory (*Marvel et al.*, 2009). We will set up the formalism for this dissertation by defining the model, basic concepts and frequently-used terms. We will also derive the governing equations for evolutions in a group orbit of Möbius transformations. Finally, we will connect this group-theoretic approach to the Watabane-Strogatz (WS) theory.

2.1 Watanabe-Strogatz Transformation

The system studied by WS consists of N globally coupled identical phase variables,

$$\dot{\theta}_j = A + B\cos\theta_j + C\sin\theta_j \qquad j = 1, \ldots N, \tag{2.1}$$

where A, B, and C are real functions of phases $\{\theta_j\}$, and are identical for all oscillators. This is equivalent to a more symmetrical form (*Marvel et al.*, 2009; *Stewart*, 2011),

$$\dot{\theta}_j = fe^{i\theta_j} + g + \bar{f}e^{-i\theta_j} \qquad j = 1, \ldots, N, \tag{2.2}$$

where the real function g and the complex function f are given by

$$A = g,\ B = 2\mathrm{Re}f,\ C = -2\mathrm{Im}f \Leftrightarrow f = \frac{1}{2}(B - iC).$$

People (*Strogatz and Mirollo*, 1991; *Nichols and Wiesenfeld*, 1992) had noticed that the incoherent states of Kuramoto model has neutral stability. The system also exhibits low-dimensional dynamics. Namely, although the full state space is an N-dimensional torus (T^N), the long-time evolution of variables is constrained in two-dimensional or three-dimensional manifolds.

To understand these observations, WS proposed a set of implicit coordinate transformations,

$$\tan\left(\frac{\theta_j(t) - \Theta(t)}{2}\right) = \sqrt{\frac{1+\gamma(t)}{1-\gamma(t)}}\tan\left(\frac{\psi_j - \Psi(t)}{2}\right), \tag{2.3}$$

where ψ_j are constants which are the initial configuration of the N oscillators. This transformation introduces three time-dependent variables: $\gamma \in [0,1)$; $\Psi, \Theta \in [0, 2\pi]$. They satisfy three coupled ODEs:

$$\dot{\gamma} = -(1-\gamma^2)(B\sin\Theta - C\cos\Theta), \tag{2.4}$$

$$\gamma\dot{\Psi} = -\sqrt{1-\gamma^2}(B\cos\Theta + C\sin\Theta), \tag{2.5}$$

$$\gamma\dot{\Theta} = A\gamma - B\cos\Theta - C\sin\Theta. \tag{2.6}$$

Given an initial condition $\{\psi_j\}$, the three variables live in a $3D$ manifold that is characterized by $N-3$ constants of motion. The full state space T^N is then foliated into a stack of $3D$ manifolds. WS showed that each manifold is neutrally stable and has at least one incoherent fixed point. Therefore, an incoherent state in a given $3D$ manifold has neutral stability in at least $N-3$ directions.

In addition, WS discussed the "cosine" model

$$\dot{\theta}_j = \omega + \frac{1}{N}\sum_{k=1}^{N} \cos(\theta_k - \theta_j - \delta), \tag{2.7}$$

which originated from averaging over Josephson-junction arrays with RLC loads in the weak coupling limit. The phase shift δ depends on physical parameters R, L, and C. Equation (2.7) is invariant under a phase shift, $\theta_j \to \theta_j + c$ with a constant angle c.

Due to this additional symmetry, the Θ dynamics in Eq. (2.6) decouple from γ and Ψ. The neutral invariant manifold becomes two-dimensional. WS constructed an $\mathcal{H}$ function on each $2D$ manifold for a given set of $\{\psi_k\}$,

$$\mathcal{H}(\gamma, \Psi) = \frac{1}{N}\sum_{k=1}^{N} \ln \frac{1 - \gamma\cos(\psi_k - \Psi)}{\sqrt{1-\gamma^2}}. \tag{2.8}$$

When $\delta = 0$, $\mathcal{H}$ is just the Hamiltonian and the model [Eq. (2.7)] becomes integrable.

The WS theory immediately received a lot of attention. It has been generalized to deal with non-identical (*Pikovsky and Rosenblum*, 2008; *Vlasov et al.*, 2016), noisy (*Braun et al.*, 2012), and externally-driven (*Pikovsky and Rosenblum*, 2009) systems. It also has connection (*Pikovsky and Rosenblum*, 2009, 2015) to the Ott-Antonsen (OA) ansatz (*Ott and Antonsen*, 2008, 2009).

Why does the WS theory work? Goebel (*Goebel*, 1995) first pointed out that the WS system [Eq. (2.1)] is essentially a set of complex Riccati equations. The $N-3$ constants of motion can be interpreted as cross-ratios of points on the unit circle. Calculations can be simplified using Möbius transformations. However, three questions remain:

1) What is the origin of those low-dimensional manifolds?

2) Where do the transformation [Eq. (2.3)] and new variables (γ, Ψ, Θ) come from?

3) How do we understand the Hamiltonian structure in the cosine model [Eq. (2.7)]?

2.2 Group Theoretic Approach

Using group theory, Marvel et al. (*Marvel et al.*, 2009) revisited the WS system and answered the first two remaining questions in the last section. We will adopt their approach to gain new insights on the WS system and to address the question on Hamiltonian structure.

2.2.1 The Riccati Equation

Let us start with the identical Kuramoto model with a phase shift α[1] (a.k.a. the Kuramoto-Sakaguchi model)

$$\dot{\theta}_j = \omega + \frac{K}{N}\sum_{l=1}^{N}\sin(\theta_l - \theta_j + \alpha). \tag{2.9}$$

Absorbing the order parameter $Z_1 = \frac{1}{N}\sum_{l=1}^{N} e^{i\theta_l} = Re^{i\psi}$ in the sinusoidal coupling term,

$$\begin{aligned}\frac{K}{N}\sum_{l=1}^{N}\sin(\theta_l - \theta_j + \alpha) &= K\mathrm{Im}(Z_1 e^{i\alpha}e^{-i\theta_j}) = KR\sin(\psi + \alpha - \theta_j)\\ &= KR[\sin(\psi+\alpha)\cos\theta_j - \cos(\psi+\alpha)\sin\theta_j],\end{aligned}$$

then comparing it with the general form $\dot{\theta}_j = A + B\cos\theta_j + C\sin\theta_j$, the coefficients are

$$A = \omega,\ B = KR\sin(\psi+\alpha),\ C = -KR\cos(\psi+\alpha).$$

So the Kuramoto-Sakaguchi model is indeed a special case of Eq. (2.1).

A phase variable θ_j is essentially as a point on the unit circle, which can be represented

[1]Compared with the cosine model [Eq. (2.7)], $\alpha = \frac{\pi}{2} - \delta$.

as a complex number, $z_j = e^{i\theta_j}$. Then Eq. (2.1) becomes

$$\begin{aligned}\dot{z}_j = iz_j\dot{\theta}_j &= iz_j\left[A + \frac{1}{2}B(e^{i\theta_j} + e^{-i\theta_j}) + \frac{1}{2i}C(e^{i\theta_j} - e^{-i\theta_j})\right] \\ &= iAz_j + iz_j\mathrm{Im}(\mathcal{a}\bar{z}_j) = iAz_j + \frac{1}{2}(\mathcal{a} - \overline{\mathcal{a}}z_j^2),\end{aligned} \tag{2.10}$$

where a new order parameter $\mathcal{a}$ is defined as

$$\mathcal{a} = -C + iB. \tag{2.11}$$

Equation (2.10) is a first-order ODE with a quadratic term and is called the Riccati equation, which plays a central role in the group-theoretic approach.

For the Kuramoto-Sakaguchi model, the order parameter is simply $\mathcal{a} = Ke^{i\alpha}Z_1$ with

$$Z_1 = \frac{1}{N}\sum_{l=1}^{N} e^{i\theta_l} = \frac{1}{N}\sum_{l=1}^{N} z_l.$$

Note that Z_1 is the first moment of a configuration $p = (\theta_1, \ldots, \theta_N) = (z_1, \ldots, z_N)$. For this reason, we will refer the Kuramoto-Sakaguchi model as the Z_1 model, and write[2]

$$\mathcal{a}(p) = e^{i\alpha}Z_1(p). \tag{2.12}$$

In the representation of the Riccati equation [Eq. (2.10)], the evolution of an oscillator $z_j(t)$ for a specific model is determined by the function A and the order parameter $\mathcal{a}$, both should be evaluated for a given configuration p. Further reduction can be made if A and $\mathcal{a}$ enjoy simple dependence on p. Before we proceed to solving the Riccati equation, let us make a short digression on such simplification.

[2]The coupling strength K is not essential in determining the fixed point structure, and can be safely set to unity by rescaling the speed of the flow. So we will often ignore it in the following sections.

2.2.2 Homogeneous Condition and Phase Models

A function $F(x)$ is said to be homogeneous with degree k if

$$F(ax) = a^k F(x), \quad k \in \mathbb{Z}. \tag{2.13}$$

Then it satisfies Euler's homogeneous function theorem[3], $x \cdot \nabla_x F(x) = kF(x)$. This relation is useful in Chapter 3 when we derive a general condition for gradient flows.

Of particular interest is when the coupling function A and the order parameter $\mathcal{a}$ are homogeneous of degree 0 and 1, respectively:

$$A(\zeta p) = A(p), \quad \mathcal{a}(\zeta p) = \zeta \mathcal{a}(p), \qquad |\zeta| = 1. \tag{2.14}$$

The multiplier $\zeta = e^{ic}$ applies a constant phase shift to all oscillators in a given configuration $p = (z_1, \ldots, z_N)$. The Riccati equation [Eq. (2.10)] is invariant under $z_j \to \zeta z_j$:

$$\zeta \dot{z}_j = iA(\zeta p)\zeta z_j + \frac{1}{2}(\mathcal{a}(\zeta p) - \overline{\mathcal{a}(\zeta p)}(\zeta z_j)^2) = \zeta \left[iA(p) z_j + \frac{1}{2}(\mathcal{a}(p) - \overline{\mathcal{a}(p)} z_j^2) \right].$$

Then we call such a system a Kuramoto phase model. For example, the Z_1 model satisfies

$$A(\zeta p) = \omega = A(p), \quad \mathcal{a}(\zeta p) = e^{i\alpha} Z_1(\zeta p) = \zeta e^{i\alpha} Z_1(p) = \zeta \mathcal{a}(p). \tag{2.15}$$

So it is a phase model. We will encounter other phase models that involve products of higher moments in the order parameters. Their time-evolutions are restricted in $2D$ manifolds. The origin of such low-dimensional dynamics lies within a generic form of solutions to the Riccati equation, also known as the Möbius transformation.

[3]This can be proved by taking the derivative with respect to a on both sides, $\frac{\partial F(ax)}{\partial (ax)} \cdot x = ka^{k-1}F(x)$, and setting $a = 1$.

2.2.3 Möbius Transformations

The generic form of Möbius transformations (linear fractional transformations) on the complex plane is given by

$$M(z) = \frac{az+b}{cz+d}, \quad z, a, b, c, d \in \mathbb{C}, \tag{2.16}$$

provided that $ad - bc \neq 0$, so as to exclude the degenerate case. Here, all coefficients (a, b, c, d) can be time-dependent. So the image of a transformation on a complex number z_0 is a function of time,

$$z(t) = M_t(z_0) = \frac{a(t)z_0 + b(t)}{c(t)z_0 + d(t)} \tag{2.17}$$

with an inverse transformation

$$z_0 = M_t^{-1}(z(t)) = \frac{d(t)z(t) - b(t)}{-c(t)z(t) + a(t)}.$$

Taking the derivative of $z(t)$ with respect to t yields the standard form of a Riccati equation:

$$\begin{aligned}
\dot{z} &= \frac{\dot{a}z_0 + \dot{b}}{cz_0 + d} - z\frac{\dot{c}z_0 + \dot{d}}{cz_0 + d} = \frac{\dot{a}\frac{dz-b}{-cz+a} + \dot{b} - z\left(\dot{c}\frac{dz-b}{-cz+a} + \dot{d}\right)}{c\frac{dz-b}{-cz+a} + d} \\
&= \frac{(a\dot{b} - \dot{a}b) + (\dot{a}d - \dot{d}a + \dot{c}b - \dot{b}c)z + (\dot{d}c - \dot{c}d)z^2}{ad - bc} \equiv P(t) + Q(t)z + R(t)z^2,
\end{aligned}$$

where the coefficients are

$$P = \frac{\dot{b}a - \dot{a}b}{ad - bc}, \quad Q = \frac{\dot{a}d - \dot{d}a + \dot{c}b - \dot{b}c}{ad - bc}, \quad R = \frac{\dot{d}c - \dot{c}d}{ad - bc}.$$

Therefore, a Möbius transformation on z_0 is the trajectory of a dynamical variable $z(t)$ that satisfies the Riccati equation. In other words, one can solve a Riccati equation by applying

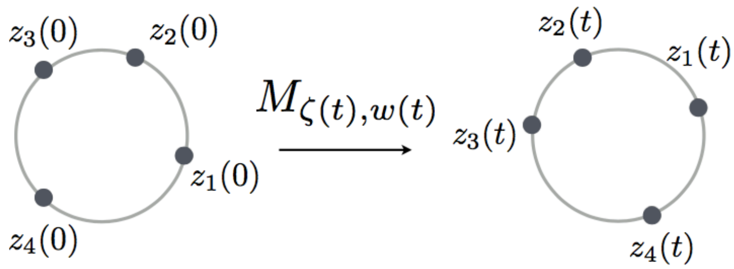

Figure 2.1: A schematic illustration of the evolution of N identical Kuramoto oscillators under the same Möbius transformation [Eq. (2.18)] $z_j(t) = M_{\zeta(t),w(t)}z_j(0)$ with an initial condition $(z_1(0), \ldots, z_N(0))$.

the corresponding Möbius transformation on an initial condition z_0.

The Möbius transformation that solves the Riccati equation for N Kuramoto oscillators [Eq. (2.10)] has the form (*Marvel et al.*, 2009; *Mirollo*, 2012)

$$M_{\zeta,w}(z) = \zeta \frac{z - w}{1 - \bar{w}z}, \quad |\zeta| = 1, \, |w| < 1, \tag{2.18}$$

which depends on three real parameters (r, φ, χ) since we can write $w = re^{i\varphi}$ and $\zeta = e^{i\chi}$.[4]

As a result, the time evolution $z_j(t)$ of N identical Kuramoto oscillators can be found by applying the Möbius transformation $M_{\zeta(t),w(t)}$ on an initial condition $z_j(0)$,

$$z_j(t) = M_{\zeta(t),w(t)}z_j(0) \equiv M_t\beta_j \qquad j = 1, \ldots, N. \tag{2.19}$$

In other words, for a given initial condition (a base point) $p = (z_1(0), \ldots, z_N(0)) = (\beta_1, \ldots, \beta_N) \in T^N$, the trajectory $p(t)$ of N oscillators is a time-t flow map $M_tp = (M_t\beta_1, \ldots, M_t\beta_N)$, as shown in Figure 2.1.

[4]In fact, $M_{\zeta,w}$ is the Lorentz transformation in $(2+1)D$ spacetime, see e.g. (*Weltin and Hua*, 2012) for more details.

More about of $M_{\zeta,w}$

The Möbius transformation $M_{\zeta,w}$ has a number of nice properties (*Weltin and Hua*, 2012). We briefly summarize them in the following.

1. Unit-disk preserving: Let $z' = M_{\zeta,w}(z)$ be the image of a point z ($|z| \leq 1$) under the Möbius transformation,

$$1 - |z'|^2 = 1 - \frac{(z-w)(\bar{z}-\bar{w})}{(1-\bar{w}z)(1-w\bar{z})} = \frac{(1-|z|^2)(1-|w|^2)}{|1-\bar{w}z|^2} \geq 0. \tag{2.20}$$

   The image z' is still within the unit disk. Thus, $M_{\zeta,w}$ preserves the unit disk $\Delta = \{|z| < 1\}$ and the unit circle $S^1 = \{|z| = 1\}$.

2. Linking to hyperbolic metric: Fixing $\zeta = 1$ and differentiating $z' = M_w z$,

$$dz' = \frac{1 - w\bar{w}}{(1-\bar{w}z)^2} dz, \tag{2.21}$$

   we then take the absolute value and divide $1 - |z'|^2$ on both sides,

$$\frac{|dz'|}{1-|z'|^2} = \frac{\frac{1-|w|^2}{|1-\bar{w}z|^2}|dz|}{\frac{(1-|z|^2)(1-|w|^2)}{|1-\bar{w}z|^2}} = \frac{|dz|}{1-|z|^2}. \tag{2.22}$$

   This invariant differential is essentially the hyperbolic metric in the unit disk (a.k.a. the Poincaré disk), which will be of great importance for our discussion on gradient systems in Chapter 3.

3. Connection to Poisson kernel: Let us consider two points $\beta = e^{i\theta}$ and $\beta' = e^{i\theta'}$ on the unit circle that are connected by $M_{\zeta,w}$,

$$\beta' = \zeta \frac{\beta - w}{1 - \bar{w}\beta} = \zeta \frac{1 - w\bar{\beta}}{1 - \bar{w}\beta} \beta.$$

The differential

$$d\beta' = i\beta' d\theta' = \zeta \frac{1 - w\bar{w}}{(1-\bar{w}\beta)^2} d\beta = \zeta \frac{1 - w\bar{w}}{(1-\bar{w}\beta)^2} i\beta d\theta$$

is just the change caused by an infinitesimal transformation. Dividing these two equations, the change on the unit circle is

$$d\theta' = \frac{1 - w\bar{w}}{(1-\bar{w}\beta)(1-w\bar{\beta})} d\theta \equiv \rho_\beta(w) d\theta. \tag{2.23}$$

The function $\rho_\beta(w)$ is just the Jacobian associated with the Möbius transformation and is called the Poisson kernel,

$$\rho_\beta(w) = \frac{1 - |w|^2}{|1-\bar{w}\beta|^2} = \frac{1 - r^2}{1 - 2r\cos(\theta - \varphi) + r^2}, \tag{2.24}$$

which has several interesting features and is connected to the OA ansatz:

- $\rho_\beta(w)$ is positive in the disk: $\rho_\beta(w) \geq 0$ for $|w| \leq 1$.

- $\rho_\beta(w)$ behaves like the Dirac delta function on the circle,

$$\rho_\beta(w) = \begin{cases} 0 & w \neq \beta \\ \\ \infty & w = \beta \end{cases}. \tag{2.25}$$

- $\rho_\beta(w)$ can be thought of as a probability density function since it normalizes to unity,

$$\frac{1}{2\pi}\int_0^{2\pi} \rho_\beta(w) d\theta = \frac{1}{2\pi}\int_0^{2\pi} d\theta' = 1. \tag{2.26}$$

- $\rho_\beta(w)$ satisfies the Laplace equation in the disk

$$\nabla^2 \rho = 0 \tag{2.27}$$

with $\nabla^2 = \partial_r^2 + r^{-1}\partial_r + r^{-2}\partial_\theta^2$ in polar coordinates, because $\rho_\beta(w)$ can be written as Fourier series,

$$\begin{aligned}\rho_\beta(w) = 1 + \frac{\bar{w}\beta}{1-\bar{w}\beta} + \frac{w\bar{\beta}}{1-w\bar{\beta}} = 1 + \sum_{n=1}^{\infty}(\bar{w}\beta)^n + \sum_{n=1}^{\infty}(w\bar{\beta})^n \Rightarrow \\ \rho_\theta(r,\varphi) = 1 + \sum_{n=1}^{\infty} r^n (e^{in(\theta-\varphi)} + e^{-in(\theta-\varphi)}) = 1 + 2\sum_{n=1}^{\infty} r^n \cos[n(\theta-\varphi)],\end{aligned} \tag{2.28}$$

then the Laplace equation is satisfied term by term:

$$\nabla^2 r^n \cos[n(\theta-\varphi)] = r^{n-2}\cos[n(\theta-\varphi)](n(n-1)+n-n^2) = 0.$$

Thus $\rho_\beta(w)$ is a harmonic function. It is also related to the Dirichlet problem: Finding a function $\rho(w)$ in the unit disk such that it satisfies the Laplace equation for $|w| < 1$ while being continuous (periodic) on the unit circle.

2.2.4 Möbius Group and Group Orbits (G-orbits)

As we have seen in the previous section, the Kuramoto oscillator system [Eq. (2.10)] evolves under the action of Möbius transformation $M_{\zeta,w}$ with three real parameters. All such transformations form a three-dimensional Lie group under function compositions. We call this group as the Möbius group G, which essentially contains all information about the original oscillator system. For instance, the time-evolution of oscillators $z_j(t)$, $\forall j$ can be interpreted as an orbit of the Möbius group.

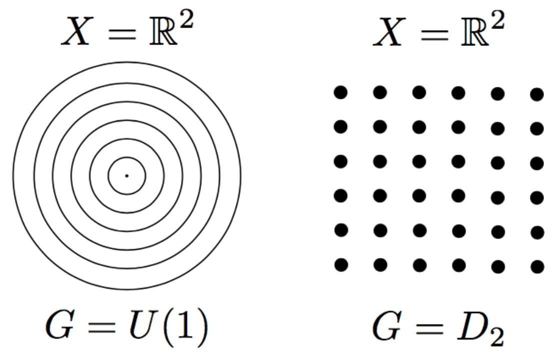

Figure 2.2: Group orbits of $U(1)$ group (left) and D_2 group (right) acting on $\mathbb{R}^2$.

For a group G, the group orbit Gx is the image of a set X under group actions,

$$Gx = \{g \cdot x | g \in G\} \subset X, \qquad \forall x \in X. \tag{2.29}$$

Since Gx is a subset of X, its dimension is at most the dimension of the group G, $\dim Gx \leq \dim G$. For example (Figure 2.2), if we take $X = \mathbb{R}^2$, and choose the group as all rotations in the plane, i.e., $G = U(1)$, then its group orbit are a family of concentric circles. If we choose the group as the dihedral group, $G = D_2$, then the group orbit are some planar lattices. Both examples are one-dimensional subsets of $\mathbb{R}^2$.

Likewise, the group orbit of the Möbius group acting on T^N (the state space of N Kuramoto oscillators) is

$$Gp = \{Mp | M \in G\} \subset T^N, \qquad \forall p \in T^N, \tag{2.30}$$

which is at most a three-dimensional manifold, which we refer to as the G-orbit Gp. A specific solution (with a base point p) to the Riccati equation [Eq. (2.10)] lies in a G-orbit. The whole state space T^N is then partitioned into a family of G-orbits.

2.2.5 Cross-ratios as Constants of Motion

A useful quantity to distinguish different G-orbits is the cross-ratio, defined as a crossed ratio of four points $\{z_1, z_2, z_3, z_4\}$ on the unit circle,[5]

$$\lambda_{(1234)} = \frac{(z_1 - z_2)(z_3 - z_4)}{(z_1 - z_4)(z_3 - z_2)} \in \mathbb{R}. \tag{2.31}$$

It is invariant under the Möbius transformation, $\beta_j = M z_j = \frac{a z_j + b}{c z_j + d}$ with the inverse $z_j = M^{-1}(\beta_j) = \frac{d\beta_j - b}{-c\beta_j + a}$:

$$\lambda_{(1234)} = \frac{(M^{-1}\beta_1 - M^{-1}\beta_2)(M^{-1}\beta_3 - M^{-1}\beta_4)}{(M^{-1}\beta_1 - M^{-1}\beta_4)(M^{-1}\beta_3 - M^{-1}\beta_2)} = \frac{(\beta_1 - \beta_2)(\beta_3 - \beta_4)}{(\beta_1 - \beta_4)(\beta_3 - \beta_2)}.$$

Since the Möbius transformation $z_j(t) = M_t z_j(0)$ is the solution to the Riccati equation, being invariant under the Möbius transformation implies that $\lambda_{(1234)}$ is also invariant under the time evolution. Therefore, it is a constant of motion.

For $N > 3$ Kuramoto oscillators, there are $N - 3$ cross-ratios (*Marvel et al.*, 2009). Trajectories in a G-orbit have the same cross-ratios. Different G-orbits are labeled by cross-ratios.

ODEs for w and ζ

Since the dynamics of oscillators are determined by the Möbius transformation, there is correspondence between the trajectory $z_j(t)$ and the group parameters $w(t)$ and $\zeta(t)$.

Given a base point $p = (\beta_1, \dots, \beta_N)$, using the pre-image [from Eq. (2.18)]

$$\beta_j = M_{\zeta,w}^{-1}(z_j) = \frac{\zeta w + z_j}{\zeta + \bar{w} z_j},$$

[5]Generically the cross-ratio is defined for four points in the complex plane. But it yields a real value only when the four points are in a line or on a circle.

we differentiate $M_t\beta_j$ with respect to t,

$$\begin{aligned}\partial_t(M_t\beta_j) &= \frac{\dot{\zeta}(\beta_j - w) - \zeta\dot{w}}{1-\bar{w}\beta_j} + \frac{\zeta(\beta_j - w)\beta_j\dot{\bar{w}}}{(1-\bar{w}\beta_j)^2} \\ &= \frac{-\zeta\dot{w}}{1-|w|^2} + \Big(\bar{\zeta}\dot{\zeta} + \frac{\dot{\bar{w}}w - \dot{w}\bar{w}}{1-|w|^2}\Big)z_j + \frac{\bar{\zeta}\dot{\bar{w}}}{1-|w|^2}z_j^2;\end{aligned}$$

then comparing with $\dot{z}_j$ in Eq. (2.10), we obtain two ODEs for w and ζ (*Chen et al.*, 2017):

$$\dot{w} = -\frac{1}{2}(1-|w|^2)\bar{\zeta}\mathcal{a}, \tag{2.32}$$

$$\dot{\zeta} = iA\zeta - \frac{1}{2}(\bar{w}\mathcal{a} - w\overline{\mathcal{a}}\zeta^2). \tag{2.33}$$

Here, $\mathcal{a} = \mathcal{a}(\zeta M_w p)$ is evaluated at the base point p with $M_w \equiv M_{\zeta=1,w}$. For a given model (A and $\mathcal{a}$ are known), starting with an initial condition [a base point $p = (z_1(0), \ldots, z_N(0))$], these two equations of $\dot{w}$ and $\dot{\zeta}$ define the Möbius transformation that evolves the N oscillators, $z_j(t) = M_{\zeta(t),w(t)}z_j(0), \forall j$.

Now it becomes clear that the WS transformation [Eq. (2.3)] stems from the Möbius transformation [Eq. (2.18)] which preserves the $N-3$ cross-ratios [Eq. (2.31)] as the $N-3$ constants of motion. The $3D$ neutral manifold found by WS is the group orbit Gp of Möbius transformations. Trajectories $z_j(t)$ in a G-orbit are equivalent to w and ζ flows. In fact, they can be expressed as the three real WS variables [Eq. (2.34)].

2.2.6 Reduced Group Orbits

For phase models with additional symmetry $\mathcal{a}(\zeta p) = \zeta\mathcal{a}(p)$, $\dot{w}$ decouples from $\dot{\zeta}$,

$$\dot{w} = -\frac{1}{2}(1-|w|^2)\mathcal{a}(M_w p), \qquad \dot{\zeta} = iA\zeta - \frac{1}{2}(\bar{w}\mathcal{a} - w\overline{\mathcal{a}}\zeta).$$

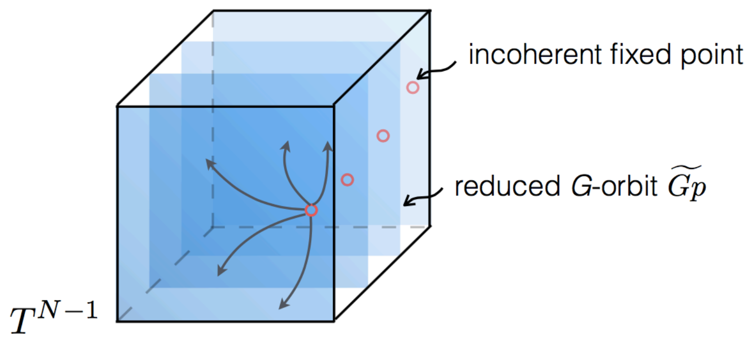

Figure 2.3: Reduced two-dimensional G-orbits (blue sheets) in the state space (the cube) of a phase model. Trajectories (black flows) and the incoherent fixed point (the red open circle) in each reduced G-orbit correspond to the $w(t)$ flow [Eq. (3.1)] and $\dot{w} = 0$.

Note that ζ is slaved to w and does not have interesting dynamics[6]. So we will focus on the w variable which lives in the (open) unit disk, $|w| < 1$. The $\dot{w}$ flows in this $2D$ manifold are equivalent to trajectories $z_j(t)$ in a reduced G-orbit (denoted as $\widetilde{Gp}$).

Figure 2.3 schematically shows how the state space of a phase model is partitioned into different $2D$ reduced G-orbits. For a phase model, every phase variable θ_j is identified with $\theta_j + c$. The state space is topologically folded into an $(N-1)$-dim torus, and is depicted as a cube. Each $2D$ reduced G-orbit (featuring distinct cross-ratios) is represented as a sheet. Trajectories $\theta_j(t)$ on each sheet are equivalent to $w(t)$ given by Eq. (3.1). There is at least one incoherent fixed point in each reduced G-orbit, which corresponds to $\dot{w} = 0$.

An Example: $N = 4$

So far, we have been using three different representations to describe the system of N identical Kuramoto oscillators: $\theta_j(t)$, $z_j(t)$, and $w(t)$. Let us demonstrate their relations with an example.

As shown in Figure 2.4, we start a system of four identical Kuramoto oscillators in the

[6]After all, in the Möbius transformation [Eq. (2.18)], ζ can be thought of as a pure rotation.

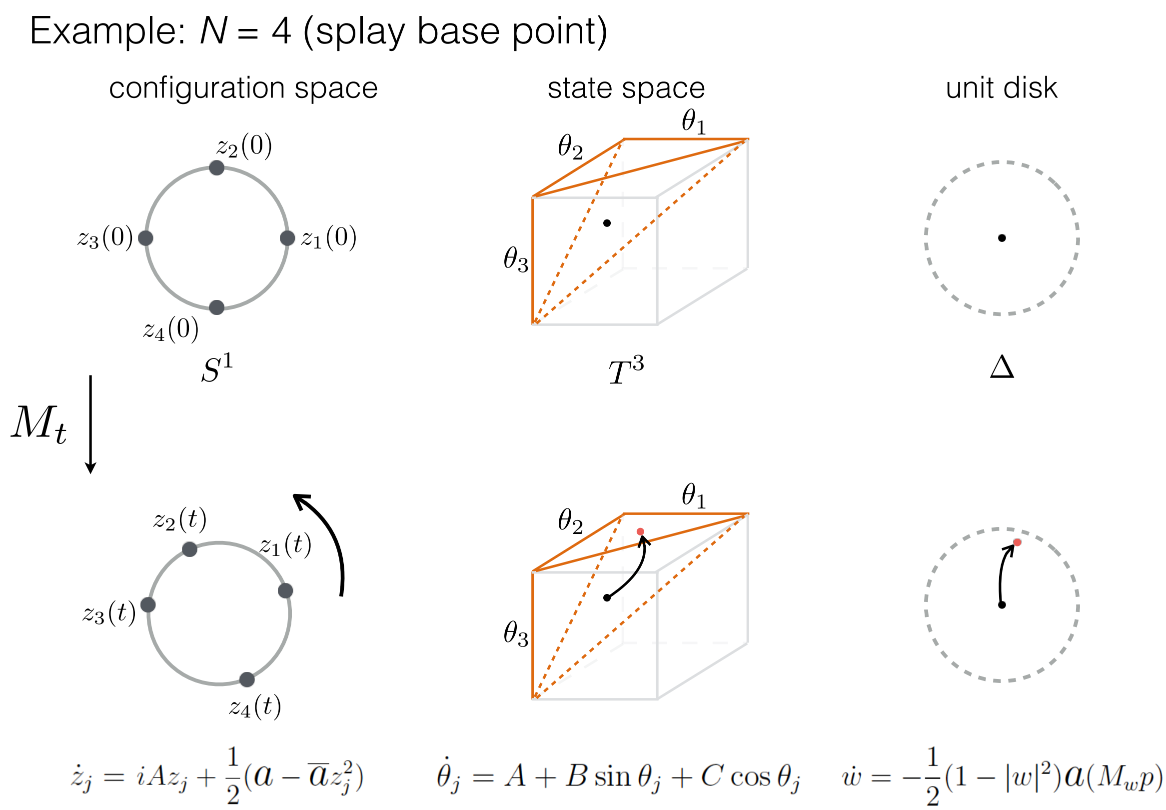

Figure 2.4: Three representations for N identical Kuramoto oscillators. Left panel: z_j as N points on the unit circle S^1. Middle panel: θ_j as a base point p in T^{N-1} (the orange tetrahedron). Right panel: The group parameter w in the unit disk Δ. The origin $w = 0$ is the identity element of the Möbius group and correspond to the base point. The system evolves according to a Möbius transformation M_t, manifested as rotations in S^1 (left), trajectories in T^3 (middle), and flows in Δ (right).

splay configuration, $\theta_j(0) = \frac{(j-1)\pi}{2}$ with $j = 1, \dots, 4$, or equivalently, $z_j(0) = e^{i\theta_j(0)} = \{1, i, -1, -i\}$. They can be depicted as four equally-spaced points on the unit circle, or as a base point p in the state space T^4.

However, under the Poincaré section (e.g. when $z_4 = 2n\pi$, $\forall n \in \mathbb{N}$), the state space is reduced to T^3, which is a cube with each edge having a length 2π and two end-points being identified one. Since oscillators are the same, they cannot pass each other. So the initial ordering $\theta_1 \leq \theta_2 \leq \theta_3 \leq \theta_4$ is kept as the system evolves. Then the trajectory $\theta_j(t)$ is restricted in one of the six tetrahedra (representing $3! = 6$ orderings) in the T^3 cube.[7]

In the group theory language, the splay state base point is the origin of the unit disk, $w = 0$, which is the identity element $M_{w=0}$ of the Möbius group. In fact, a new base point (a new initial configuration) still corresponds to the origin. Since different base points are related via Möbius transformations, changing base points amounts to choosing another w-coordinate system for the unit disk (*Chen et al.*, 2017). So focusing our discussion on a specific base point (the splay state) does not lose generality.

As the system evolves under a Möbius transformation M_t, there is one-to-one correspondence among the evolution $z_j(t)$ on the unit disk, the trajectory $\theta_j(t)$ in the tetrahedron, and the $w(t)$ flow in the unit disk. In particular, $\theta_j(t)$ actually lies in the reduce G-orbit $\widetilde{Gp}$ of the splay base point, which can be visualized as a $2D$ surface inside the tetrahedron. Long-time dynamics in the former two representations (S^1 and T^3) are manifested as fixed points of the flow $\dot{w} = 0$ or zeros of the order parameter $\mathcal{a}(M_w p)$.

Figure 2.5 shows trajectories $\theta_j(t)$ of four oscillators and $w(t)$ flows of the Z_1 phase model [Eq. (2.9)] with $\alpha = 0$. In the tetrahedron, colored curves consist of four "lobes", separated by four blue saddle connections linking the center (the splay state) and mid-points [$(3, 1)$ states] on four solid edges. There is no attractors on the two lightgray edges,

[7] The center of a tetrahedron is the splay base point. The four vertices represent the fully synchronized state (the sync state). Edges represent partially synchronized states.

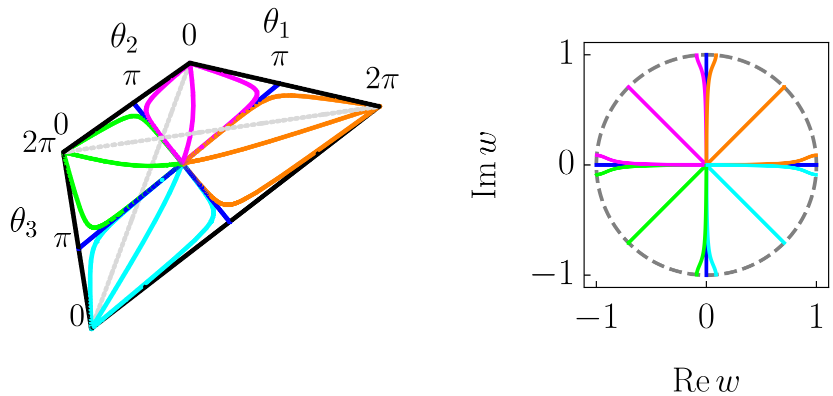

$N = 4$

Figure 2.5: Left panel: Trajectories $\theta_j(t)$ in the reduced G-orbit of the splay base point for the Z_1 phase model [Eq. (2.9)] with $\alpha = 0$. Right panel: The $w(t)$ flows in the unit disk given by Eq. (3.1). Detailed correspondence is listed in Table 2.1.

States	$\widetilde{Gp}$	Δ
base point	$p = (\beta_1, \dots, \beta_{N-1})$	$w = 0$
sync	vertices	arcs excluding β_j
$(N-1, 1)$	edges excluding vertices	base point β_j
fixed points	$\dot{z}_j(t) = 0, \quad \forall j$	$a(w) = 0$

Table 2.1: A dictionary between the reduced G-orbit $\widetilde{Gp}$ and the unit disk Δ.

meaning that the $(2, 2)$ state is not a fixed point. Trajectories within one lobe flow to the same vertex (the sync state). All trajectories lie in a $2D$ surface (the reduce G-orbit) that is inside the tetrahedron and is bounded by the four solid edges.

In the unit disk, the $w(t)$ flows are labeled by the same color-coding. For example, the orange lobe enclosed by two blue saddle connections in the tetrahedron is mapped to the first quadrant in the w-plane. In the same manner, the entire reduced G-orbit $\widetilde{Gp}$ maps to the unit disk Δ with correspondence summarized in Table 2.1.[8]

[8] The angle of approaching a $\beta_j \in \Delta$ gives the location of a $(N-1, 1)$ fixed point on an edge in the tetrahedron.

2.3 Connecting Möbius to Watanabe-Strogatz

To understand the WS transformation in terms of Möbius transformation, let us consider a base point $p = (\beta_1, \ldots, \beta_N) = (e^{i\psi_1}, \ldots, e^{i\psi_N})$. There is a Möbius transformation to map p to a new configuration $p(t) = (e^{i\theta_1(t)}, \ldots, e^{i\theta_N(t)})$ with $w = re^{i\varphi}$ and $\zeta = e^{i\chi}$,

$$M_{\zeta(t),w(t)}(\beta_j) = \zeta(t)\frac{\beta_j - w(t)}{1 - \bar{w}(t)\beta_j} = e^{i\chi(t)}\frac{e^{i\psi_j} - r(t)e^{i\varphi(t)}}{1 - r(t)e^{-i\varphi(t)}e^{i\psi_j}} = e^{i\theta_j(t)}.$$

Rearranging both sides, we have

$$e^{i(\theta_j - \varphi - \chi)} = \frac{e^{i(\psi_j - \varphi)} - r}{1 - re^{i(\psi_j - \varphi)}}.$$

Using trigonometric identities (*Marvel et al.*, 2009), $\tan(x)$ can be written as

$$\tan(x) = \frac{\sin(x)}{\cos(x)} = \frac{\frac{1}{2i}(e^{ix} - e^{-ix})}{\frac{1}{2}(e^{ix} + e^{-ix})} = i\frac{1 - e^{2ix}}{1 + e^{2ix}}.$$

Then we have

$$\tan\left(\frac{\theta_j - (\varphi + \chi)}{2}\right) = i\frac{1 - e^{i(\theta_j - (\varphi + \chi))}}{1 + e^{i(\theta_j - (\varphi + \chi))}} = i\frac{1 + r}{1 - r}\frac{1 - e^{i(\psi_j - \varphi)}}{1 + e^{i(\psi_j - \varphi)}} = \frac{1 + r}{1 - r}\tan\left(\frac{\psi_j - \varphi}{2}\right).$$

Compared with Eq. (2.3), if we require $\sqrt{\frac{1+\gamma}{1-\gamma}} = \frac{1+r}{1-r}$, then the three WS variables (γ, Ψ, Θ) are identified with three real parameters (r, φ, χ) in the Möbius transformation,

$$\gamma = \frac{2r}{1 + r^2} = \frac{2|w|}{1 + |w|^2}, \quad \Psi = \varphi = \arg(w), \quad \Theta = \varphi + \chi = \arg(\zeta w). \tag{2.34}$$

Equations of $\dot{w}$ and $\dot{\zeta}$ [Eqs. (3.1), (2.33)] are equivalent to ODEs of WS variables. First let us look at $\dot{w}$:

$$\dot{w} = -\frac{1}{2}(1-|w|^2)\bar{\zeta}\mathsf{a} \Rightarrow e^{i\varphi}(\dot{r} + ir\dot{\varphi}) = -\frac{1}{2}(1-r^2)e^{-i\chi}(-C+iB) \Rightarrow$$

$$e^{i\Theta}(\dot{r} + ir\dot{\varphi}) = \dot{r}\cos\Theta - r\dot{\varphi}\sin\Theta + i(\dot{r}\sin\Theta + r\dot{\varphi}\cos\Theta) = \frac{1}{2}(1-r^2)(C-iB) \Rightarrow$$

$$\begin{cases} \dot{r}\cos\Theta - r\dot{\varphi}\sin\Theta = \frac{1}{2}(1-r^2)C \\ \dot{r}\sin\Theta + r\dot{\varphi}\cos\Theta = -\frac{1}{2}(1-r^2)B \end{cases} \Rightarrow$$

$$\dot{r} = \frac{1}{2}(1-r^2)(C\cos\Theta - B\sin\Theta) \Rightarrow \dot{\gamma} = -(1-\gamma^2)(B\sin\Theta - C\cos\Theta),$$

$$r\dot{\varphi} = -\frac{1}{2}(1-r^2)(B\cos\Theta + C\sin\Theta) \Rightarrow \gamma\dot{\Psi} = -\sqrt{1-\gamma^2}(B\cos\Theta + C\sin\Theta).$$

Here we have used $\Theta = \varphi + \chi$, $\Psi = \varphi$, and

$$\dot{\gamma} = \frac{2(1-r^2)}{(1+r^2)^2}\dot{r} \Rightarrow \dot{r} = \frac{(1+r^2)^2}{2(1-r^2)}\dot{\gamma}, \quad 1-\gamma^2 = \left(\frac{1-r^2}{1+r^2}\right)^2.$$

Similarly, the equation for $\dot{\zeta}$ leads to the equation for $\dot{\Theta}$ as Eq. (2.6).

$$\dot{\zeta} = iA\zeta - \frac{1}{2}(\bar{w}\mathsf{a} - w\overline{\mathsf{a}}\zeta^2) \Rightarrow e^{i\chi}i\dot{\chi} = iAe^{i\chi} - \frac{1}{2}(re^{-i\varphi}\mathsf{a} - re^{i\varphi}\overline{\mathsf{a}}e^{2i\chi}) \Rightarrow$$

$$\dot{\chi} = A - \frac{1}{2i}(r\mathsf{a}e^{-i(\varphi+\chi)} - r\overline{\mathsf{a}}e^{i(\varphi+\chi)}) = A - r\mathrm{Im}(\mathsf{a}e^{-i(\varphi+\chi)})$$

$$= A - r\mathrm{Im}((-C+iB)e^{i\Theta}) = A - r(C\sin\Theta + B\cos\Theta) \Rightarrow$$

$$\gamma\dot{\varphi} + \gamma\dot{\chi} = A\gamma - (r\gamma + \sqrt{1-\gamma^2})(B\cos\Theta + C\sin\Theta) = A\gamma - (B\cos\Theta + C\sin\Theta) \Rightarrow$$

$$\gamma\dot{\Theta} = A\gamma - B\cos\Theta - C\sin\Theta.$$

2.4 Summary

In this chapter, using a group-theoretic approach, we establish the formalism for later chapters. We demonstrate that dynamics of N identical Kuramoto oscillators are determined by applying a unit-disk-preserving Möbius transformation on an initial condition. Trajectories in the state space of oscillators are identified as group orbits of such Möbius transformations. In particular, for phase models, flows in the reduced group orbits are equivalent to flows in the unit disk.

CHAPTER III

Phase Models

As shown in Chapter 2, dynamics of phase models live in reduced G-orbits of Möbius transformations, and can be fully described as flows in the unit disk,

$$\dot{w} = -\frac{1}{2}(1 - |w|^2)a(M_w p), \qquad |w| < 1. \tag{3.1}$$

In this chapter, we will focus on Eq. (3.1) and fixed points in the disk Δ that has an intrinsic hyperbolic metric. We are particularly interested in the implication of hyperbolic geometry on dynamics of Kuramoto oscillators, which leads to a condition for gradient systems. We will discuss bifurcations on a partially synchronized edge.

3.1 Flows in Reduced Group Orbits

3.1.1 Fixed Points

According to (*Engelbrecht and Mirollo*, 2014), there are only three types of asymptotic fixed points for phase models with $N \geq 4$. They are the fully synchronized state (sync), the partially synchronized state with only one outlier known as the $(N-1, 1)$ state, and limit cycles.

The simple classification of fixed points does not imply that the dynamics are simple: There can be saddle points and saddle connections in the G-orbit and the unit disk. Let us examine a few examples.

3.1.1.1 Z_1 model

Starting from the order parameter $a(M_w p) = Z_1(M_w p)$ at a base point $p = (\beta_1, \ldots, \beta_N)$, the first moment $Z_1(M_w p)$ can be expanded into a series of moments evaluated at p,

$$Z_1(M_w p) = \frac{1}{N}\sum_{k=1}^{N} \frac{\beta_k - w}{1 - \bar{w}\beta_k} = \frac{1}{N}\sum_{k}(\beta_k - w)\sum_{n=0}^{\infty}(\bar{w}\beta_k)^n = \sum_{n=0}^{\infty}\bar{w}^n(Z_{n+1}(p) - wZ_n(p)). \tag{3.2}$$

Splay base point The $\dot{w}$ flow has a closed form if we take the base point in the splay G-orbit,

$$\tilde{p} = (\eta, \eta^2, \ldots, \eta^N),\ \eta = e^{2\pi i/N}.$$

Note that $\eta^{kN} = 1, \forall k \in \mathbb{N}$, so

$$Z_n(\tilde{p}) = \overline{Z_n(\tilde{p})} = \delta_{n,kN},$$

with δ denoting the Kronecker delta. As a result, $Z_1(M_w\tilde{p})$ reduces to

$$\begin{aligned} Z_1(M_w\tilde{p}) &= \sum_{n=0}^{\infty}\bar{w}^n(Z_{n+1}(\tilde{p}) - wZ_n(\tilde{p})) = \sum_{n=0}^{\infty}\bar{w}^n(\delta_{n+1,kN} - w\delta_{n,kN}) \\ &= \bar{w}^{-1}\sum_{k=1}^{\infty}\bar{w}^{kN} - w\sum_{k=0}^{\infty}\bar{w}^{kN} \\ &= \frac{\bar{w}^{N-1} - w}{1 - \bar{w}^N} = -w + \frac{\bar{w}^{N-1}\left(1 - |w|^2\right)}{1 - \bar{w}^N}. \end{aligned} \tag{3.3}$$

For finite N, the $\dot{w}$ flow is given by

$$\dot{w} = -\frac{1}{2}(1-|w|^2)\mathcal{a}(M_w\tilde{p}) = -\frac{1}{2}\frac{(1-|w|^2)(\bar{w}^{N-1}-w)}{1-\bar{w}^N}. \tag{3.4}$$

Near the base point $w = \eta^k = e^{2\pi ik/N}$, $1-\bar{w}^N \to 0$. But the flow is not singular, it actually vanishes: Let $w = re^{i\phi}$ with $r \in [0,1)$, using L'Hopital's rule, the flow near η^k is

$$\begin{aligned}
\lim_{w\to\eta^k}\dot{w} &= -\frac{1}{2}\lim_{r\to 1}\lim_{\phi\to 2\pi k/N}\frac{(1-r^2)(r^{N-1}e^{-i(N-1)\phi}-re^{i\phi})}{1-r^Ne^{-iN\phi}} \\
&= -\frac{1}{2}\lim_{r\to 1}(1-r^2)\lim_{\phi\to 2\pi k/N}\frac{r^{N-1}(-i(N-1))e^{-i(N-1)\phi}-rie^{i\phi}}{-r^N(-iN)e^{-iN\phi}} \\
&= -\frac{1}{2}\lim_{r\to 1}(1-r^2)\lim_{\phi\to 2\pi k/N}\left(-\frac{1}{r}\frac{N-1}{N}e^{i\phi}-\frac{1}{r^{N-1}}\frac{1}{N}e^{i(N+1)\phi}\right) = 0.
\end{aligned}$$

On the other hand, the large N limit for Z_1 and the $\dot{w}$ flow is simple, since $|w| < 1$ then $\bar{w}^N$ approaches zero as $N \to \infty$,

$$\lim_{N\to\infty} Z_1(M_w\tilde{p}) = -w,\ \lim_{N\to\infty}\dot{w} = \frac{1}{2}(1-|w|^2)w.$$

Fixed points Finding the fixed point such that $\dot{w} = 0$ amounts to solving

$$(1-|w|^2)(\bar{w}^{N-1}-w) = 0,$$

assuming $\bar{w}^N \neq 1 \Leftrightarrow w \neq e^{2\pi ik/N}$. This assumption is valid because w is defined only inside the unit disk, $|w| < 1$, not on the unit circle. Although $|w|^2 = 1$ does satisfy $\dot{w} = 0$, it should not be considered as a fixed point for the flow.

The remaining equation $w = \bar{w}^{N-1}$ has a solution at the origin, $r = 0$. Other than that, since $0 < |w| < 1 \Rightarrow 0 < |\bar{w}^{N-1}| < |w|$, so $w = 0$ is the only solution in Δ. In the large

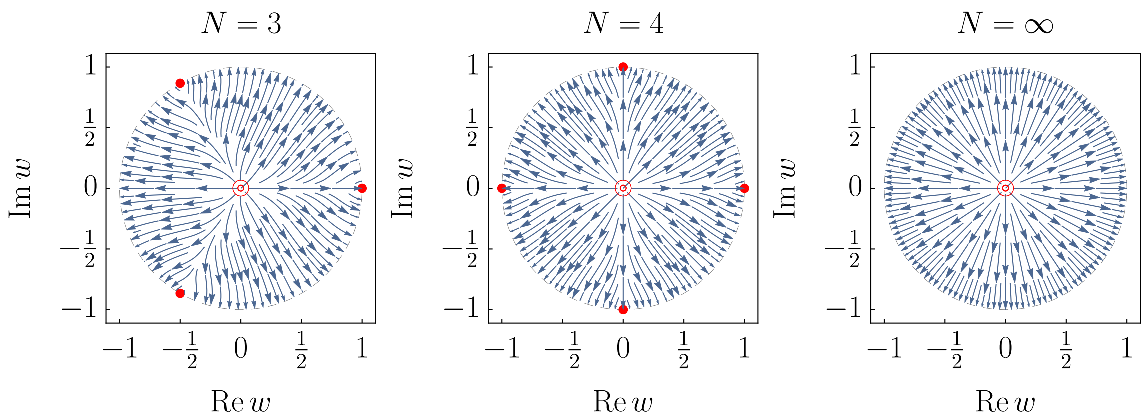

Figure 3.1: $\dot{w}$ flow for Z_1 model on the splay base point (red solid circles) $\tilde{p} = (\eta, \eta^2, \ldots, \eta^N)$ with $\eta = e^{2\pi i/N}$. The open circle at $w = 0$ denotes an unstable fixed point.

N limit, $\dot{w} \to \frac{1}{2}(1 - |w|^2)w$ and also vanishes at $w = 0$. The stability is easy to analyze,

$$\frac{d\dot{w}}{dw}\bigg|_{w=0} = -\bar{w}w + \frac{1}{2}(1 - |w|^2)\bigg|_{w=0} = \frac{1}{2}.$$

Since the origin is the identity element of the Möbius group, it corresponds to the unstable splay state on the splay G-orbit.

Figure 3.1 shows the $\dot{w}$ flows and fixed points for the Z_1 model with different N at the splay base point.

3.1.1.2 $Z_2 Z_{-1}$ model

We expect richer fixed point structures in other phase models. The first example is the $Z_2 Z_{-1}$ model with Z_2 denoting the second moment,

$$a(p) = Z_2(p) Z_{-1}(p) = \frac{1}{N^2} \sum_{j,k=1}^{N} z_j^2 z_k^{-1}.$$

Evaluated at $M_w p$, the product $Z_2 Z_{-1}$ can be expanded into a power series of moments,

$$Z_2 Z_{-1}(M_w p) = \sum_{n=0}^{\infty}(n+1)\bar{w}^n (Z_{n+2} - 2wZ_{n+1} + w^2 Z_n) \sum_{m=0}^{\infty} w^m (\bar{Z}_{m+1} - \bar{w}\bar{Z}_m).$$

The summation over m is for $Z_{-1} = \bar{Z}_1$, and the summation over n is for the Z_2 moment,

$$\begin{aligned}
Z_2(M_w p) &= \frac{1}{N}\sum_{l=1}^{N}\left(\frac{\beta_l - w}{1-\bar{w}\beta_l}\right)^2 = \frac{1}{N}\sum_{l=1}^{N}(\beta_l - w)^2 \sum_{n=0}^{\infty}(n+1)(\bar{w}\beta_l)^n \\
&= \sum_{n=0}^{\infty}(n+1)\,\bar{w}^n \frac{1}{N}\sum_{l=1}^{N}\left(\beta_l^{n+2} - 2w\beta_l^{n+1} + w^2\beta_l^n\right) \\
&= \sum_{n=0}^{\infty}(n+1)\bar{w}^n (Z_{n+2} - 2wZ_{n+1} + w^2 Z_n).
\end{aligned}$$

Splay base point At the splay base point $\tilde{p} = (\eta, \ldots \eta^N)$, summing over all the Kronecker deltas, the Z_2 moment becomes a function of w and $\bar{w}$,

$$\begin{aligned}
Z_2(M_w \tilde{p}) &= \sum_{n=0}^{\infty}(n+1)\,\bar{w}^n\left(\delta_{n+2,kN} - 2w\delta_{n+1,kN} + w^2\delta_{n,kN}\right) \\
&= \sum_{k=1}(kN-1)\,\bar{w}^{kN-2} - 2w\sum_{k=1} kN\bar{w}^{kN-1} + w^2\sum_{k=0}(kN+1)\,\bar{w}^{kN} \\
&= \frac{\bar{w}^{N-2}\left(N-1+\bar{w}^N\right)}{(1-\bar{w}^N)^2} - 2w\frac{N\bar{w}^{N-1}}{(1-\bar{w}^N)^2} + w^2\frac{1+(N-1)\,\bar{w}^N}{(1-\bar{w}^N)^2}. \qquad (3.5)
\end{aligned}$$

The Z_{-1} moment is just the conjugate of Z_1,

$$Z_{-1}(M_w\tilde{p}) = \overline{Z_1(M_w\tilde{p})} = \overline{\left(\frac{\bar{w}^{N-1} - w}{1-\bar{w}^N}\right)} = \frac{w^{N-1} - \bar{w}}{1-w^N}.$$

So the product of moments $Z_2 Z_{-1}$ reduces to

$$Z_2 Z_{-1}(M_w\tilde{p}) = \frac{f(w,\bar{w})}{(1-\bar{w}^N)^2}\frac{(w^{N-1} - \bar{w})}{(1-w^N)}, \qquad (3.6)$$

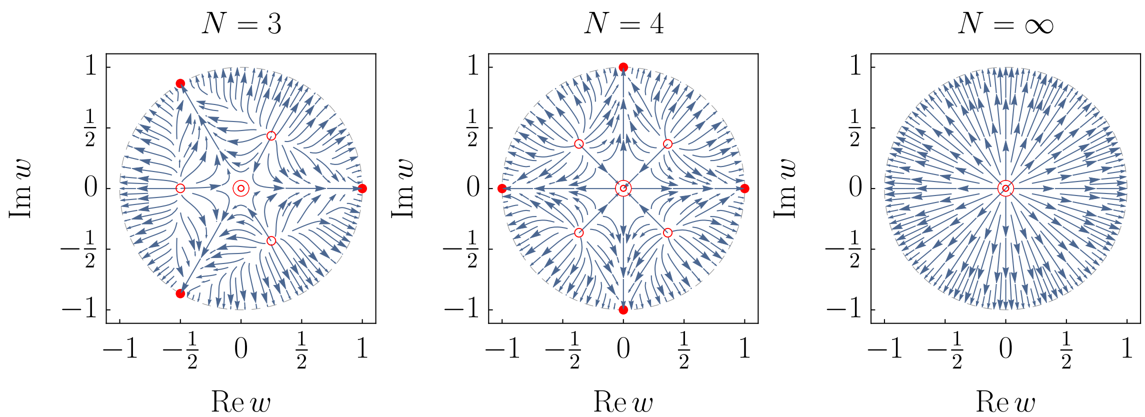

Figure 3.2: $\dot{w}$ flow for $Z_2 Z_{-1}$ model on the splay base point (red solid circles) $\tilde{p} = (\eta, \eta^2, \ldots, \eta^N)$ with $\eta = e^{2\pi i/N}$. The open circle at $w = 0$ denotes an non-hyperbolic, unstable fixed point.

where the numerator in Z_2 adds up to a polynomial f in w and $\bar{w}$,

$$f(w, \bar{w}) = \bar{w}^{2(N-1)} + (N-1)\bar{w}^{N-2} - 2N\bar{w}^{N-1}w + (N-1)\bar{w}^N w^2 + w^2. \tag{3.7}$$

In the large N limit, the flow is even simpler,

$$\lim_{N\to\infty} Z_2 Z_{-1}(M_w \tilde{p}) = -w^2 \bar{w}.$$

Figure 3.2 shows the $\dot{w}$ flow for $Z_2 Z_{-1}$ model at the splay base point with different N. New fixed points appear due to the second moment Z_2, particularly the zeros of $f(w, \bar{w})$.

Fixed points In addition to zeros at the origin $w = 0$ and on the unit circle $|w| = 1$, solving $f(w, \bar{w}) = 0$ with $w = re^{i\phi}$ leads to

$$r^{2(N-2)} + e^{iN\phi}\left[(N-1)\, r^N - 2N r^{N-2} + (N-1)\, r^{N-4}\right] + e^{2iN\phi} = 0.$$

Let $\varphi = N\phi$ and define a polynomial of r,

$$P_N(r) \equiv (N-1)\, r^N - 2Nr^{N-2} + (N-1)\, r^{N-4},$$

we have two equations for the real part and the imaginary part:

$$\begin{aligned} r^{2(N-2)} + P_N(r)\cos\varphi + \cos 2\varphi = 0, \\ P_N(r)\sin\varphi + \sin 2\varphi = 0. \end{aligned}$$

1. $\sin\varphi \neq 0$ ($\phi \neq \frac{n\pi}{N}$, $n \in \mathbb{N}$): The imaginary part yields $P_N(r) = -\frac{\sin 2\varphi}{\sin\varphi} = -2\cos\varphi$. Substituting it to the real part gives

$$r^{2(N-2)} = -P_N(r)\cos\varphi - \cos 2\varphi = 2\cos^2\varphi - \cos 2\varphi = 1.$$

So $r = 1$ when N is odd, $r = \pm 1$ when N is even.

2. $\sin\varphi = 0$ ($\phi = \frac{n\pi}{N}$, $n \in \mathbb{N}$): The imaginary part always holds. For the real part, there are two possibilities:

- $n = 0$ (the real axis): Since $\varphi = N\phi = 0$, $\cos\varphi = \cos 2\varphi = 1$. The real part is

$$r^{2(N-2)} + P_N(r) + 1 = 0.$$

Table 3.1 lists all solutions to the above equation for small N with $n = 0$. Noticeably, when $N \geq 6$, there is no real root except for $r = \pm 1$ (depending on N being even or odd), which means no fixed point exists on the real axis.

N	1	2	3	4	5	≥ 6
r	1	± 1	$\left\{-\frac{1}{2}, 1\right\}$	± 1	$\left\{\frac{-3+\sqrt{5}}{2}, 1\right\}$	$\begin{cases} 1 & \text{odd } N \\ \pm 1 & \text{even } N \end{cases}$

Table 3.1: Zeros of Z_2 on the real axis ($\phi = 0$).

N	1	2	3	4	5	≥ 6
r	-1	$\pm(1-\sqrt{2})$	$\left\{-1, \frac{1}{2}\right\}$	$\pm\sqrt{2-\sqrt{3}}$	$\left\{-1, \frac{3-\sqrt{5}}{2}\right\}$	$\begin{cases} -1 & \text{odd } N \\ \emptyset & \text{even } N \end{cases}$

Table 3.2: Zeros of Z_2 on the first symmetry axis ($\phi = \pi/N$).

- $n = 1$ (the symmetry axis): Since $\varphi = N\phi = \pi$, $\cos\varphi = -1 = -\cos 2\varphi$. The real part becomes

  $$r^{2(N-2)} - P_N(r) + 1 = 0.$$

  Solutions for small N with $n = 1$ are listed in Table 3.2.

In sum, there are several interesting observations:

- The fixed point at the origin $w = 0$ is non-hyperbolic;
- Fixed points in the disk only exist on symmetric axes ($\varphi = n\pi/N$) since Z_2 is invariant under rotations $e^{i\varphi}$;
- For $N \geq 6$, the origin is the only fixed point.

This cut-off effect can be seen from Figure (3.3). Zero-crossings are solutions to $f(r) = 0$, which determine locations of fixed points in the w vector field. For $N = 6$, the curve is positive-definite on the real axis ($\varphi = 0$) and the symmetry axis ($\varphi = \pi/N$). Thus there is no solution except for $r = \pm 1$ which is on the unit circle.

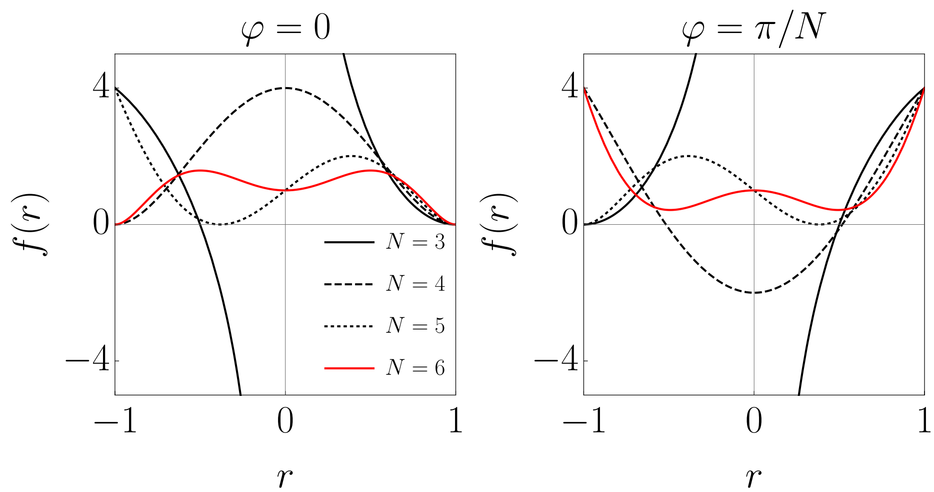

Figure 3.3: Plot of the radial component $f(r)$ in Z_2 moment for different N along the real axis ($\varphi = 0$) and the symmetry axis ($\varphi = \pi/N$). The zero-crossings correspond to fixed point of $\dot{w}$ flows.

3.1.2 Flows for $Z_q Z_{1-q}$ Models

A natural generalization is to consider $Z_q Z_{1-q}$ models with $q \in \mathbb{N}$. Since the order parameter $a = Z_q Z_{1-q}(M_w p)$ is a product of moments, it would be useful to have an explicit expression for $Z_q(M_w p)$ as a function of w and $\bar{w}$. Using expansions

$$(1-\bar{w}\beta_j)^{-1} = \sum_{n=0}^{\infty} (\bar{w}\beta_j)^n,$$

$$(1-\bar{w}\beta_j)^{-q} = \sum_{n=0}^{\infty} \frac{(n+1)(n+2)\cdots(n+m-1)}{(m-1)!} (\bar{w}\beta_j)^n,\ q \geq 2,$$

we expand Z_q into a series of moments,

$$\begin{aligned} Z_q(M_w p) &= \frac{1}{N}\sum_{j=1}^{N}\left(\frac{\beta_j - w}{1-\bar{w}\beta_j}\right)^q = \frac{1}{N}\sum_j (\beta_j - w)^q \sum_{n=0}^{\infty}\frac{(n+1)_{q-1}}{(q-1)!}\bar{w}^n\beta_j^n \\ &= \sum_n \frac{(n+1)_{q-1}}{(q-1)!}\bar{w}^n \frac{1}{N}\sum_j \beta_j^n \sum_{s=0}^{q}(-1)^{q-s}\binom{q}{s}\beta_j^s w^{q-s} \\ &= \sum_{s=0}^{q}(-1)^{q-s}\binom{q}{s} w^{q-s}\sum_{n=0}^{\infty}\frac{(n+1)_{q-1}}{(q-1)!}\bar{w}^n Z_{n+s}(p) \\ &= \sum_{s=0}^{q}\frac{(-1)^{q-s}q}{s!(q-s)!}w^{q-s}\sum_{n=0}^{\infty}(n+1)_{q-1}\bar{w}^n Z_{n+s}(p). \end{aligned}$$

Reorganizing it, we obtain

$$Z_q(M_w p) = q\sum_{s=0}^{q}\frac{(-1)^{q-s}}{s!(q-s)!}w^{q-s}\Sigma_q(\bar{w}, s; p), \tag{3.8}$$

$$\Sigma_q(\bar{w}, s; p) \equiv \sum_{n=0}^{\infty}(n+1)_{q-1}\bar{w}^n Z_{n+s}(p), \tag{3.9}$$

where $\binom{q}{s} = \frac{q!}{s!(q-s)!}$ and the Pochhammer symbol is defined as

$$(n+1)_{q-1} \equiv \prod_{l=0}^{q-2}(n+1+l) = (n+1)(n+2)\cdots(n+m-1) = \frac{\Gamma(n+q)}{\Gamma(n+1)}$$

where Γ is the gamma function, $(n+1)_0 = 1$ and $(n+1)_1 = n+1$.

3.1.2.1 Simplification at splay base point

At the splay base point $\tilde{p}$, using $Z_n(M_w\tilde{p}) = \delta_{n,kN}$, $\forall k \in \mathbb{N}$, the summation Σ_q for the q-th moment reduces to

$$\Sigma_q(\bar{w}, s; \tilde{p}) = \sum_{n=0}^{\infty}(n+1)_{q-1}\bar{w}^n\delta_{n+s,kN} = \sum_{k(s)}^{\infty}(kN+1-s)_{q-1}\bar{w}^{kN-s} \equiv \Sigma_q(s). \tag{3.10}$$

	$q=1$	$q=2$	$q=3$
$s=0$	$\frac{1}{1-\bar{w}^N}$	$\frac{(N-1)\bar{w}^N+1}{(1-\bar{w}^N)^2}$	$\frac{\bar{w}^N(N-1)(\bar{w}^N(N-2)+(N+4))+2}{(1-\bar{w}^N)^3}$
$s=1$	$\frac{\bar{w}^{N-1}}{1-\bar{w}^N}$	$\frac{N\bar{w}^{N-1}}{(1-\bar{w}^N)^2}$	$\frac{N\bar{w}^{N-1}(\bar{w}^N(N-1)+(N+1))}{(1-\bar{w}^N)^3}$
$s=2$		$\frac{\bar{w}^{N-2}(\bar{w}^N+N-1)}{(1-\bar{w}^N)^2}$	$\frac{N\bar{w}^{N-2}(\bar{w}^N(N+1)+(N-1))}{(1-\bar{w}^N)^3}$
$s=3$			$\frac{\bar{w}^{N-3}[\bar{w}^N(2\bar{w}^N+(N+4)(N-1))+(N-1)(N-2)]}{(1-\bar{w}^N)^3}$

Table 3.3: A Table of $\Sigma_q(s)$ on the splay base point.

The lower-bound of the summation over k depends on s: When $s=0$, k should start from 0; otherwise k runs from 1 as long as $N \geq \max(s) = q$. For example,

$$\Sigma_1(0) = \sum_{k=0}^{\infty} \bar{w}^{kN},\ \Sigma_1(1) = \sum_{k=1}^{\infty} \bar{w}^{kN-1};$$
$$\Sigma_2(0) = \sum_{k=0}^{\infty} (kN+1)\bar{w}^{kN},\ \Sigma_2(1) = \sum_{k=1}^{\infty} kN\bar{w}^{kN-1},\ \Sigma_2(2) = \sum_{k=1}^{\infty} (kN-1)\bar{w}^{kN-2};$$
$$\Sigma_3(0) = \sum_{k=0}^{\infty} (kN+1)(kN+2)\bar{w}^{kN},\ \Sigma_3(1) = \sum_{k=1}^{\infty} kN(kN+1)\bar{w}^{kN-1},$$
$$\Sigma_3(2) = \sum_{k=1}^{\infty} kN(kN-1)\bar{w}^{kN-2},\ \Sigma_3(3) = \sum_{k=1}^{\infty} (kN-2)(kN-1)\bar{w}^{kN-3}.$$

Results of these summations are listed in Table 3.3.

Then the q-th moment can be written as a weighted sum of $\Sigma_q(s)$. The lowest three cases are listed below

$$q=1:\ Z_1(M_w\tilde{p}) = \Sigma_1(1) - w\Sigma_1(0);$$
$$q=2:\ Z_2(M_w\tilde{p}) = \Sigma_2(2) - 2w\Sigma_2(1) + w^2\Sigma_2(0);$$
$$q=3:\ Z_3(M_w\tilde{p}) = \frac{1}{2}(\Sigma_3(3) - 3w\Sigma_3(2) - 3w^2\Sigma_3(1) + \Sigma_3(0)).$$

3.1.2.2 Zeros of Z_3 moment at splay base point

Now we can examine the zeros of $Z_3(M_w\tilde{p})$. Using the above formula,

$$Z_3(M_w\tilde{p}) = \frac{f_3(w,\bar{w})}{2(1-\bar{w}^N)^3}, \tag{3.11}$$

where the numerator is a polynomial of w and $\bar{w}$,

$$\begin{aligned} f_3(w,\bar{w}) = &(N-1)(N-2)(\bar{w}^{N-3} - \bar{w}^{2N}w^3) + (N+4)(N-1)(\bar{w}^{2N-3} - \bar{w}^N w^3) \\ &+ 3N(N-1)(\bar{w}^{2N-1}w^2 - \bar{w}^{N-2}w) + 3N(N+1)(w^{N-1}w^2 - \bar{w}^{2N-2}w) \\ &+ 2(\bar{w}^{3N-3} - w^3). \end{aligned} \tag{3.12}$$

Let $w = re^{i\phi}$, then f_3 becomes

$$\begin{aligned} f_3(r,\phi) = e^{-i(2N-3)\phi}[&-(N-1)(N-2)r^{2N+3} + 3N(N-1)r^{2N+1} \\ &- 3N(N+1)r^{2N-1} + (N+4)(N-1)r^{2N-3}] \\ + e^{-i(N-3)\phi}[&-(N+4)(N-1)r^{N+3} + 3N(N+1)r^{N+1} \\ &- 3N(N-1)r^{N-1} + (N-1)(N-2)r^{N-3}] \\ + 2e^{-i3(N-1)\phi}&r^{3N-3} - 2e^{i3\phi}r^3. \end{aligned}$$

Splitting f_3 into the real and the imaginary parts, and solving $f_3 = \mathrm{Re}f_3 + \mathrm{iIm}f_3 = 0$,

$$\begin{aligned} 0 &= P_1(r)\cos[(2N-3)\phi] + P_2(r)\cos[(N-3)\phi] \\ &\quad + 2r^{3N-3}\cos[3(N-1)\phi] - 2r^3\cos(3\phi), \\ 0 &= P_1(r)\sin[(2N-3)\phi] + P_2(r)\sin[(N-3)\phi] \\ &\quad + 2r^{3N-3}\sin[3(N-1)\phi] + 2r^3\sin(3\phi), \end{aligned}$$

N	r	N	r
3	1 $-1+2\cos\left(\frac{2\pi}{9}\right) \approx 0.532089$ $-\cos\left(\frac{\pi}{9}\right)+\sqrt{3}\sin\left(\frac{\pi}{9}\right) \approx -0.347296$ $-1+2\sin\left(\frac{\pi}{18}\right) \approx -0.652704$	7	1 0.62273 0.0679779 0
4	± 1 $\pm\frac{1}{\sqrt{3}} \approx 0.57735$ 0	8	± 1 ± 0.615633 ± 0.248274 0
5	1 0.603593 0	9	1 0.577835 0.438031 0
6	± 1 $\pm\frac{\sqrt{5}-1}{2} \approx 0.618034$ 0	≥ 10	$0,\ \pm 1$

Table 3.4: Zeros of Z_3 on the real axis ($\phi = 0$).

where the polynomials in r are defined as

$$\begin{aligned}
P_1(r) &= -(N-1)(N-2)r^{2N+3} + 3N(N-1)r^{2N+1} \\
&\quad - 3N(N+1)r^{2N-1} + (N+4)(N-1)r^{2N-3}, \\
P_2(r) &= -(N+4)(N-1)r^{N+3} + 3N(N+1)r^{N+1} \\
&\quad - 3N(N-1)r^{N-1} + (N-1)(N-2)r^{N-3}.
\end{aligned}$$

Observing that all zeros are on symmetric axis $\phi_n = \frac{n\pi}{N}$, $n = 0, \ldots, N-1$, we only need to examine $\phi_0 = 0$ and $\phi_1 = \frac{\pi}{N}$ due to the rotational symmetry. Results for locations of zeros are listed in Table 3.4 and Table 3.5. For $N \geq 10$, there are only zeros at 0 or ± 1.

N	r	N	r
3	$1-2\sin\left(\frac{\pi}{18}\right) \approx 0.652704$ $\cos\left(\frac{\pi}{9}\right)-\sqrt{3}\sin\left(\frac{\pi}{9}\right) \approx 0.347296$ $1-2\cos\left(\frac{2\pi}{9}\right) \approx -0.532089$ -1	7	0 -0.0679779 -0.62273 -1
4	$\pm\sqrt{\frac{1}{3}(4-\sqrt{7})} \approx \pm 0.671875$ $\pm\sqrt{2-\sqrt{3}} \approx \pm 0.517638$ 0	8	0
5	0 -0.603593 -1	9	0 -0.438031 -0.577835 -1
6	0	≥ 10	$0, \pm 1$

Table 3.5: Zeros of Z_3 on the first symmetry axis ($\phi = \pi/N$).

3.2 Geometry of Reduced Group Orbits

3.2.1 Poincaré Disk

For phase models, the base point $p = (\beta_1, \ldots, \beta_N)$ is identified with $e^{ic}p$ where c is a constant angle. This symmetry makes the state space topologically equivalent to T^{N-1}. Then the reduced G-orbit $\widetilde{Gp}$ is a two dimensional subspace in T^{N-1} formed by actions of Möbius transformations on a base point p. There are $N-2$ constants of motion and the flow in $\widetilde{Gp}$ is characterized by $\dot{w}$ ($\dot{\zeta}$ becomes irrelevant), $\dot{w} = -\frac{1}{2}(1-|w|^2)\mathcal{A}(M_w p)$, which is a vector field in the unit disk $\Delta = \{|w| < 1\}$.

The factor $(1-|w|^2)$ in $\dot{w}$ implies that the flow vanishes as w approaches the unit circle $|w| = 1$. It stems from the invariant differential of Möbius transformations on points in the unit disk (see Chapter 2). This factor naturally shows up in the metric of Poincaré disk model for $2D$ hyperbolic geometry. To further explore this correspondence between the reduced G-orbit $\widetilde{Gp}$ and the Poincaré disk Δ, we need to briefly review some basic facts about hyperbolic geometry.

3.2.1.1 Metrics and isometries

Isometries are transformations that keep the distance function (a metric) in a space invariant. In $2D$ Euclidean space $\mathbb{R}^2$, for example, the distance between two points $r_i = (x_i, y_i)$ with $i = 1, 2$ is defined through Pythagorean theorem,

$$d(r_1, r_2) = \sqrt{(\Delta x)^2 + (\Delta y)^2} = \sqrt{(x_1 - x_2)^2 + (y_1 - y_2)^2}.$$

Using complex variables $w = x + iy$, the metric can be expressed as

$$ds = |dw| = |dx + idy| = \sqrt{dx^2 + dy^2}, \tag{3.13}$$

which is invariant under translations, rotations and reflections with respect to an axis. These transformations are isometries of $\mathbb{R}^2$ and form a group.

Likewise, Möbius transformations $M \in G$ are orientation-preserving isometries on the unit disk with hyperbolic metric

$$ds = \frac{2\,|dw|}{1 - |w|^2} = \lambda(w)\,|dw|\,, \quad \lambda(w) = \frac{2}{1 - |w|^2}, \tag{3.14}$$

where the multiplier $\lambda(w)$ is a geometric factor that captures the "deformation" from the Euclidean metric.

We have shown (in Chapter 2) that base points p and p' related by a Möbius transformation in a reduced G-orbit corresponds to coordinates w and w' in the unit disk, also related by the same Möbius transformation. Changing base points in $\widetilde{Gp}$ amounts to applying Möbius transformations on Δ, which does not change the metric. Therefore, the hyperbolic metric is intrinsic on the unit disk, independent of the choice of base points in a given reduced G-orbit. Since there is a one-to-one correspondence between $\widetilde{Gp}$ and Δ,

Figure 3.4: Escher's woodcut "Circle Limit I" as an illustration for the Poincaré disk (From `https://www.wikiart.org/`). The metric gets distorted so that all the birds and fish have the same size and shape. Points on the boundary are infinitely far away. They connected by geodesics along spines of birds and fish.

we can transfer this natural metric from the unit disk to the reduced G-orbit, and make an identification between these two spaces.

3.2.1.2 Geodesics and vector fields

Geodesics on the Poincaré disk are lines or circular arcs that are perpendicular to the boundary. A vivid illustration is the woodcut "Circle Limit I " by M. C. Escher (see Figure 3.4). In a finite disk, the artist masterfully presented infinite numbers of equally-shaped and sized (under the hyperbolic metric) birds and fish, whose spines are geodesics connecting two points on the boundary.

In our case, there is an intriguing connection between the geodesics through a point $w \in \Delta$ and the vector field $\dot{w}$ for Z_1 phase model. It can be shown that there exists a unique geodesic connecting a point $w \in \Delta$ to any point on S^1, which gives a unit vector at w tangential to the geodesic. $\dot{w}$ is the average of unit vectors pointing to each β_j.

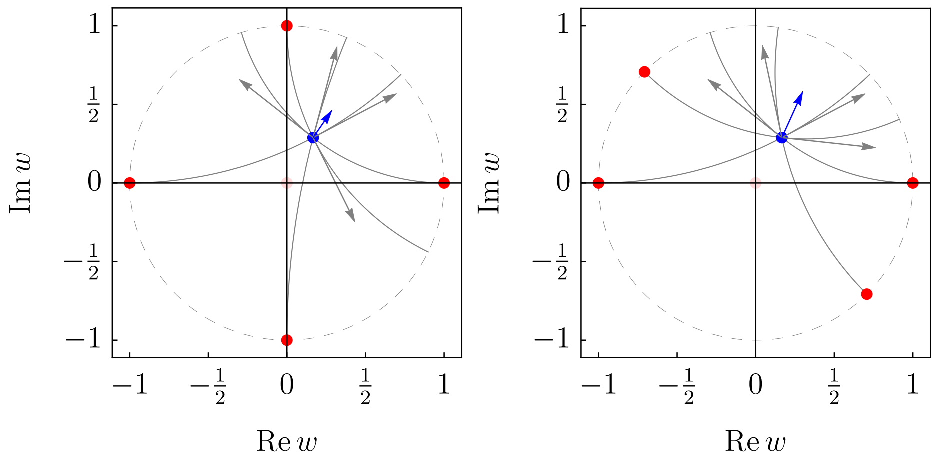

Figure 3.5: Plot of geodesics for Z_1 model on two different base points.

3.2.2 Gradient Condition

3.2.2.1 Hyperbolic gradient operator

We have discussed the vector field $\dot{w}$ on the unit disk and seen several explicit examples for phase models in previous sections. Now with the metric function defined on Δ, we may ask: When is the vector field $\dot{w}$ a gradient flow? Namely, there exists a potential function h whose gradient gives the flow, $\dot{w} = \nabla h$. To answer this question, we need to derive a gradient operator ∇_{hyp} that is compatible with the hyperbolic metric.

Using $w = x + iy \in \Delta$, then $x = (w + \bar{w})/2$, $y = (w - \bar{w})/2i$, the partial derivatives of any smooth function h on Δ can be expressed in terms of w and $\bar{w}$,

$$\frac{\partial h}{\partial w} = \frac{\partial h}{\partial x}\frac{\partial x}{\partial w} + \frac{\partial h}{\partial y}\frac{\partial y}{\partial w} = \frac{1}{2}\left(\frac{\partial}{\partial x} - i\frac{\partial}{\partial y}\right)h,$$
$$\frac{\partial h}{\partial \bar{w}} = \frac{\partial h}{\partial x}\frac{\partial x}{\partial \bar{w}} + \frac{\partial h}{\partial y}\frac{\partial y}{\partial \bar{w}} = \frac{1}{2}\left(\frac{\partial}{\partial x} + i\frac{\partial}{\partial y}\right)h.$$

So the ordinary gradient (with respect to Euclidean metric $ds = |dw|$) can be written as

(using complex notation)

$$\nabla_{euc} h = \left(\frac{\partial h}{\partial x}, \frac{\partial h}{\partial y}\right) = \frac{\partial h}{\partial x} + i\frac{\partial h}{\partial y} = 2\frac{\partial h}{\partial \bar{w}}. \tag{3.15}$$

With the hyperbolic metric, $ds = \lambda(w)\,|dw|$, $\lambda(w) = \frac{2}{1-|w|^2}$, the gradient operator becomes

$$\nabla_{hyp} = \lambda^{-2}(w)\nabla_{euc} = 2\lambda^{-2}\frac{\partial}{\partial \bar{w}} = \frac{1}{2}(1-|w|^2)^2\frac{\partial}{\partial \bar{w}}. \tag{3.16}$$

3.2.2.2 Condition for gradient flows

For a dynamical system on Δ, $\dot{w} = f(w) = f(x+iy) = u(x,y) + iv(x,y)$ where u and v are real functions, the gradient condition in the Euclidean metric is just

$$\dot{w} = \dot{x} + i\dot{y} = \frac{\partial h}{\partial x} + i\frac{\partial h}{\partial y} = \nabla_{euc} h = 2\frac{\partial h}{\partial \bar{w}} \Leftrightarrow$$

$$\begin{pmatrix} \dot{x} \\ \dot{y} \end{pmatrix} = \begin{pmatrix} u \\ v \end{pmatrix} = \begin{pmatrix} \partial_x h \\ \partial_y h \end{pmatrix} \Rightarrow \begin{cases} \partial_x u + \partial_y v = (\partial_x^2 + \partial_y^2)h = \nabla^2 h \\ \partial_y u - \partial_x v = (\partial_{yx}^2 - \partial_{xy}^2)h = 0 \end{cases}$$

for some real potential function $h(x,y)$. Notice that

$$\frac{\partial f}{\partial w} = \frac{1}{2}\left(\frac{\partial}{\partial x} - i\frac{\partial}{\partial y}\right)(u+iv) = \frac{1}{2}\left[\frac{\partial u}{\partial x} + \frac{\partial v}{\partial y} + i\left(\frac{\partial v}{\partial x} - \frac{\partial u}{\partial y}\right)\right],$$
$$\frac{\partial f}{\partial \bar{w}} = \frac{1}{2}\left(\frac{\partial}{\partial x} + i\frac{\partial}{\partial y}\right)(u+iv) = \frac{1}{2}\left[\frac{\partial u}{\partial x} - \frac{\partial v}{\partial y} + i\left(\frac{\partial v}{\partial x} + \frac{\partial u}{\partial y}\right)\right],$$

then the gradient condition implies $\mathrm{Im}(\partial_w f) = 0$. Since $\dot{w} = f = 2\partial_{\bar{w}} h$, this is equivalent to $\mathrm{Im}(\partial_w \partial_{\bar{w}} h = 0)$.

Likewise, with the hyperbolic metric multiplier $\lambda = \frac{2}{1-|w|^2}$, a gradient system satisfies

$$\dot{w} = \dot{x} + i\dot{y} = \nabla_{hyp} h = \lambda^{-2}\nabla_{euc} h = \lambda^{-2}(x,y)\left(\frac{\partial h}{\partial x} + i\frac{\partial h}{\partial y}\right)$$

$$\begin{pmatrix} \dot{x} \\ \dot{y} \end{pmatrix} = \begin{pmatrix} u \\ v \end{pmatrix} = \begin{pmatrix} \lambda^{-2}\partial_x h \\ \lambda^{-2}\partial_y h \end{pmatrix}$$

$$\Rightarrow \begin{cases} \partial_x u + \partial_y v = -2\lambda^{-3}(\partial_x\lambda\partial_x h + \partial_y\lambda\partial_y h) + \lambda^{-2}(\partial_x^2 + \partial_y^2)h \\ \partial_y u - \partial_x v = -2\lambda^{-3}(\partial_y\lambda\partial_x h - \partial_x\lambda\partial_y h) \end{cases} .$$

If we look at the partial derivative

$$\begin{aligned} \frac{\partial}{\partial w}(\lambda^2 f) &= \frac{1}{2}\left(\frac{\partial}{\partial x} - i\frac{\partial}{\partial y}\right)(\lambda^2 u + i\lambda^2 v) \\ &= \frac{1}{2}\left[\frac{\partial(\lambda^2 u)}{\partial x} + \frac{\partial(\lambda^2 v)}{\partial y} + i\left(\frac{\partial(\lambda^2 v)}{\partial x} - \frac{\partial(\lambda^2 u)}{\partial y}\right)\right] \\ &= \frac{1}{2}\left\{2\lambda\left(\frac{\partial\lambda}{\partial x}u + \frac{\partial\lambda}{\partial y}v\right) + \lambda^2\left(\frac{\partial u}{\partial x} + \frac{\partial v}{\partial y}\right)\right. \\ &\quad \left. +i\left[2\lambda\left(\frac{\partial\lambda}{\partial x}v - \frac{\partial\lambda}{\partial y}u\right) + \lambda^2\left(\frac{\partial v}{\partial x} - \frac{\partial u}{\partial y}\right)\right]\right\}, \end{aligned}$$

its imaginary part would vanish when the flow $f = u + iv$ is a gradient of a potential h with $u = \partial_x h$ and $v = \partial_y h$,

$$\begin{aligned} \mathrm{Im}\frac{\partial(\lambda^2 f)}{\partial w} &= 2\lambda\left(\frac{\partial\lambda}{\partial x}v - \frac{\partial\lambda}{\partial y}u\right) + \lambda^2\left(\frac{\partial v}{\partial x} - \frac{\partial u}{\partial y}\right) \\ &= 2\lambda(\partial_x\lambda\partial_y h - \partial_y\lambda\partial_x h) + \lambda^2[2\lambda^{-3}(\partial_y\lambda\partial_x h - \partial_x\lambda\partial_y h)] = 0. \end{aligned}$$

Similarly, since $\dot{w} = f = 2\lambda^{-2}\partial_{\bar{w}} h$, this condition implies

$$\mathrm{Im}\frac{\partial^2 h}{\partial w\partial\bar{w}} = 0. \tag{3.17}$$

3.2.2.3 Gradient condition for phase models

For phase models, the flow in the unit disk is

$$\dot{w} = f(w) = -\frac{1}{2}(1-|w|^2)a(M_w p) = -\lambda^{-1}a(M_w p).$$

The hyperbolic gradient condition is

$$\mathrm{Im}\frac{\partial(\lambda^2 f)}{\partial w} = \mathrm{Im}\frac{\partial(\lambda a(M_w p))}{\partial w} = \mathrm{Im}\left[\frac{\partial \lambda}{\partial w}a(M_w p) + \lambda\frac{\partial a(M_w p)}{\partial w}\right] = 0.$$

Calculating directly, the derivatives yield

$$\begin{aligned}
\frac{\partial \lambda}{\partial w} &= \frac{\partial}{\partial w}\frac{2}{1-|w|^2} = \frac{2\bar{w}}{(1-|w|^2)^2} \\
\frac{\partial a(M_w p)}{\partial w} &= \sum_{j=1}^{N}\frac{\partial a(z)}{\partial z_j}\frac{\partial z_j}{\partial w} = \sum_j \frac{\partial a(z)}{\partial z_j}\frac{z_j}{w-\beta_j}, \\
\frac{\partial \lambda}{\partial w}a(z) + \lambda\frac{\partial a(z)}{\partial w} &= \frac{2\bar{w}}{(1-|w|^2)^2}a(z) + \frac{2}{1-|w|^2}\sum_j \frac{\partial a(z)}{\partial z_j}\frac{z_j}{w-\beta_j} \\
&= \frac{2}{1-|w|^2}\sum_j\left(\frac{\bar{w}z_j}{1-|w|^2}\frac{\partial a(z)}{\partial z_j} + \frac{\partial a(z)}{\partial z_j}\frac{z_j}{w-\beta_j}\right) \\
&= \frac{2}{1-|w|^2}\sum_j z_j\frac{\partial a(z)}{\partial z_j}\frac{1-\bar{w}\beta_j}{(1-w\bar{w})(w-\beta_j)} \\
&= -\frac{2}{(1-|w|^2)^2}\sum_j \frac{\partial a}{\partial z_j},
\end{aligned}$$

where we have used

$$z_j = M_w\beta_j = \frac{\beta_j - w}{1-\bar{w}\beta_j},\ \frac{\partial z_j}{\partial w} = -\frac{1}{1-\bar{w}\beta_j} = \frac{z_j}{w-\beta_j},$$

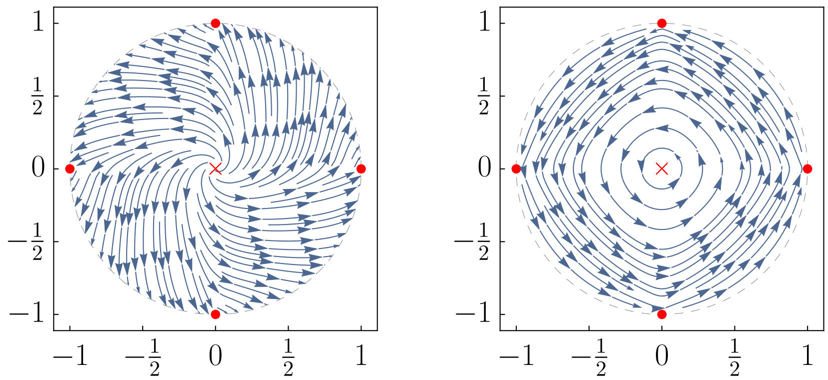

Figure 3.6: Applying global rotations to $\dot{w}$ flow for Z_1 model on the splay base point with $N = 4$. Left panel: Spirals with $\alpha = \pi/4$; Right panel: Closed orbits with $\alpha = \pi/2$.

and Euler's theorem for homogeneous functions

$$\sum_j z_j \frac{\partial a(z)}{\partial z_j} = a(z).$$

Then the gradient condition is essentially

$$\text{Im} \sum_j \frac{\partial a}{\partial z_j} \equiv \text{Im}\mathcal{D}a = 0, \tag{3.18}$$

where $\mathcal{D} = \sum_j \partial_{z_j}$ is a differential operator acting on the order parameter a. In other words, if a satisfies this condition, the flow of $\dot{w}$ can be written as the gradient of a real function. We will denote this function as a potential Φ with $\dot{w} = \nabla_{hyp}\Phi$.

3.2.2.4 Gradient vs. Hamiltonian

If we apply a global rotation $e^{i\alpha}$ to a gradient vector field $\dot{w} = \nabla_{hyp}\Phi$, then it becomes $\dot{w} = e^{i\alpha}\nabla_{hyp}\Phi$, which is clearly not gradient unless $e^{i\alpha} = \pm 1$. Figure 3.6 shows $\dot{w}$ flows under two global rotations of $\pi/4$ and $\pi/2$, which lead to spirals and closed orbits.

For phase models, rotating the vector field is equivalent as rotating a,

$$\dot{w} = e^{i\alpha}\nabla_{hyp}\Phi = -\frac{1}{2}e^{i\alpha}(1-|w|^2)a(M_w p).$$

The gradient condition ($\mathrm{Im}(\mathcal{D}a) = 0 \Leftrightarrow \mathcal{D}a \in \mathbb{R}$) gives

$$\mathrm{Im}\mathcal{D}(e^{i\alpha}a) = \mathrm{Im}(e^{i\alpha}\mathcal{D}a) = \sin\alpha\mathcal{D}a,$$

which is zero only when $\alpha = k\pi$, $k \in \mathbb{N}$. So when $\alpha \neq k\pi$, the rotated phase model is not a gradient flow.

However, when $\alpha = \pm\frac{\pi}{2}$ ($e^{i\alpha} = \pm i$), $\dot{w} = \pm\nabla_{hyp}(i\Phi)$. Taking the complex conjugate and using the metric factor $\lambda = 2(1-|w|^2)^{-1}$, we have

$$\dot{w} = \pm\frac{1}{2}(1-|w|^2)^2\frac{\partial(i\Phi)}{\partial\bar{w}} = 2\lambda^{-2}\frac{\partial(\pm i\Phi)}{\partial\bar{w}}, \tag{3.19}$$

$$\dot{\bar{w}} = \mp\frac{1}{2}(1-|w|^2)^2\frac{\partial(i\Phi)}{\partial w} = -2\lambda^{-2}\frac{\partial(\pm i\Phi)}{\partial w}, \tag{3.20}$$

which remind us of the Hamilton equations, $\dot{q} = \frac{\partial H}{\partial p}$, $\dot{p} = -\frac{\partial H}{\partial q}$. This analogy can be made precise if we introduce a transformation from $(w,\bar{w})$ to (q,p),

$$q = Q(w,\bar{w}), \quad \frac{\partial}{\partial w} = \frac{\partial Q}{\partial w}\frac{\partial}{\partial q} + \frac{\partial P}{\partial w}\frac{\partial}{\partial p}, \tag{3.21}$$

$$p = P(w,\bar{w}), \quad \frac{\partial}{\partial\bar{w}} = \frac{\partial Q}{\partial\bar{w}}\frac{\partial}{\partial q} + \frac{\partial P}{\partial\bar{w}}\frac{\partial}{\partial p}, \tag{3.22}$$

and identify $H = \pm i\Phi$ such that

$$\dot{q} = \frac{\partial Q}{\partial w}\dot{w} + \frac{\partial Q}{\partial\bar{w}}\dot{\bar{w}} = 2\lambda^{-2}\left(\frac{\partial Q}{\partial w}\frac{\partial}{\partial\bar{w}} - \frac{\partial Q}{\partial\bar{w}}\frac{\partial}{\partial w}\right)(\pm i\Phi) = \frac{\partial H}{\partial p},$$
$$\dot{p} = \frac{\partial P}{\partial w}\dot{w} + \frac{\partial P}{\partial\bar{w}}\dot{\bar{w}} = -2\lambda^{-2}\left(\frac{\partial P}{\partial\bar{w}}\frac{\partial}{\partial w} - \frac{\partial P}{\partial w}\frac{\partial}{\partial\bar{w}}\right)(\pm i\Phi) = -\frac{\partial H}{\partial q}.$$

This implies

$$\frac{\partial}{\partial p} = 2\lambda^{-2}\left(\frac{\partial Q}{\partial w}\frac{\partial}{\partial \bar{w}} - \frac{\partial Q}{\partial \bar{w}}\frac{\partial}{\partial w}\right), \quad \frac{\partial}{\partial q} = 2\lambda^{-2}\left(\frac{\partial P}{\partial \bar{w}}\frac{\partial}{\partial w} - \frac{\partial P}{\partial w}\frac{\partial}{\partial \bar{w}}\right).$$

Using the relation between $(\partial_w, \partial_{\bar{w}})$ and (∂_q, ∂_p),

$$\begin{aligned}
\frac{\partial}{\partial w} &= 2\lambda^{-2}\frac{\partial Q}{\partial w}\left(\frac{\partial P}{\partial \bar{w}}\frac{\partial}{\partial w} - \frac{\partial P}{\partial w}\frac{\partial}{\partial \bar{w}}\right) + 2\lambda^{-2}\frac{\partial P}{\partial w}\left(\frac{\partial Q}{\partial w}\frac{\partial}{\partial \bar{w}} - \frac{\partial Q}{\partial \bar{w}}\frac{\partial}{\partial w}\right) \\
&= 2\lambda^{-2}\left(\frac{\partial Q}{\partial w}\frac{\partial P}{\partial \bar{w}} - \frac{\partial P}{\partial w}\frac{\partial Q}{\partial \bar{w}}\right)\frac{\partial}{\partial w} + 2\lambda^{-2}\left(\frac{\partial Q}{\partial w}\frac{\partial P}{\partial w} - \frac{\partial P}{\partial w}\frac{\partial Q}{\partial w}\right)\frac{\partial}{\partial \bar{w}}, \\
\frac{\partial}{\partial \bar{w}} &= 2\lambda^{-2}\frac{\partial Q}{\partial \bar{w}}\left(\frac{\partial P}{\partial \bar{w}}\frac{\partial}{\partial w} - \frac{\partial P}{\partial w}\frac{\partial}{\partial \bar{w}}\right) + 2\lambda^{-2}\frac{\partial P}{\partial \bar{w}}\left(\frac{\partial Q}{\partial w}\frac{\partial}{\partial \bar{w}} - \frac{\partial Q}{\partial \bar{w}}\frac{\partial}{\partial w}\right) \\
&= 2\lambda^{-2}\left(\frac{\partial Q}{\partial \bar{w}}\frac{\partial P}{\partial \bar{w}} - \frac{\partial P}{\partial \bar{w}}\frac{\partial Q}{\partial \bar{w}}\right)\frac{\partial}{\partial w} + 2\lambda^{-2}\left(\frac{\partial P}{\partial \bar{w}}\frac{\partial Q}{\partial w} - \frac{\partial Q}{\partial \bar{w}}\frac{\partial P}{\partial w}\right)\frac{\partial}{\partial \bar{w}},
\end{aligned}$$

we obtain a constraint on the transformations Q and P,

$$\frac{\partial Q}{\partial w}\frac{\partial P}{\partial \bar{w}} - \frac{\partial P}{\partial w}\frac{\partial Q}{\partial \bar{w}} \equiv \{Q, P\}_{(w,\bar{w})} = \frac{\lambda^2}{2} = \frac{2}{(1 - w\bar{w})^2}, \tag{3.23}$$

where $\{\dots\}_{(w,\bar{w})}$ is the Poisson bracket with respect to w and $\bar{w}$. The transformed variables q and p then satisfy Hamilton's equation and the Poisson algebra,

$$\begin{aligned}
\{q, p\}_{(q,p)} &= \frac{\partial q}{\partial q}\frac{\partial p}{\partial p} - \frac{\partial p}{\partial q}\frac{\partial q}{\partial p} \\
&= \left(2\lambda^{-2}\right)^2\left(\frac{\partial P}{\partial \bar{w}}\frac{\partial Q}{\partial w} - \frac{\partial P}{\partial w}\frac{\partial Q}{\partial \bar{w}}\right)^2 \\
&\quad - \left(2\lambda^{-2}\right)^2\left(\frac{\partial P}{\partial \bar{w}}\frac{\partial P}{\partial w} - \frac{\partial P}{\partial w}\frac{\partial P}{\partial \bar{w}}\right)\left(\frac{\partial Q}{\partial w}\frac{\partial Q}{\partial \bar{w}} - \frac{\partial Q}{\partial \bar{w}}\frac{\partial Q}{\partial w}\right) = 1.
\end{aligned} \tag{3.24}$$

In other words, if we can find such transformations Q and P, then q and p can be thought of as the canonical coordinate and momentum.

It is straightforward to verify the following choice

$$q = Q(w, \bar{w}) = \frac{1}{2}\ln\frac{w}{\bar{w}}, \qquad p = P(w, \bar{w}) = \frac{1 + w\bar{w}}{1 - w\bar{w}}, \tag{3.25}$$

$$w = \pm e^{q}\sqrt{\frac{p-1}{p+1}}, \qquad \bar{w} = \pm e^{-q}\sqrt{\frac{p-1}{p+1}}, \tag{3.26}$$

satisfies the Poisson bracket relation, Eq. (3.23):

$$\{Q, P\}_{(w,\bar{w})} = \frac{1}{2w}\frac{2w}{(1-w\bar{w})^2} - \frac{2\bar{w}}{(1-w\bar{w})^2}\frac{-1}{2\bar{w}} = \frac{2}{(1-w\bar{w})^2}.$$

Therefore the $\dot{w}$ flow can be described by a Hamiltonian function $H = \pm i\Phi$ and a set of canonically conjugate variables (q, p). Clearly the Hamiltonian itself is a constant of motion, $\dot{H} = \{H, H\}_{(q,p)} = 0$. So this $2D$ system is completely integrable: All trajectories $(q(t), p(t))$ lie on levels curves of H.

In sum, when $e^{i\alpha} = \pm 1$, the system is a gradient flow with $\pm\Phi$ being the potential. When $e^{i\alpha} = \pm i$, the system is a Hamiltonian flow with $H = \pm i\Phi$ being the Hamiltonian. [1]

3.2.2.5 Classes of gradient phase models

Revisiting the WS theory (Z_1 model) from a geometric perspective yields new insights:

- Existence of low-dimensional dynamics on a $2D$ manifold with a hyperbolic metric.
- The Z_1 (iZ_1) model is a gradient (Hamiltonian) flow
- For phase models, the gradient condition is equivalent to an analytic constraint on the order parameter, $\mathrm{Im}\mathcal{D}a = 0$.

[1] Despite its appearance, the Hamiltonian $H = i\Phi$ is a real function because the canonical coordinate q is purely imaginary. If we put the imaginary unit i into q and define $q = -i\ln(w\bar{w}^{-1})^{1/2} = \arg(w)$ as the angular variable, then both q and p are real. The canonical equations become $\dot{q} = \partial_p\Phi$, and $\dot{p} = -\partial_q\Phi$.

The differential operator $\mathcal{D}$ acts on functional spaces of Z_n moments. It links the geometry of a dynamical system with algebra. This condition also provides us an operational criteria for finding new gradient models, since it acts on Z_n like an ordinary differential,

$$\mathcal{D}Z_n = nZ_{n-1}, \quad \mathcal{D}(Z_n Z_m) = nZ_{n-1}Z_m + mZ_n Z_{m-1}, \quad n.m \in \mathbb{N}. \tag{3.27}$$

With it, we can find new classes of models that are also gradient. The first a few examples contain double, triple, and quadruple products of moments,

$$\mathcal{D}_n = Z_n Z_{1-n}, \tag{3.28}$$

$$\mathcal{T}_n = Z_{1+2n}Z_{-n}^2 - Z_{1-2n}Z_n^2 + Z_{1+n}Z_n Z_{-2n} - Z_{1-n}Z_{-n}Z_{2n}, \tag{3.29}$$

$$\mathcal{Q}_n = (Z_{1+n}Z_{-n} - Z_{1-n}Z_n)|Z_n|^2. \tag{3.30}$$

It is straightforward to verify:

$$\begin{aligned}
\mathcal{D}(Z_n Z_{1-n}) &= nZ_{n-1}Z_{1-n} - (n-1)Z_n Z_{-n} = n|Z_{n-1}|^2 - (n-1)|Z_n|^2 \in \mathbb{R}, \\
\mathcal{D}(\mathcal{T}_n) &= 3n(Z_{2n}Z_{-n}^2 + Z_{-2n}Z_n^2) - 2n(Z_{n+1}Z_n Z_{-2n-1} + Z_{-n-1}Z_{-n}Z_{2n+1}) \\
&\quad - 2n(Z_n Z_{n-1}Z_{1-2n} + Z_{-n}Z_{1-n}Z_{2n-1}) \\
&\quad + n(Z_{n+1}Z_{n-1}Z_{-2n} + Z_{-n-1}Z_{1-n}Z_{2n}) \in \mathbb{R}, \\
\mathcal{D}(\mathcal{Q}_n) &= 2n|Z_n|^4 - 2n(|Z_{n+1}|^2 + |Z_{n-1}|^2)|Z_n|^2 \\
&\quad + n(Z_{n+1}Z_{n-1}Z_{-n}^2 + Z_{-n-1}Z_{1-n}Z_n^2) \in \mathbb{R}.
\end{aligned}$$

For example, the double product $\mathcal{D}_n = Z_n Z_{1-n}$ involves higher-order harmonics coupling,

$$\begin{aligned}\dot{\theta}_j = \frac{\dot{z}_j}{iz_j} = \mathrm{Im}(\mathcal{a}\bar{z}_j) = \mathrm{Im}\frac{1}{N^2}\sum_{k,\,l=1}^{N} z_k^n z_l^{1-n} z_j^{-1} = \frac{1}{N^2}\sum_{k,\,l}\mathrm{Im}e^{i(n\theta_l+(1-n)\theta_k-\theta_j)} \\ = \frac{1}{N^2}\sum_{k,\,l=1}^{N}\sin(n\theta_k+(1-n)\theta_l-\theta_j). \qquad (3.31)\end{aligned}$$

More importantly, these models are all gradient flows, which means that they have similar "nice" properties as the Z_1 model: The existence of potential functions and constants of motion, and integrability and Hamiltonian dynamics upon $\frac{\pi}{2}$-rotations, etc. In short, simply by applying the gradient condition $\mathrm{Im}\mathcal{D}\mathcal{a} = 0$, we have a much richer family of coupled oscillator systems that are reducible to low-dimensional dynamics.

3.3 Potentials for Phase Models

In the previous section, we showed that if the order parameter of a phase model satisfies $\mathrm{Im}\mathcal{D}\mathcal{a} = 0$, then the flow can be written as a hyperbolic gradient of a real potential,

$$\dot{w} = -\frac{1}{2}(1-|w|^2)\mathcal{a}(M_w p) = \nabla_{hyp}\Phi = \frac{1}{2}(1-|w|^2)^2\frac{\partial\Phi}{\partial\bar{w}}. \qquad (3.32)$$

For instance, moment-models like Z_1 and $Z_q Z_{1-q}$ satisfy the gradient condition. So they can be described by potential functions.

To find the potential, notice that it is related to $\mathcal{a}$ in Eq. (3.32),

$$\frac{\partial\Phi(w,\bar{w})}{\partial\bar{w}} = -\frac{\mathcal{a}(M_w p)}{1-|w|^2}. \qquad (3.33)$$

Integrating over $\bar{w}$,

$$\Phi(w,\bar{w}) = -\int d\bar{w}\frac{a(M_w p)}{1-w\bar{w}} + f(w) = F(w,\bar{w}) + f(w), \tag{3.34}$$

where the function $f(w)$ is analytic in w. Substituting the above equation into the conjugate for the potential's gradient, and using the fact that Φ is real, $f(w)$ can be found by integrating over w,

$$-\frac{\overline{a(M_w p)}}{1-|w|^2} = \overline{\left(\frac{\partial\Phi}{\partial\bar{w}}\right)} = \frac{\partial\Phi}{\partial w} = \frac{\partial F}{\partial w} + \frac{df}{dw} \Rightarrow f(w) = -\int dw\frac{\overline{a(M_w p)}}{1-|w|^2} - \int dw\frac{\partial F}{\partial w}.$$

Then the potential is given by

$$\Phi(w,\bar{w}) = F(w,\bar{w}) + F^{\dagger}(w,\bar{w}) - \int dw\frac{\partial\bar{F}}{\partial w}, \tag{3.35}$$

$$F(w,\bar{w}) = -\int d\bar{w}\frac{a(M_w p)}{1-w\bar{w}},\ F^{\dagger}(w,\bar{w}) = -\int dw\frac{\overline{a(M_w p)}}{1-|w|^2}. \tag{3.36}$$

3.3.1 Z_1 Model

At a base point $p = (\beta_1,\ldots,\beta_N)$, the order parameter for a gradient Z_1 model is $a(p) = Z_1(p)$. Upon a Möbius transformation on p,

$$a(M_w p) = \frac{1}{N}\sum_{k=1}^{N}\frac{\beta_k - w}{1-\bar{w}\beta_k},$$

we can calculate the integral F

$$F(w,\bar{w}) = -\int d\bar{w}\frac{a(M_w p)}{1-w\bar{w}} = -\frac{1}{N}\sum_k(\beta_k - w)\int \frac{d\bar{w}}{(1-w\bar{w})(1-\beta_k\bar{w})}$$
$$= -\frac{1}{N}\sum_k(\beta_k - w)\left(\frac{a_0}{-w}\ln(1-|w|^2) + \frac{a_1}{-\beta_k}\ln(1-\beta_k\bar{w})\right)$$
$$= -\frac{1}{N}\sum_k \ln\frac{1-|w|^2}{1-\beta_k\bar{w}} \tag{3.37}$$

by partial fractions,

$$\frac{1}{(1-\beta_k\bar{w})(1-w\bar{w})} = \frac{a_0}{1-w\bar{w}} + \frac{a_1}{1-\beta_k\bar{w}}; \quad a_0 = \frac{w}{w-\beta_k},\, a_1 = -\frac{\beta_k}{w-\beta_k}.$$

The conjugate term $F^\dagger$ can be found in a similar way:

$$F^\dagger(w,\bar{w}) = -\int dw\frac{\overline{a(M_w p)}}{1-\bar{w}w}$$
$$= -\frac{1}{N}\sum_k(\bar{\beta}_k - \bar{w})\int\frac{dw}{(1-\bar{w}w)(1-\bar{\beta}_k w)} = -\frac{1}{N}\sum_k \ln\frac{1-|w|^2}{1-\bar{\beta}_k w}.$$

Integrating the derivative $\frac{\partial F}{\partial w}$ over w,

$$\frac{\partial F}{\partial w} = -\frac{1}{N}\sum_k \frac{\partial}{\partial w}\ln\frac{1-\bar{w}w}{1-\beta_k\bar{w}} = -\frac{1}{N}\sum_k\frac{-\bar{w}}{1-\bar{w}w},$$
$$\int dw\frac{\partial F}{\partial w} = -\frac{1}{N}\sum_k\int\frac{-\bar{w}dw}{1-\bar{w}w} = -\frac{1}{N}\sum_k \ln(1-|w|^2),$$

so the potential is

$$\Phi(w,\bar{w}) = -\ln(1-|w|^2) + \frac{1}{N}\sum_k \ln(1-\beta_k\bar{w})(1-\bar{\beta}_k w) \equiv \Phi_0 + \Phi_1. \tag{3.38}$$

Here Φ_1 depends on the configuration of $\{\beta_k\}$, since its argument is the Euclidean distance between β_k and w,

$$\Phi_1 = \frac{1}{N}\sum_k \ln|\beta_k - w|^2, \tag{3.39}$$

which is an analog of the potential for 2D electrostatics, or the potential energy of vortices. The more intriguing part is Φ_0: It is intrinsic to the disk's geometry and it is the potential for the $\dot{w}$ flow as $N \to \infty$,

$$\nabla_{hyp}\Phi_0 = -\frac{1}{2}(1-|w|^2)^2\frac{\partial}{\partial\bar{w}}\ln(1-|w|^2) = \frac{1}{2}(1-|w|^2)w. \tag{3.40}$$

If we denote $\beta_j = e^{i\psi_j}$, $w = re^{i\varphi}$ and $\zeta = e^{i\chi}$, then from the relation between WS variables (γ, Ψ, Θ) and (r, φ, χ):

$$\gamma = \frac{2r}{1+r^2}, \quad \Psi = \varphi, \quad \Theta = \varphi + \chi,$$

the potential Φ is just the $\mathcal{H}$ function defined in WS theory,

$$\begin{aligned}\Phi(w,\bar{w}) &= -\frac{1}{N}\sum_k \ln\frac{1-|w|^2}{(1-\beta_k\bar{w})(1-\bar{\beta}_k w)} = \frac{1}{N}\sum_k \ln\frac{1-2\mathrm{Re}(\beta_k\bar{w})+|w|^2}{1-|w|^2}\\ &= \frac{1}{N}\sum_k \ln\frac{1+r^2-2r\cos(\psi_k-\varphi)}{1-r^2} = \frac{1}{N}\sum_k \ln\frac{1-\frac{2r}{1+r^2}\cos(\psi_k-\varphi)}{\frac{1-r^2}{1+r^2}}\\ &= \frac{1}{N}\sum_k \ln\frac{1-\gamma\cos(\psi_k-\Psi)}{\sqrt{1-\gamma^2}} = \mathcal{H}(\gamma,\Psi).\end{aligned} \tag{3.41}$$

In addition, the canonical coordinate and momentum for the Hamiltonian flow coincide with the ones found by WS,

$$q = -\frac{i}{2}\ln\frac{w}{\bar{w}} = \varphi = \Psi, \quad p = \frac{1+w\bar{w}}{1-w\bar{w}} = \frac{1+r^2}{1-r^2} = \frac{1}{\sqrt{1-\gamma^2}}. \tag{3.42}$$

We can expand the logarithmic function in a power series, $\ln(1-x) = -\sum_{n=1}^{\infty} \frac{x^n}{n}$, so the potential Φ_1 becomes a series of moments,

$$\Phi_1 = \frac{1}{N} \sum_{k=1}^{N} (\ln(1 - \beta_k \bar{w}) + \ln(1 - \bar{\beta}_k w)) = -\sum_{n=1}^{\infty} \left(\frac{\bar{w}^n}{n} Z_n(p) + \frac{w^n}{n} \bar{Z}_n(p) \right).$$

If the base point p has additional symmetry in its configuration, then the summation further simplifies.

Splay base point At the splay base point $\tilde{p} = (\eta, \eta^2, \ldots, \eta^N)$ with $\eta = e^{2\pi i/N}$, $Z_n(\tilde{p}) = \overline{Z_n(\tilde{p})} = \delta_{n,kN}$, $\forall k \in \mathbb{N}$. The series expansion for Φ_1 becomes

$$\begin{aligned}\Phi_1 &= -\frac{1}{N} \sum_{k=1}^{\infty} \left(\frac{\bar{w}^{kN}}{k} + \frac{w^{kN}}{k} \right) \\ &= -\frac{1}{N} (\ln(1 - \bar{w}^N) + \ln(1 - w^N)) = \ln[(1 - \bar{w}^N)^{1/N} (1 - w^N)^{1/N}]. \end{aligned} \tag{3.43}$$

This can be verified by integrating $\partial_{\bar{w}} \Phi = -a(w, \bar{w})(1 - |w|^2)^{-1}$ with the order parameter $a(w, \bar{w}) = Z_1(M_w \tilde{p}) = (\bar{w}^{N-1} - w)(1 - \bar{w}^N)^{-1}$. Thus, the full potential Φ at the splay base point is

$$\Phi = -\ln \frac{1 - |w|^2}{(1 - \bar{w}^N)^{1/N} (1 - w^N)^{1/N}}; \quad \lim_{N \to \infty} \Phi = -\ln(1 - |w|^2), \tag{3.44}$$

as shown in Figure 3.7.

3.3.2 $Z_2 Z_{-1}$ Model

Since the $Z_2 Z_{-1}$ model also satisfies the gradient condition, $\mathcal{D} Z_2 Z_{-1} = 2|Z_1|^2 - |Z_2|^2 \in \mathbb{R}$, there is a potential function whose hyperbolic gradient is the $\dot{w}$ flow. Under

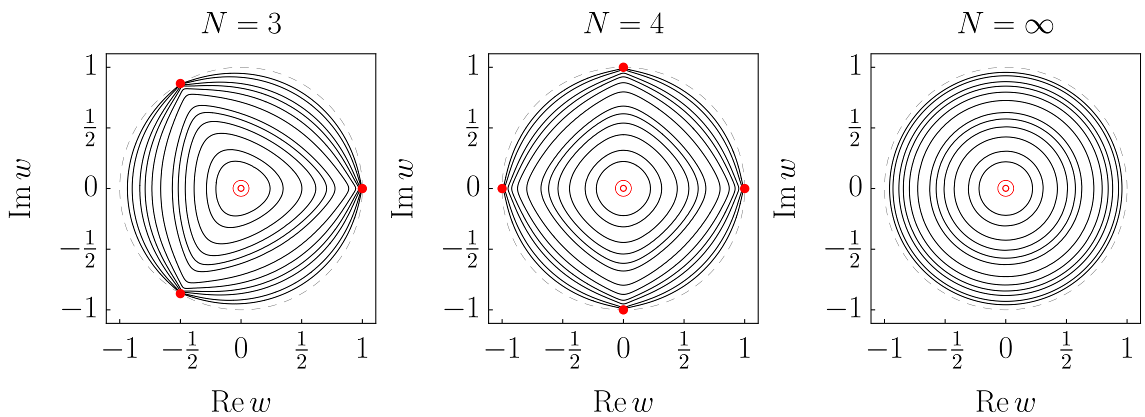

Figure 3.7: Equipotential lines for Z_1 model on the splay base point (red solid circles) $\tilde{p} = (\eta, \eta^2, \ldots, \eta^N)$ with $\eta = e^{2\pi i/N}$. The open circle at $w = 0$ denotes an unstable fixed point.

Möbius transformation with respect to base point p, the order parameter is

$$a(w,\bar{w}) = Z_2(M_w p)\overline{Z_1(M_w p)} = \frac{1}{N^2}\sum_{l,k}\left(\frac{\beta_l - w}{1-\bar{w}\beta_l}\right)^2 \frac{\bar{\beta}_k - \bar{w}}{1 - w\bar{\beta}_k}.$$

Similar to the previous section, evaluating $F(w,\bar{w})$ gives

$$\begin{aligned} F(w,\bar{w}) &= -\int d\bar{w}\frac{a\,(w,\bar{w})}{1-|w|^2} = -\frac{1}{N^2}\sum_{l,k}\frac{(\beta_l - w)^2}{1-\bar{\beta}_k w} I_{lk}, \\ &= -\frac{1}{N^2}\sum_{l,k}\ln\left(\frac{1-|w|^2}{1-\beta_l\bar{w}} + \frac{(\beta_l - w)(\bar{\beta}_k - \bar{\beta}_l)}{(1-\bar{\beta}_k w)(1-\beta_l \bar{w})}\right) \end{aligned}$$

with the integral I_{lk}

$$\begin{aligned} I_{lk} &= \int d\bar{w}\frac{\bar{\beta}_k - \bar{w}}{(1-w\bar{w})(1-\bar{w}\beta_l)^2} = \int d\bar{w}\left(\frac{a_0}{1-w\bar{w}} + \frac{a_1}{1-\beta_l\bar{w}} + \frac{a_2}{(1-\beta_l\bar{w})^2}\right) \\ &= \frac{1-\bar{\beta}_k w}{(w-\beta_l)^2}\ln\frac{1-|w|^2}{1-\beta_l\bar{w}} + \frac{\bar{\beta}_k - \bar{\beta}_l}{\beta_l - w}\frac{1}{1-\beta_l\bar{w}}; \\ a_0 &= \frac{-w(1-\bar{\beta}_k w)}{(w-\beta_l)^2},\ a_1 = \frac{\beta_l(1-\bar{\beta}_k w)}{(w-\beta_l)^2},\ a_2 = \frac{1-\bar{\beta}_k\beta_l}{w-\beta_l}. \end{aligned}$$

For the conjugate $F^\dagger(w,\bar{w})$, it is straightforward to show

$$\begin{aligned}
\overline{a(w,\bar{w})} &= \overline{Z_2(M_w p)} Z_1(M_w p) = \frac{1}{N^2}\sum_{l,k}\frac{\beta_l - w}{1-\bar{w}\beta_l}\left(\frac{\bar{\beta}_k-\bar{w}}{1-w\bar{\beta}_k}\right)^2, \\
F^\dagger(w,\bar{w}) &= -\int dw \frac{\overline{a(w,\bar{w})}}{1-|w|^2} = -\frac{1}{N^2}\sum_{l,k}\frac{(\bar{\beta}_k-\bar{w})^2}{1-\beta_l\bar{w}}\bar{I}_{kl} \\
&= -\frac{1}{N^2}\sum_{l,k}\left(\ln\frac{1-|w|^2}{1-\bar{\beta}_k w} + \frac{(\bar{\beta}_k-\bar{w})(\beta_l-\beta_k)}{(1-\beta_l\bar{w})(1-\bar{\beta}_k w)}\right). \qquad (3.45)
\end{aligned}$$

with $\bar{I}_{kl}$ being the transposed conjugate of the integral I_{lk},

$$\bar{I}_{kl} = \int dw \frac{\beta_l - w}{(1-\bar{w}w)(1-\bar{\beta}_k w)^2}.$$

Lastly, integrating the derivative $\frac{\partial F}{\partial w}$ over w gives

$$\begin{aligned}
\frac{\partial F}{\partial w} &= \frac{1}{N^2}\sum_{l,k}\left(\frac{\bar{w}}{1-|w|^2} + \frac{(\bar{\beta}_k-\bar{\beta}_l)(1-\beta_l\bar{\beta}_k)}{(1-\beta_l\bar{w})(1-\bar{\beta}_k w)^2}\right), \\
\int dw \frac{\partial F}{\partial w} &= \frac{1}{N^2}\sum_{l,k}\left(-\ln(1-|w|^2) + \frac{(\bar{\beta}_k-\bar{\beta}_l)(\beta_k-\beta_l)}{(1-\beta_l\bar{w})(1-\bar{\beta}_k w)}\right).
\end{aligned}$$

Putting all pieces together, the potential Φ is

$$\begin{aligned}
\Phi(w,\bar{w}) &= -\frac{1}{N^2}\sum_{l,k}\left(\ln\frac{1-|w|^2}{(1-\beta_l\bar{w})(1-\bar{\beta}_k w)} + \frac{(\bar{\beta}_k-\bar{\beta}_l)(\beta_k-w)+(\beta_l-\beta_k)(\bar{\beta}_k-\bar{w})}{(1-\bar{\beta}_k w)(1-\beta_l\bar{w})}\right) \\
&= \Phi_0+\Phi_1+\Phi_2, \qquad (3.46) \\
\Phi_2(w,\bar{w}) &= -\frac{1}{N^2}\sum_{l,k}\frac{(\bar{\beta}_k-\bar{\beta}_l)(\beta_k-w)+(\beta_l-\beta_k)(\bar{\beta}_k-\bar{w})}{(1-\bar{\beta}_k w)(1-\beta_l\bar{w})} \\
&= -\frac{1}{N^2}\sum_{l,k}\frac{(\bar{\beta}_k-\bar{\beta}_l)(\beta_l-w)+(\beta_l-\beta_k)(\bar{\beta}_k-\bar{w})+(\beta_k-\beta_l)(\bar{\beta}_k-\bar{\beta}_l)}{(1-\bar{\beta}_k w)(1-\beta_l\bar{w})}.
\end{aligned}$$

Here, the potential Φ_2 (due to the second-order moment Z_2) is a real function, since the matrix of terms in the summation is equal to its transposed conjugate, i.e. is self adjoint, as can be observed from the second line of the above equation by switching $w \leftrightarrow \bar{w}$ and $l \leftrightarrow k$.

Note that the potential function is additive, just as expected for a scalar. Using $(1-x)^{-1} = \sum_{n=0}^{\infty} x^n$, we expand Φ_2 into a series of moments,

$$
\begin{aligned}
\Phi_2(w,\bar{w}) = & \sum_{n_l,n_k=0}^{\infty} \bar{w}^{n_l} w^{n_k} \times \\
& \left[Z_{n_l+1}\bar{Z}_{n_k+1} - w\left(Z_{n_l}\bar{Z}_{n_k+1} - Z_{n_l-1}\bar{Z}_{n_k}\right)\right. \\
& \left. -\bar{w}\left(Z_{n_l+1}\bar{Z}_{n_k} - Z_{n_l}\bar{Z}_{n_k-1}\right) - Z_{n_l-1}\bar{Z}_{n_k-1}\right].
\end{aligned}
$$

Splay base point At the splay base point $\tilde{p} = (\eta, \ldots, \eta^N)$, the potential for $Z_2 Z_{-1}$ model has the following form,

$$
\Phi(w,\bar{w}) = -\left(\ln \frac{1-|w|^2}{(1-\bar{w}^N)^{1/N}(1-w^N)^{1/N}} + \frac{\bar{w}^{N-1}w^{N-1} - \left(\bar{w}^N + w^N\right) + \bar{w}w}{(1-\bar{w}^N)(1-w^N)} \right), \tag{3.47}
$$

$$
\lim_{N\to\infty} \Phi = -\left(\ln(1-\bar{w}w) + \bar{w}w\right). \tag{3.48}
$$

It is straightforward to check this result by integrating $\partial_{\bar{w}}\Phi = -\frac{a(w,\bar{w})}{1-|w|^2}$ with $a(w,\bar{w}) = \frac{f(w,\bar{w})\left(w^{N-1}-\bar{w}\right)}{(1-\bar{w}^N)^2(1-w^N)} \sim -w^2\bar{w}$ as $N \to \infty$. Figure 3.8 shows the potentials for $Z_2 Z_{-1}$ model. Notice the origin becomes a non-hyperbolic node with additional attractive directions, coming from new repelling fixed points in the disk.

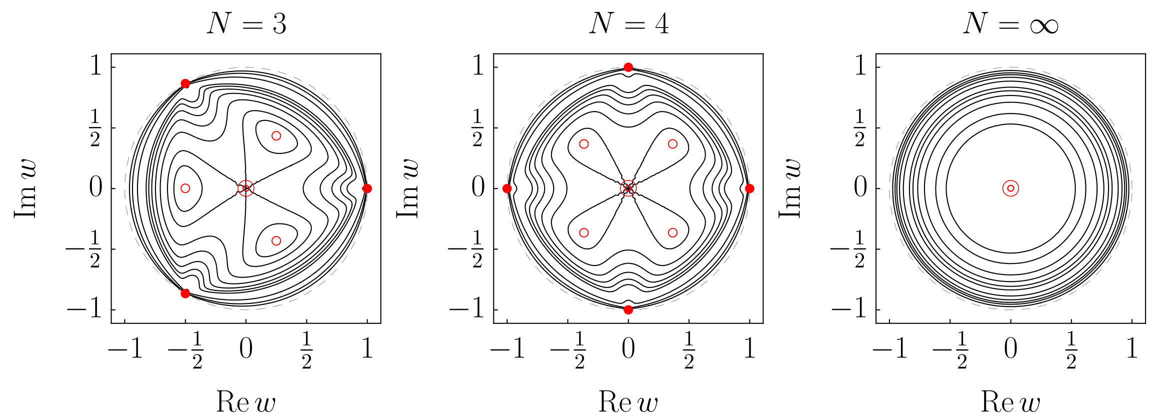

Figure 3.8: Potentials for $Z_2 Z_{-1}$ model on the splay base point (red solid circles) $\tilde{p} = (\eta, \eta^2, \dots, \eta^N)$ with $\eta = e^{2\pi i/N}$. The open circle at $w = 0$ denotes an unstable fixed point.

3.4 Flows on $(N-1, 1)$ Edges

3.4.1 Bifurcation Diagrams

For a two-cluster state characterized by two complex numbers on the unit circle (β_1 and β_2), the moment Z_p gets simplified,

$$Z_p = \frac{1}{N} \sum_{j=1}^{N} \beta_j^p = \frac{M}{N} \beta_1^p + \frac{N-M}{N} \beta_2^p = s\beta_1^p + (1-s)\beta_2^p. \tag{3.49}$$

Here $s = \frac{M}{N}$ is the size of a cluster. For the $(N-1, 1)$ state, $s = \frac{1}{N}$.

Reduced dynamics on the partially synchronized edge is described by the relative phase

$$\delta = \beta_1 \bar{\beta}_2 = e^{i\varphi}. \tag{3.50}$$

Each cluster satisfies the Riccati equation $\dot{\beta}_j = i\omega\beta_j + \frac{1}{2}(a - \bar{a}\beta_j^2)$, where the order parameter a becomes

$$a = e^{i\alpha} Z_p Z_{1-p} = c Z_p Z_{1-p}$$

$$= c[s^2\beta_1 + s(1-s)\beta_1^p\beta_2^{1-p} + s(1-s)\beta_1^{1-p}\beta_2^p + (1-s)^2\beta_2].$$

The dynamics of δ is determined by

$$\dot{\delta} = \Big(\frac{\dot{\beta}_1}{\beta_1} - \frac{\dot{\beta}_2}{\beta_2}\Big)\delta = \frac{1}{2}[a(\bar{\beta}_1 - \bar{\beta}_2) - \text{c.c.}]\delta = i\text{Im}[a(\bar{\beta}_1 - \bar{\beta}_2)]\delta, \tag{3.51}$$

where the order parameter is

$$a(\bar{\beta}_1 - \bar{\beta}_2) = c[(2s-1) - s(1-s)(\delta^p - \bar{\delta}^p) + s(1-s)(\delta^{p-1} - \bar{\delta}^{p-1}) - s^2\delta + (1-s)^2\bar{\delta}]$$

$$= c[s(1-s)\bar{\delta}^p - s(1-s)\bar{\delta}^{p-1} + (1-s)^2\bar{\delta} + (2s-1)$$

$$- s^2\delta + s(1-s)\delta^{p-1} - s(1-s)\delta^p].$$

Since $|\delta|^2 = 1$, the fixed point solution $\dot{\delta} = 0$ implies $\text{Im}[a(\bar{\beta}_1 - \bar{\beta}_2)] = 0$. Direct calculations show

$$\text{Im}[a(\bar{\beta}_1 - \bar{\beta}_2)] = (2s-1)\sin\alpha(1-\cos\varphi)$$

$$- \cos\alpha\{2s(1-s)[\sin p\varphi - \sin(p-1)\varphi] + [s^2 + (1-s)^2]\sin\varphi\},$$

leading to an implicit trigonometric relationship between α and φ:

$$\tan\alpha = \frac{1}{2s-1}\frac{2s(1-s)[\sin p\varphi - \sin(p-1)\varphi] + [s^2 + (1-s)^2]\sin\varphi}{1-\cos\varphi} \tag{3.52}$$

Figure 3.9 illustrates bifurcation diagrams $\varphi(\alpha)$ for various ranks p and number of oscillators N. We observe a few interesting features:

1. Bifurcation diagrams are symmetric under $-\pi \Leftrightarrow \pi$ due to periodicity in α and φ.

2. The sync state ($\varphi = 0$) is a fixed point for all α. Its stability depends on the sign of $\left.\frac{d\dot{\delta}}{d\delta}\right|_{\delta=1}$, which is further determined jointly by p, N and α.

3. When $\alpha = 0$, the symmetric splay state ($\varphi = \pm\pi$) is a fixed point. For higher-degree models (larger p), there are more "wiggles" in the bifurcation curve, giving rise to more zero-crossing at the vertical axis ($\alpha = 0$) thus more fixed points. They are non-symmetric splay states in which the two clusters are locked up to a constant phase φ^*. The term $\sin p\varphi - \sin(p-1)\varphi$ in Eq. (3.9) is the reason why the number of new fixed points grows with p. For very large p, the difference between the two sine functions are diminishing. The bifurcation curve is centered around an N-dependent asymptotic curve (Figure 3.10):

$$\tan\alpha = \frac{s^2 + (1-s)^2}{2s-1} \cot\frac{\varphi}{2}. \tag{3.53}$$

4. When N is large, $s = \frac{1}{N} \to 0$. The bifurcation curve converges to a straight line:

$$\tan\alpha = -\cot\frac{\varphi}{2} \Rightarrow \varphi = -2\cot^{-1}(\tan\alpha) = 2\alpha - \pi, \tag{3.54}$$

   as shown in Figure 3.10. The number of new splay fixed points only depends on N. So there is competition between p and N, which will be demonstrated in greater detail in the next sub-section.

5. For fixed p and N, as α increases, saddle-node bifurcations occur between two splay

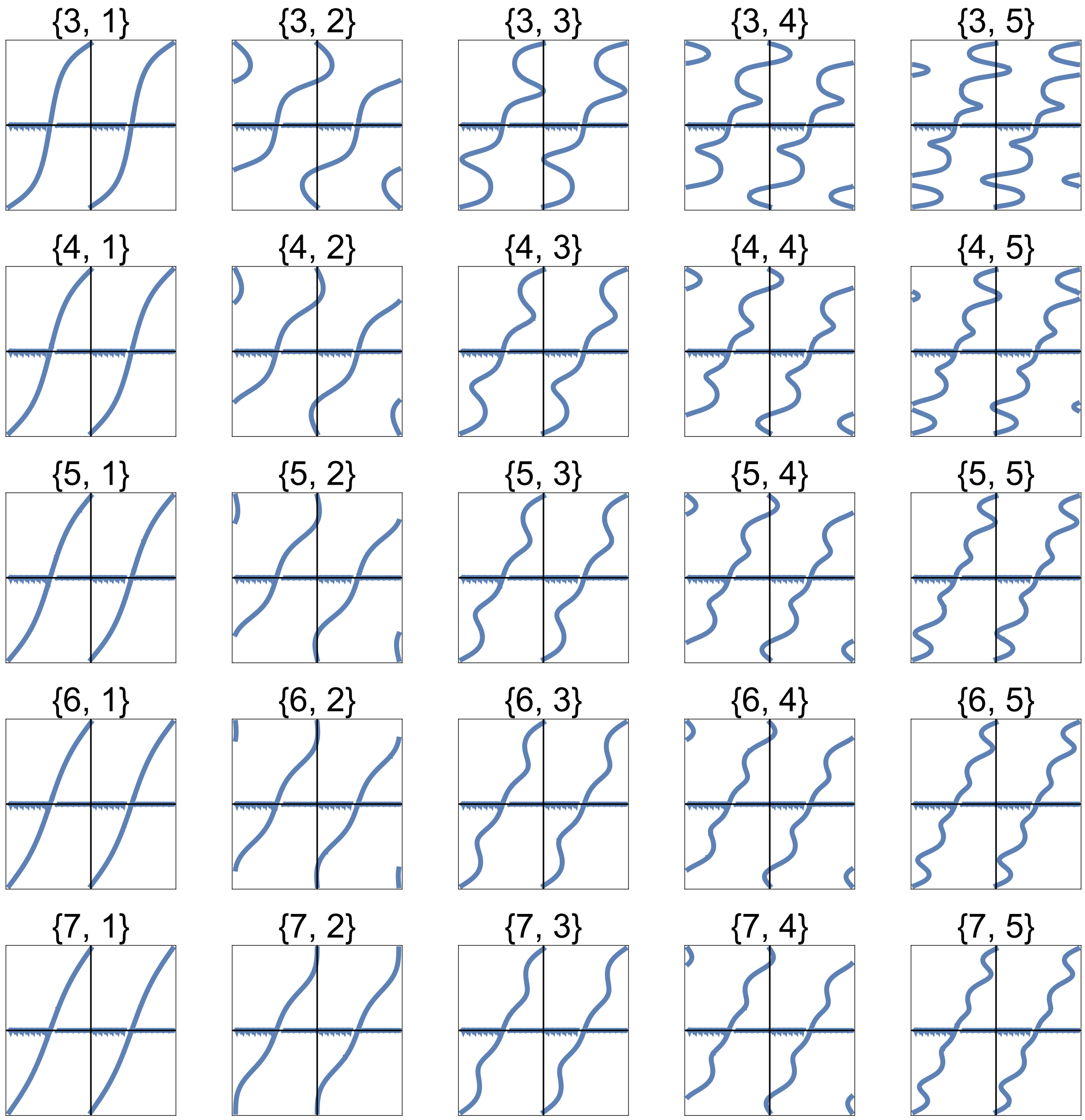

Figure 3.9: Bifurcation diagrams $\varphi(\alpha)$ on the $(N-1, 1)$ edge for various models, given by Eq. (3.52). Each panel is labelled by the degree p and the number of oscillators N: $\{N, p\}$. The horizontal axis is the phase shift α, and the vertical axis the relative phase difference φ between the two clusters. The ranges for α and φ are $[-\pi, \pi]$.

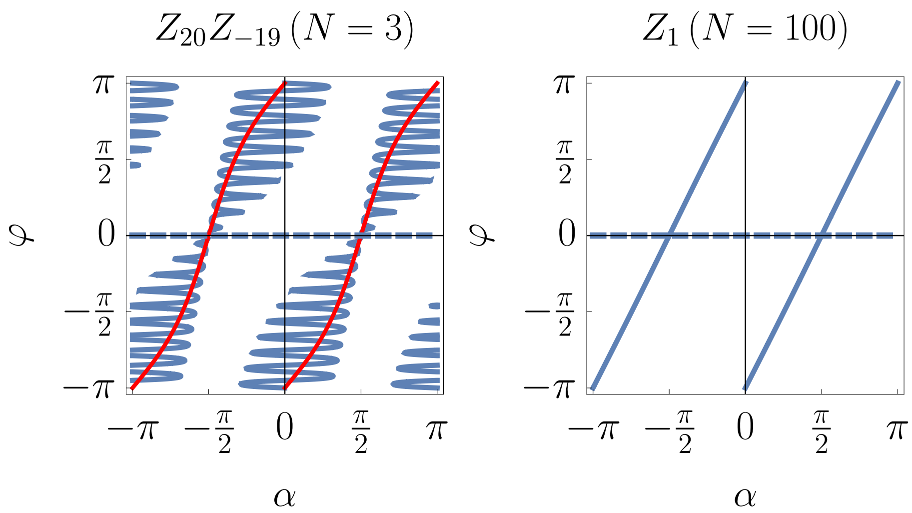

Figure 3.10: Left panel: The bifurcation diagram for the $Z_{20}Z_{-19}$ model with $N = 3$. The horizontal dashed line is the sync state ($\varphi = 0$). The red line is the asymptotic curve for $p \to \infty$, given by Eq. (3.53).
Right panel: The bifurcation diagram for the Z_1 model with $N = 100$. The curve becomes a straight line since N is large, as predicted by Eq. (3.54).

states. With large p and N large and lots of new fixed points, there can be a cascade of saddle-node and anti-saddle-node bifurcations. At $\alpha = \pi/2$, the sync state collides with the splay state in a transcritical bifurcation.

3.4.1.1 Polynomial Representation

Alternative to using trigonometric functions, we can set $2\dot{\delta} = [a(\bar{\beta}_1 - \bar{\beta}_2) - \text{c.c.}]\delta = 0$ and solve a polynomial of δ,

$$
\begin{aligned}
0 = {} & s(1-s)(c+\bar{c})\bar{\delta}^{p-1} - s(1-s)(c+\bar{c})\bar{\delta}^{p-2} + (1-s)^2 c + s^2 \bar{c} \\
& + (2s-1)(c-\bar{c})\delta - [(1-s)^2\bar{c} + s^2 c]\delta^2 + s(1-s)(c+\bar{c})\delta^p - s(1-s)(c+\bar{c})\delta^{p+1}.
\end{aligned}
$$

As for the Z_1 model, the above equation reduces to

$$\bar{a}\delta^2 - b\delta - a = 0$$

with $a = s\bar{c} + (1-s)c$ and $b = (2s-1)(c-\bar{c})$. There are two roots for this equation,

$$\delta_\pm = \frac{b \pm \sqrt{b^2 + 4|a|^2}}{2\bar{a}} = \frac{\pm|\text{Re}c| + i(2s-1)\text{Im}c}{sc + (1-s)\bar{c}} = \frac{\pm\cos\alpha + i(2s-1)\sin\alpha}{\cos\alpha + i(2s-1)\sin\alpha}.$$

For $\alpha \in [-\pi/2, \pi/2]$, $\cos\alpha \in [0,1]$. Then these roots become

$$\delta_+ = 1, \quad \delta_- = -\frac{\cos\alpha - i(2s-1)\sin\alpha}{\cos\alpha + i(2s-1)\sin\alpha}.$$

As for the Z_2Z_{-1} model, the resulting equation is a quartic polynomial of δ,

$$\delta^4 + B\delta^3 - C\delta^2 - \bar{B}\delta - 1 = 0, \quad B = \frac{(1-2s)[(1-s)\bar{c} - sc]}{s(1-s)(c+\bar{c})}, \quad C = \frac{(2s-1)(c-\bar{c})}{s(1-s)(c+\bar{c})}.$$

For the Z_pZ_{1-p} model with an arbitrary phase shift α (thus an arbitrary c), locations of fixed points are roots of a polynomial in δ with degree $2p$.

3.4.2 New Fixed Points for Z_pZ_{1-p} Models

When $\alpha = 0$, we can find all fixed points on the $(N-1,1)$ edge explicitly. Since the order parameter a is homogeneous for phase models, i.e., $a(\zeta z) = \zeta a(z)$, rewriting it in terms of the relative phase variable $\delta = e^{i\varphi}$ ($\varphi \in [-\pi, \pi]$) for the two-cluster state,

$$\begin{aligned}\dot{\delta} = \dot{\beta}_1\bar{\beta}_2 + \beta_1\dot{\bar{\beta}}_2 &= \frac{1}{2}(1-\delta)[\bar{\beta}_2 a(\beta_1,\beta_2) + \beta_1\overline{a(\beta_1,\beta_2)}] \\ &= \frac{1}{2}(1-\delta)[a(\delta,1) + \bar{a}(1,\bar{\delta})] = \frac{1}{2}(1-\delta)[a(\delta,1) + \delta\bar{a}(\delta,1)]. \qquad (3.55)\end{aligned}$$

In this case, the q-th moment is $Z_p = s\delta^p + (1-s)$ and the order parameter reads

$$a = Z_p Z_{1-p} = (s\delta^p + 1 - s)(s\delta^{1-p} + 1 - s) = s^2\delta + (1-s)^2 + s(1-s)(\delta^p + \delta^{1-p}). \quad (3.56)$$

Then the dynamics of $\dot{\delta}$ is determined by

$$\begin{aligned}\dot{\delta} &= \frac{1}{2}(1-\delta)\{[s+(1-s)^2](1+\delta) + 2s(1-s)(\delta^p + \delta^{1-p})\} \\ &= \frac{1}{2}\delta(\delta^{-1/2} - \delta^{1/2})\{[s^2+(1-s)^2](\delta^{1/2}+\delta^{-1/2}) + 2s(1-s)(\delta^{p-1/2}+\delta^{-p+1/2})\}.\end{aligned} \quad (3.57)$$

Clearly, $\delta = 1$ is a fixed point such that $\dot{\delta} = 0$, which corresponds to $\cos\varphi = 1 \Leftrightarrow \varphi = 0$.

Other fixed points are solutions to

$$\begin{aligned}[s^2+(1-s)^2](\delta^{1/2}+\delta^{-1/2}) + 2s(1-s)(\delta^{p-1/2}+\delta^{-p+1/2}) = 0 \Rightarrow \\ [s^2+(1-s)^2]Q + 2s(1-s)R_{2p-1} = 0.\end{aligned} \quad (3.58)$$

Here we denote $x = \delta^{1/2}$, $\delta^{p-1/2} = x^{2p-1}$, $x + x^{-1} \equiv Q$ and $x^n + x^{-n} \equiv R_n$. Notice that

$$\begin{aligned}(x+x^{-1})^{2p-1} &= \sum_{k=0}^{2p-1} \binom{2p-1}{k} x^{2p-1-k}x^{-k} \\ &= \sum_{k=0}^{2p-1} \binom{2p-1}{k} x^{2p-1-2k} = \sum_{k=0}^{p-1} \binom{2p-1}{k}(x^{2p-1-2k} + x^{-2p+1+2k}).\end{aligned}$$

There is a recurrence relation (with $2p-1=n$),

$$\begin{aligned}x^{2p-1} + x^{1-2p} = (x+x^{-1})^{2p-1} - \sum_{k=1}^{p-1}\binom{2p-1}{k}(x^{2p-1-2k} + x^{1+2k-2p}) \Rightarrow \\ R_n = Q^n - \sum_{k=1}^{\frac{n-1}{2}} \binom{n}{k} R_{n-2k}.\end{aligned}$$

Then for small p,

$$
\begin{aligned}
&p = 1,\, n = 1: \quad R_1 = Q, \\
&p = 2,\, n = 3: \quad R_3 = Q(Q^2 - 3) \\
&p = 3,\, n = 5: \quad R_5 = Q(Q^4 - 5Q^2 + 5) \\
&p = 4,\, n = 7: \quad R_7 = Q(Q^6 - 7Q^4 + 14Q^2 - 7) \\
&p = 5,\, n = 9: \quad R_9 = Q(Q^8 - 9Q^6 + 27Q^4 - 30Q^2 + 9) \\
&\quad \ldots
\end{aligned}
$$

we factor out R as polynomials of Q and solve the following equation (define $\sigma \equiv 2s(1-s)$)

$$(1 - \sigma)Q + \sigma R_{2p-1} = 0. \tag{3.59}$$

Let us consider a few cases with small p.

1. $p = 1$: Equation (3.59) gives $Q = 0$. Since $Q = \delta^{1/2} + \delta^{-1/2} = 2\cos\frac{\varphi}{2}$, then $\varphi = \pm\pi$. So when $\alpha = 0$, the Z_1 model has two fixed points: the sync and the splay at $\varphi = \{0, \pm\pi\}$.

2. $p = 2$: Solving Eq. (3.59) for non-zero solutions,

$$(1 - \sigma)Q + \sigma Q(Q^2 - 3) = Q(\sigma Q^2 - 4\sigma + 1) = 0 \Rightarrow Q^2 = 4 - \sigma^{-1}.$$

   Since $Q = 2\cos\frac{\varphi}{2} \in [-2, 2]$, then $Q^2 \in [0, 4]$. This puts a constraint on σ, i.e., on the cluster's size s. Or equivalently, there will be a constraint on the number of oscillators:

For the $(N-1,1)$ state, $s=\frac{1}{N}$, $\sigma=\frac{2(N-1)}{N^2}$. The critical condition $Q^2=0$ implies

$$4-\frac{N^2}{2(N-1)}=-\frac{N^2-8N+8}{2(N-1)}=0 \Rightarrow N_\pm=4\pm 2\sqrt{2}=\{1.17157, 6.82843\}.$$

When $N=\{3,4,5,6\}$, $Q^2=\frac{(N-N_-)(N_+-N)}{2(N-1)}\in[0,4]$. The fixed points locate at

$$\varphi_\pm=2\arccos\frac{Q}{2}=2\arccos\left(\pm\sqrt{\frac{(N-N_-)(N_+-N)}{8(N-1)}}\right). \tag{3.60}$$

So when $\alpha=0$, the Z_2Z_{-1} model has three fixed points, $\varphi=\{0,\pm\pi,\varphi_\pm\}$, on the $(N-1,1)$ edge for $N=\{3,4,5,6\}$.

3. $p=3$: Equation (3.59) becomes

$$Q^4-5Q^2+4+\sigma^{-1}=0 \Rightarrow Q^2=\frac{1}{2}(5\pm\sqrt{9-4\sigma^{-1}}).$$

For the $(N-1,1)$ state, the critical condition $\sqrt{9-4\sigma^{-1}}=0$ yields

$$9-\frac{2N^2}{N-1}=-\frac{2N^2-9N+9}{N-1}=0 \Rightarrow N_\pm=\frac{1}{4}(9\pm 3)=\{\frac{3}{2},3\}.$$

Q^2 is real only when $N=3$, corresponding to two fixed points at $\varphi_\pm=2\cos^{-1}\left(\pm\sqrt{\frac{5}{8}}\right)$. So when $\alpha=0$ and $N=3$, the Z_3Z_{-2} model has tangent fixed points at $\varphi_\pm$ and a splay state on the $(N-1,1)$ edge

4. $p=4$: Equation $Q^6-7Q^4+14Q^2-8+\sigma^{-1}=0$ has real solutions up to $N_{max}=14$ for $(N-1,1)$ state, $Q^2_{N_{max}}=0.0335263$. The two fixed points are $\varphi_\pm\approx\pm 2.95823$, which is consistent with the result of trigonometric representations.

From the above observations, we know that the number of new fixed points and associated saddle-node bifurcations depend subtly on the degree p and the number of oscillators N.

Specifically, with a given p, there is a maximal $N_{max}(p)$ above which the symmetric splay state ($\varphi = \pm\pi$) and the sync state ($\varphi = 0$) are the only fixed points. In other words, the non-symmetric splay state can exists when $N \leq N_{max}(p)$. The following table lists $N_{max}(p)$ and the number of non-symmetric splay fixed points for $p \leq 4$.

p	1	2	3	4
$N_{max}(p)$	3	6	3	14
# of non-symmetric splay states	0	2	1	2

3.5 Summary

In this chapter, we investigate several aspects of Kuramoto phase models whose dynamics are equivalent to two-dimensional flows $w(t)$ [Eq. (3.1)] in the Poincaré disk of hyperbolic geometry.

We systematically explore the fixed point structure of the w flow for the Z_1 and $Z_p Z_{1-p}$ models. Using the hyperbolic metric, we derive a general condition for the flow to be a gradient of some potential function. With this condition, we are able to show that the Z_1 phase model (the identical Kuramoto-Sakaguchi model) is a gradient system when the phase shift $\alpha = 0$. It becomes a Hamiltonian system when $\alpha = \pi/2$. This gradient/Hamiltonian duality provides a natural way of understanding the integrability in the "cosine" model discussed in the WS theory.

Moreover, we find new classes of phase models that satisfy the gradient condition. They include families of double, triple, and quadruple products of higher moments of oscillators' configurations. These models enjoy all features of as the Z_1 model (existence of potentials and Hamiltonians, low-dimensional dynamics, constants of motion, etc.), and have richer fixed point structures and bifurcations, especially on the partially synchronized subspace.

CHAPTER IV

Extended Phase Models

Up to now, we have been considering identical Kuramoto oscillators, which are subject to dimension-reduction and yield interesting features such as $2D$ dynamics, a gradient condition, and integrability.

It is tempting to ask, can this formalism be applied to non-identical system? We will address this question in this chapter. It turns out that if identical oscillators contribute unequally to the order parameter, the similar group-theoretic approach can be adopted. In other words, we can study extended phase models with non-identical coupling under the same framework.

Of particular interest is when different contributions to the order parameter sum up to zero. Then the system is simultaneously gradient and Hamiltonian. The w flows are analogous to field lines of a two-dimensional electrostatic system with equal numbers of positive and negative charges.

4.1 Extended Z_1 Phase Models

A natural generalization to simple phase models is including unequal weights in the order parameter. Let us start with the Z_1 model,

$$\mathcal{a}(p) = \sum_{j=1}^{N} c_j \beta_j, \qquad c_j \in \mathbb{C}. \tag{4.1}$$

Here the coefficient c_j can be any complex number. It is clear that this weighted moment still satisfies the condition $\mathcal{a}(\zeta p) = \zeta \mathcal{a}(p)$ for phase models.

Since all β_j follow the Riccati equation $\dot{\beta}_j = i\omega\beta_j + \frac{1}{2}(\mathcal{a} - \bar{\mathcal{a}}\beta_j^2)$ with $\mathcal{a} = \sum_{l=1}^{N} c_l \beta_l$, using $\beta_j = e^{i\theta_j}$, $\dot{\beta}_j = i\beta_j\dot{\theta}_j$ and $c_l = K_l e^{i\alpha_l}$, the equation for θ_j is,

$$\begin{aligned}\dot{\theta}_j &= \omega + \frac{1}{2i}\sum_{l=1}^{N}(c_l\beta_l\bar{\beta}_j - \bar{c}_l\bar{\beta}_l\beta_j) = \omega + \sum_{l=1}^{N}\mathrm{Im}(c_l\beta_l\bar{\beta}_j) \\ &= \omega + \sum_{l=1}^{N} K_l \sin(\theta_l - \theta_j + \alpha_l).\end{aligned} \tag{4.2}$$

In other words, the weights c_l in the order parameter determine an inhomogeneous coupling K_l and a phase lag α_l between the l-th oscillator and the whole population. The coupling matrix has N identical rows,

$$\mathbf{K} = \begin{pmatrix} K_1 & K_2 & \cdots & K_N \\ K_1 & K_2 & \cdots & K_N \\ \vdots & \vdots & \ddots & \vdots \\ K_1 & K_2 & \cdots & K_N \end{pmatrix}, \tag{4.3}$$

which is clearly not symmetric unless all K_j are the same. [1]

[1] Even with identical couplings $K_j = K_l = K$ for all nodes, the phase lags can still be node-dependent: $c_j = Ke^{i\alpha_j}$.

In Chapter 3, depending on the phase shift α in the order parameter $\mathcal{a}$, we have seen that the simple Z_1 phase model can be a gradient flow $(\alpha = 0, \pi)$ or a Hamiltonian flow $(\alpha = \pm\pi/2)$. This is further embodied by two constraints on $\mathcal{a}$:

$$\begin{cases} \mathrm{Im}\mathcal{D}\mathcal{a} = 0 & \text{Gradient flows,} \\ \mathrm{Re}\mathcal{D}\mathcal{a} = 0 & \text{Hamiltonian flows.} \end{cases} \tag{4.4}$$

For the extended Z_1 phase model, the differential $\mathcal{D}\mathcal{a}$ is the sum of all weights, which is the weight of the zeroth moment C, given by

$$\mathcal{D}\mathcal{a} = (\partial_{\beta_1} + \ldots + \partial_{\beta_N}) \sum_{j=1}^{N} c_j \beta_j = \sum_{j=1}^{N} c_j = C. \tag{4.5}$$

So there are three interesting cases:

1. Gradient flows: $\mathrm{Im}\mathcal{D}\mathcal{a} = \mathrm{Im}\sum_j c_j = 0$;

2. Hamiltonian flows: $\mathrm{Re}\mathcal{D}\mathcal{a} = \mathrm{Re}\sum_j c_j = 0$;

3. Gradient and Hamiltonian flows: $\mathcal{D}\mathcal{a} = \sum_j c_j = 0$.

In the following subsections, we will discuss each case in detail.

4.1.1 Gradient-Hamiltonian Structures

Gradient flows: $\mathrm{Im}\sum_j c_j = 0$

When the sum of all coupling weights is real, $\sum_j c_j \in \mathbb{R}$, the flow is given by a hyperbolic gradient a (real) potential $\dot{w} = \nabla_{hyp}\Phi$ with Φ related to the order parameter,

$$\frac{\partial \Phi}{\partial \bar{w}} = -\frac{\mathcal{a}(M_w p)}{1 - |w|^2}, \quad \mathcal{a}(M_w p) = \sum_j c_j \frac{\beta_j - w}{1 - \bar{w}\beta_j}.$$

Integrating over $\bar{w}$, the potential is

$$\Phi = -\int d\bar{w}\frac{a(M_w p)}{1-|w|^2} + f(w) = -\sum_j c_j(\beta_j - w)\int \frac{d\bar{w}}{(1-\bar{w}\beta_j)(1-w\bar{w})} + f(w).$$
$$= -\sum_j c_j \ln \frac{1-w\bar{w}}{1-\beta_j\bar{w}} + f(w).$$

The holomorphic function $f(w)$ can be found via an integration over w,

$$\frac{\partial\Phi}{\partial w} = -\sum_j c_j\partial_w \ln\frac{1-w\bar{w}}{1-\beta_j\bar{w}} + \frac{df}{dw} = -\frac{\overline{a(M_w p)}}{1-w\bar{w}} \Rightarrow$$
$$f(w) = -\int dw\frac{\overline{a(M_w p)}}{1-w\bar{w}} + \sum_j c_j\int\frac{-\bar{w}dw}{1-\bar{w}w} = -\sum_j \bar{c}_j \ln\frac{1-w\bar{w}}{1-\bar{\beta}_j w} + \sum_j c_j\ln(1-\bar{w}w).$$

Since $\sum_j c_j = \sum_j \bar{c}_j \in \mathbb{R}$, $f(w)$ only depends on w. In fact, $f(w) = \sum_j \bar{c}_j \ln(1-\bar{\beta}_j w)$. Then the potential can be written as

$$\Phi \equiv \Phi_0 + \Phi_1, \tag{4.6}$$
$$\Phi_0 = -\ln(1-w\bar{w})\sum_j \bar{c}_j = -\ln(1-w\bar{w})\sum_j c_j, \tag{4.7}$$
$$\Phi_1 = \sum_j[\bar{c}_j\ln(1-\bar{\beta}_j w) + c_j\ln(1-\beta_j\bar{w})] = \mathrm{Re}\sum_j \bar{c}_j\ln(1-\bar{\beta}_j w)^2. \tag{4.8}$$

Clearly, Φ is a real function, which is consistent with the gradient condition.

Hamiltonian flows: $\mathrm{Re}\sum_j c_j = 0$

When the sum of all weights is imaginary, $\sum_j c_j \in i\mathbb{R}$, this corresponds to $\dot{w} = i\nabla_{hyp}\Phi$. The flows get rotated by 90 degrees from the gradient case, and form closed orbits.

Gradient-Hamiltonian duality

Let us first consider a gradient system in $2D$ Euclidean space with a potential Φ,

$$\dot{\mathbf{x}} = \nabla\Phi \Leftrightarrow \begin{pmatrix} \dot{x} \\ \dot{y} \end{pmatrix} = \begin{pmatrix} \Phi_x \\ \Phi_y \end{pmatrix}.$$

Here subscripts denote spatial derivatives. Using $z = x + iy$ and differentials

$$\frac{\partial}{\partial z} = \frac{1}{2}\left(\frac{\partial}{\partial x} - i\frac{\partial}{\partial y}\right), \quad \frac{\partial}{\partial \bar{z}} = \frac{1}{2}\left(\frac{\partial}{\partial x} + i\frac{\partial}{\partial y}\right),$$

then $\dot{\mathbf{x}}$ is equivalent to

$$\dot{z} = \dot{x} + i\dot{y} = \Phi_x + i\Phi_y = 2\frac{\partial\Phi}{\partial\bar{z}}.$$

Suppose we can construct a holomorphic function in the complex plane

$$F(z) = F(x+iy) = \Phi(x,y) + iH(x,y)$$

where the real part is the potential Φ. The imaginary part H is assumed to be differentiable, whose meaning will become clear in a moment. Since F is holomorphic, the Cauchy-Riemann equations are satisfied,

$$\Phi_x = H_y, \quad \Phi_y = -H_x. \tag{4.9}$$

The derivative of F is

$$\frac{dF(z)}{dz} = \frac{1}{2}\left(\frac{\partial}{\partial x} - i\frac{\partial}{\partial y}\right)(\Phi + iH) = \frac{1}{2}[\Phi_x + H_y + i(H_x - \Phi_y)] = \Phi_x + iH_x,$$

which is related to the gradient flow,

$$\dot{z} = \Phi_x + i\Phi_y = \Phi_x - iH_x = \overline{\Phi_x + iH_x} = \overline{F'(z)}. \tag{4.10}$$

Notice that $F'(z)$ can also be written as

$$F'(z) = H_y - i\Phi_y = H_y + iH_x = \overline{H_y - iH_x},$$

then H can be understood as a Hamiltonian function with

$$\begin{pmatrix} \dot{x} \\ \dot{y} \end{pmatrix} = \begin{pmatrix} H_y \\ -H_x \end{pmatrix} \Rightarrow \dot{z} = \dot{x} + i\dot{y} = H_y - iH_x = \overline{F'(z)}. \tag{4.11}$$

Therefore, a gradient (Hamiltonian) system in $2D$ can be characterized by a holomorphic function F where the real (imaginary) part is the potential (Hamiltonian) function:

$$\mathrm{Re}F = \Phi, \quad \mathrm{Im}F = H. \tag{4.12}$$

A special case: $\sum_j c_j = 0$

As for extended Z_1 phase models, the above analysis still holds if we use the hyperbolic gradient operator $\nabla_{hyp} = \lambda^{-2}\nabla_{euc} = \frac{1}{2}(1 - w\bar{w})^2\partial_{\bar{w}}$. Since we have already found the potential Φ for the gradient flow, it is tempting to find a holomorphic function F that incorporates the Hamiltonian part.

In fact, if we define F as

$$F(w) = -\sum_{j=1}^{N} \bar{c}_j \ln \frac{1 - w\bar{w}}{(1 - \bar{\beta}_j w)^2}, \tag{4.13}$$

it is holomorphic when $\sum_j c_j = \sum_j \bar{c}_j = 0$; then $F = 2\sum_j \bar{c}_j \ln(1 - \bar{\beta}_j w)$. This is a special case since every row in the coupling matrix sums up to zero, which corresponds to the so-called Laplacian condition.

It is straightforward to verify that the function F leads to the correct $\dot{w}$ flow:

$$\dot{w} = \overline{F'(w)} = \frac{1}{4}(1-w\bar{w})^2\overline{\frac{dF(w)}{dw}} = \frac{1}{4}(1-w\bar{w})^2\sum_j c_j\left(\frac{w}{1-w\bar{w}} - \frac{2\beta_j}{1-\beta_j\bar{w}}\right)$$

$$= \frac{1}{4}(1-w\bar{w})\sum_j c_j\left(w - 2\frac{\beta_j - w + w - w\beta_j\bar{w}}{1-\beta_j\bar{w}}\right) = \frac{1}{4}(1-w\bar{w})\sum_j c_j\left(-2\frac{\beta_j - w}{1-\beta_j\bar{w}} - w\right)$$

$$\overset{\sum_j c_j = 0}{=} -\frac{1}{2}(1-w\bar{w})\sum_j c_j\frac{\beta_j - w}{1-\beta_j\bar{w}} - = -\frac{1}{2}(1-w\bar{w})a(M_w p).$$

With $c_j = a_j + ib_j$ and $\ln(1-\bar{\beta}_j w) = \ln|1-\bar{\beta}_j w| + i\arg(1-\bar{\beta}_j w)$, the real and the imaginary part are

$$\begin{aligned}\Phi = \mathrm{Re}F &= \sum_j[\bar{c}_j\ln(1-\bar{\beta}_j w) + c_j\ln(1-\beta_j\bar{w})] \qquad (4.14)\\ &= \sum_j\left[a_j\ln|1-\bar{\beta}_j w|^2 + 2b_j\arg(1-\bar{\beta}_j w)\right],\\ H = \mathrm{Im}F &= -i\sum_j[\bar{c}_j\ln(1-\bar{\beta}_j w) - c_j\ln(1-\beta_j\bar{w})] \qquad (4.15)\\ &= -\sum_j\left[b_j\ln|1-\bar{\beta}_j w|^2 - 2a_j\arg(1-\bar{\beta}_j w)\right].\end{aligned}$$

Clearly, the gradient condition and the Hamiltonian condition have both been implemented in this construction.

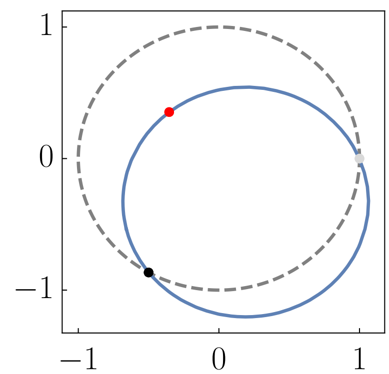

Figure 4.1: A circular trajectory of $\mathrm{Im}F = \mathrm{const}$ connecting a point w (the red dot) and two clusters β_1 (the black dot) and β_2 (the light gray dot) with opposite weights: $c_1 = -1$, $c_2 = 1$. The dashed gray line is the unit circle.

Circular Field Lines

Consider two clusters on the unit circle located at $\beta_1 = e^{i\theta_1}$ and $\beta_2 = e^{i\theta_2}$ with weights $c_1 = 1 = -c_2$. The holomorphic function is

$$F = \ln(1 - \bar{\beta}_1 w)^2 - \ln(1 - \bar{\beta}_2 w)^2 = 2 \ln \frac{1 - \bar{\beta}_1 w}{1 - \bar{\beta}_2 w}. \tag{4.16}$$

Contours of the imaginary part $\mathrm{Im}F = \mathrm{const}$ are circles that pass through β_1, w and β_2, as shown in Figure 4.1.

Since F is a holomorphic function, Φ is a harmonic function. This implies that Φ cannot have local minima or maxima inside the unit disk except for constant values, which further excludes sinks or sources in the $\dot{w}$ vector field.

The system is Hamiltonian and gradient at the same time. Contours for the Hamiltonian flows are given by $\Phi = 2\mathrm{Re}F = \mathrm{const}$, while contours for the gradient flows are given by $H = 2\mathrm{Im}F = \mathrm{const}$. Figure 4.2 illustrates both contours of the extended Z_1 phase model ($\sum_j c_j = 0$) for small N. As expected, both contours are perpendicular to each other. The $\dot{w}$ flows align with the gradient flows.

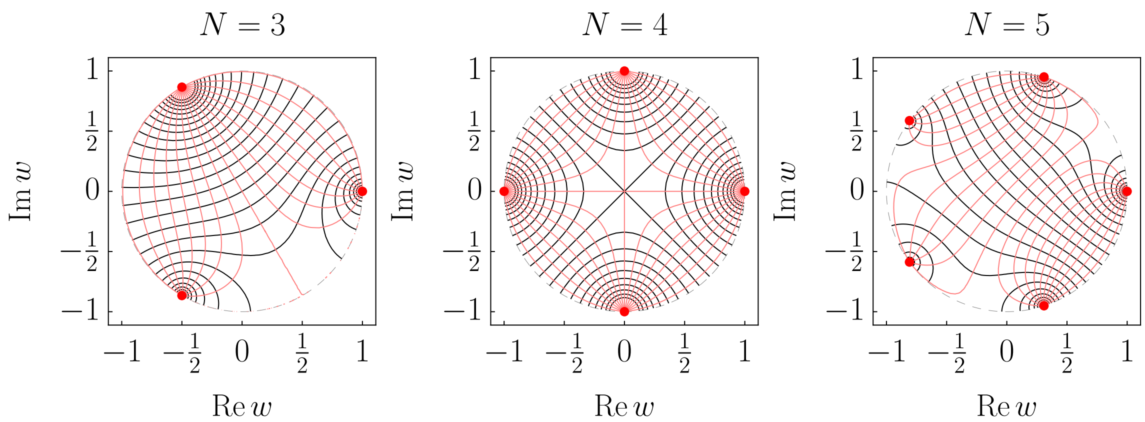

Figure 4.2: Contours of gradient flows (pink lines) and Hamiltonian flows (black lines) for the extended Z_1 phase model ($\sum_j c_j = 0$) on the splay base point (red solid circles) $\tilde{p} = (\eta, \eta^2, \ldots, \eta^N)$ with $\eta = e^{2\pi i/N}$. Both contours are perpendicular to each other. Contours of gradient flows are also the $\dot{w}$ flows. The weights are chosen to sum up to zero. Left panel ($N = 3$): $c_j = \left\{-\frac{2}{3}, \frac{1}{3}, \frac{1}{3}\right\}$; Middle panel ($N = 4$): $c_j = \left\{-\frac{1}{4}, \frac{1}{4}, -\frac{1}{4}, \frac{1}{4}\right\}$; Right panel ($N = 5$): $c_j = \left\{-\frac{2}{5}, \frac{1}{5}, \frac{1}{5}, \frac{2}{5}, -\frac{2}{5}\right\}$.

4.1.2 An Analogue with $2D$ Electrostatics

The potential for the extended Z_1 phase model with real coefficients has an interesting physical analogue: If we view the complex number $w = re^{i\varphi}$ as a point in the unit disk, and think of the weights c_j as "electric charges" q_j located on the unit circle, the potential $\Phi(w)$ mimics the electrostatic potential Φ_e due to N charges at a point w in the unit disk.

Logarithmic potentials and non-uniform charge density

Here we assume the "electric field" $\mathbf{E}$ is two-dimensional. According to Gauss' law in $2D$ (in a proper unit system), the electric field scales as the inverse of the distance measured from the charge:

$$\oint \mathbf{E} \cdot d\mathbf{s} = \int \rho da \Leftrightarrow \nabla \cdot \mathbf{E} = \rho \Rightarrow E \propto \frac{q}{r}.$$

$\rho = \nabla^2 \Phi_e = \nabla \cdot \mathbf{E}$	$\mathbf{E} = \nabla \Phi_e$	Φ_e
0	0	const.
4	$2r\mathbf{e}_r$	r^2
$\frac{4}{(1-r^2)^2}$	$\frac{2r}{1-r^2}\mathbf{e}_r$	$-\ln(1-r^2) = \sum_{n=1}^{\infty} \frac{r^{2n}}{n}$

Table 4.1: Typical charge densities, electric fields and potentials in $2D$ electrostatics

Since the electric field is the gradient of the electric potential, $\mathbf{E} = \nabla \Phi_e$, direct integration gives the potential as a logarithmic function in the (Euclidean) distance r,

$$\Phi_e = \int E(r) dr \propto q \ln r.$$

Using polar coordinates (r, φ),

$$\nabla = \frac{\partial}{\partial r}\mathbf{e}_r + \frac{1}{r}\frac{\partial}{\partial \varphi}\mathbf{e}_\varphi, \quad \nabla \cdot = \frac{1}{r}\frac{\partial}{\partial r} r + \frac{1}{r}\frac{\partial}{\partial \varphi}, \quad \nabla^2 = \frac{\partial^2}{\partial r^2} + \frac{1}{r}\frac{\partial}{\partial r} + \frac{1}{r^2}\frac{\partial^2}{\partial \varphi^2},$$

Table 4.1 summarizes typical charge distributions, electric fields, and potentials in the unit disk $(0 < r < 1)$:

Interestingly, the non-uniform charge density ρ that leads to a logarithmic potential is related to the hyperbolic metric factor λ,

$$\rho = \frac{4}{(1-r^2)^2} = \lambda^2 = \left(\frac{2}{1 - w\bar{w}}\right)^2, \quad ds = \lambda |dw| = \lambda \sqrt{dx^2 + dy^2}. \tag{4.17}$$

Note that the charge density diverges as $r \to 1$. The total charge in the disk also diverges,

$$q = 2\pi \int_0^1 \rho(r) r dr = \left. \frac{4\pi}{1 - r^2} \right|_0^1 \to \infty.$$

Another intriguing feature for a $2D$ electro-dipole is that the field lines are circles, as shown in Figure 4.3. This strikingly resonates with circular $\dot{w}$ flows when $\mathrm{Im}F = \mathrm{const.}$

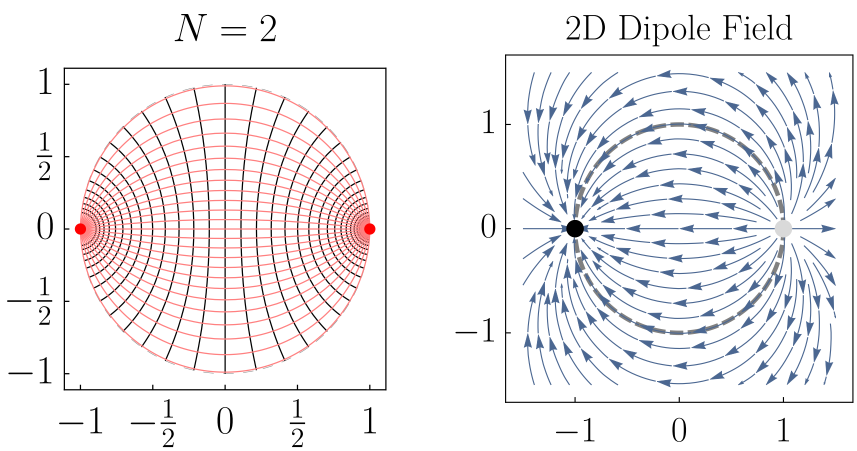

Figure 4.3: Left panel: Circular w flows (pink lines) and equal-potential curves (black lines) for the extended Z_1 phase model with $N = 2$, $c_1 = 1$, $c_2 = -1$.
Right panel: Circular field lines of a $2D$ electric dipole moment. Two charges with $q_1 = 1$ (black circle) and $q_2 = -1$ (light gray circle) locate on the horizontal axis at $(1, 0)$ and $(-1, 0)$. The dashed gray line denotes the unit circle, which is also a field line.

Potentials for $\sum_j c_j = 1$ and $\sum_j c_j = 0$

In the simple Z_1 model when $\sum_j c_j = \sum_j N^{-1} = 1$, the potential

$$\Phi = -\ln(1 - w\bar{w}) + \frac{1}{N}\sum_j \ln|\beta_j - w|^2$$

is analogous to the electric potential of a $2D$ Coulomb system: N identical charges ($q_j = 2N^{-1}$) are located on the unit circle with each at β_j. There is also a non-uniform background charge in the unit disk with density $\rho = \lambda^2 = 4(1 - w\bar{w})^{-2}$. When $\sum_j c_j = 0$, the charge background disappears, and the potential is just $\Phi = N^{-1}\sum_j \ln|\beta_j - w|^2$.

Table 4.2 summarizes several key features of this analogy.

	Extended Phase Model	$2D$ Electrostatics
Variables	w, β_j, c_j	r, r_j, q_j
Zero Weights as Charge Neutrality	$\sum_j c_j = 0, \forall c_j \in \mathbb{R}$	$\sum_j q_j = 0$
Potential	$\sum_j c_j \ln \lvert\beta_j - w\rvert^2$	$\sum_j q_j \ln \lvert r_j - r\rvert$
Background Potential	$-\ln(1 - w\bar{w})$	$-\ln(1 - r^2)$
Geometric Factor as Charge Density	$\lambda^2 = \frac{4}{(1-w\bar{w})^2}$	$\rho = \frac{4}{(1-r^2)^2}$
Circular Field Lines	$\dot{w}$ flows for $N = 2$	electric field of a dipole

Table 4.2: An analog between extended Kuramoto phase models and $2D$ electrostatics

4.1.3 Fixed Points and Stability

Now we analyze the fixed points and stability for extended Z_1 phase models. This is a generalization for the simple Z_1 model in Chapter 3.

For a given base point $p = (\beta_1, \ldots, \beta_N)$ and a set of coupling weights $c = (c_1, \ldots, c_N)$, we assume there are $r < N$ fixed points in the disk and label them as $(w_1, \ldots, w_r) \in \Delta$. Each one of them satisfies $\dot{w}_k = 0$ $(k = 1, \ldots, r)$. Equivalently, for each w_k, we have r linear equations for c_j:

$$\mathcal{a}(M_{w_k} p) = \sum_{j=1}^{N} c_j \frac{\beta_j - w_k}{1 - \bar{w}_k \beta_j} \equiv \sum_{j=1}^{N} c_j A_{jk} = 0, \quad k = 1, \ldots, r. \tag{4.18}$$

If a solution $(c_1, \ldots, c_N)$ exists, then the fixed point w_k is realizable. Since there are more unknowns than the number of equations $(N > r)$, we can get arbitrarily many fixed point in Δ and no other types of fixed points.

We can linearize the equation of motion near of one of the fixed points w_k. It is convenient to transform the coordinate system such that the fixed point sits at the origin in the new coordinate system. This can be achieved by applying a Möbius transformation on the base point p: $p \to M_{w_k} p = p_k$, i.e. $\beta_j \to M_{w_k} \beta_j = \beta'_j$, so $w_k \to M_{w_k} w_k = 0$ becomes the origin. In this coordinate system, we expand the $\dot{w}$ flow:

$$\dot{w} = -\frac{1}{2}(1-w\bar{w})\mathcal{A}(M_w p_k) = -\frac{1}{2}(1-w\bar{w})\sum_j c_j \frac{\beta'_j - w}{1-\bar{w}\beta'_j} \approx -\frac{1}{2}\sum_j c_j(\beta'_j - w)(1+\bar{w}\beta'_j)$$

$$\approx -\frac{1}{2}\sum_j c_j(\beta'_j - w + \bar{w}\beta'^2_j) = \frac{1}{2}(-Z_1 + wC - \bar{w}Z_2), \tag{4.19}$$

where the weighted second moment $Z_2 = \sum_j c_j\beta'^2_j$ should be evaluated at $p_k = M_{w_k}p$. Using $w = x+iy$ and $C = \sum_j c_j$, the above equation is equivalent to

$$\dot{x} = \frac{1}{2}\left[-\mathrm{Re}Z_1 + (\mathrm{Re}C - \mathrm{Re}Z_2)x - (\mathrm{Im}C + \mathrm{Im}Z_2)y\right],$$
$$\dot{y} = \frac{1}{2}\left[-\mathrm{Im}Z_1 + (\mathrm{Im}C - \mathrm{Im}Z_2)x + (\mathrm{Re}C + \mathrm{Re}Z_2)y\right].$$

Then the linearization matrix

$$L = \begin{pmatrix} \frac{\partial \dot{x}}{\partial x} & \frac{\partial \dot{x}}{\partial y} \\ \frac{\partial \dot{y}}{\partial x} & \frac{\partial \dot{y}}{\partial y} \end{pmatrix}_{(0,0)} = \frac{1}{2}\begin{pmatrix} \mathrm{Re}C - \mathrm{Re}Z_2 & -(\mathrm{Im}C + \mathrm{Im}Z_2) \\ \mathrm{Im}C - \mathrm{Im}Z_2 & \mathrm{Re}C + \mathrm{Re}Z_2 \end{pmatrix} \tag{4.20}$$

has $\det L = \frac{1}{4}(|C|^2 - |Z_2|^2)$ and $\mathrm{tr}L = \mathrm{Re}C$, and thus has two eigenvalues

$$\lambda_\pm = \frac{1}{2}\left[\mathrm{Re}C \pm \sqrt{|Z_2|^2 - (\mathrm{Im}C)^2}\right]. \tag{4.21}$$

Identical real weights: $c_j = \frac{1}{N}$

This corresponds to the simple Z_1 model, $C = \sum_{j=1}^N \frac{1}{N} = 1$. It is a gradient flow with two positive real eigenvalues

$$\lambda_\pm = \frac{1}{2}(1 \pm |Z_2|), \tag{4.22}$$

since the second moment $|Z_2|$ cannot exceed 1. So the fixed point is always an unstable node. As we have shown in Chapter 3, it is the only fixed point in the unit disk.

Real weights

The system is a gradient flow, $\mathrm{Im} \sum_j c_j = \mathrm{Im} C = 0$. The fixed point has two real eigenvalues,

$$\lambda_{\pm} = \frac{1}{2}(C \pm |Z_2|). \tag{4.23}$$

Without an imaginary part, it can never be a center or a spiral. In fact, since

$$|Z_2| = |\sum_j c_j \beta_j^2| \leq \sum_j |c_j \beta_j^2| = \sum_j |c_j||\beta_j^2| = \sum_j |c_j|,$$

when all weights are positive, $|Z_2| \leq \sum_j |c_j| = \sum_j c_j = C$, and then both eigenvalues are non-negative. The fixed point can be an unstable node or a non-isolated repeller (when $|Z_2| = C$), but never a saddle. On the contrary, when all weights are negative, $|Z_2| \leq -C$, then both eigenvalues are non-positive, making the fixed point a stable node or a non-isolated attractor (when $|Z_2| = -C$).

A special case is when the weights sum to zero, $C = \sum_j c_j = 0$. The fixed point becomes a saddle with two opposite eigenvalues,

$$\lambda_{\pm} = \pm\frac{1}{2}|Z_2|. \tag{4.24}$$

This is consistent with the analysis on the potential, and results shown in Figure 4.2. The system is simultaneously gradient and Hamiltonian. Clearly, the type of fixed point is determined by coupling weights. Bifurcations may occur when some c_j change signs.

Imaginary weights

The system is a Hamiltonian flow, $\mathrm{Re}\sum_j c_j = \mathrm{Re}C = 0$. The eigenvalues for the fixed point are

$$\lambda_{\pm} = \pm\frac{1}{2}\sqrt{|Z_2|^2 - (\mathrm{Im}C)^2} = \pm\frac{1}{2}\sqrt{(|Z_2| + \mathrm{Im}C)(|Z_2| - \mathrm{Im}C)}. \tag{4.25}$$

As long as all weights have the same sign, from the inequality

$$|Z_2| \leq \sum_j |c_j| = \sum_j |\mathrm{Im}c_j| = \begin{cases} \sum_j \mathrm{Im}c_j = \mathrm{Im}C & \mathrm{Im}c_j > 0,\, \forall j \\ -\sum_j \mathrm{Im}c_j = -\mathrm{Im}C & \mathrm{Im}c_j < 0,\, \forall j \end{cases}$$

both eigenvalues are imaginary, making the fixed point a center. When $C = \sum_j c_j = 0$, the system is both gradient and Hamiltonian and the fixed point must be a saddle. (Perhaps a degenerate saddle.)

Complex weights

We can write the weights as $c_j = K_j e^{i\alpha_j}$ with

$$\mathrm{Re}C = \sum_j \mathrm{Re}c_j = \sum_j K_j \cos\alpha_j, \quad \mathrm{Im}C = \sum_j \mathrm{Im}c_j = \sum_j K_j \sin\alpha_j.$$

The inequality for $|Z_2|$ reduces to $|Z_2| \leq \sum_j |c_j| = \sum_j |K_j e^{i\alpha_j}| = \sum_j |K_j|$. For a general set of c_j's, the eigenvalues are

$$\lambda_{\pm} = \frac{1}{2}\left[\sum_j K_j \cos\alpha_j \pm \sqrt{|Z_2|^2 - \left(\sum_j K_j \sin\alpha_j\right)^2}\right]. \tag{4.26}$$

Table 4.3 summarizes fixed points and their stability of the extended Z_1 model.

$C = \sum_{j=1}^{N} c_j$	$2\lambda_\pm$	Fixed points
$\sum_j \frac{1}{N} = 1$	$1 \pm \lvert Z_2 \rvert$	unstable node
0	$\pm \lvert Z_2 \rvert$	saddle
Real	$C \pm \lvert Z_2 \rvert$	node: $\begin{cases} \text{stable,} & c_j < 0\,\forall j \\ \text{unstable,} & c_j > 0\,\forall j \end{cases}$
Imaginary	$\pm\sqrt{\lvert Z_2 \rvert^2 - (\mathrm{Im}C)^2}$	center
Complex	$\mathrm{Re}C \pm \sqrt{\lvert Z_2 \rvert^2 - (\mathrm{Im}C)^2}$	multiple types

Table 4.3: Fixed points and their stability of the extended Z_1 phase model.

4.1.4 Flows on $(N-1,1)$ Edges

On a partially synchronized edge in the reduced G-orbit $\widetilde{Gp} \subset T^N$, which corresponds to $\beta_j \in S^1$ as the boundary of the unit disk Δ, there are two clusters in the population of oscillators, β_1 and β_2. Each one of them evolves according to the Riccati equation, $\dot{\beta}_j = i\omega\beta_j + \frac{1}{2}(a - \bar{a}\beta_j^2)$, $j = 1, 2$. The order parameter can be expressed as

$$a(p) = Z_1(p) = \beta_1 \sum_{j=1}^{M} c_j + \beta_2 \sum_{j=M+1}^{N} c_j = \beta_1 s_1 + \beta_2 s_2, \quad s_1 = \sum_{j=1}^{M} c_j,\ s_2 = \sum_{j=M+1}^{N} c_j.$$

We can define a relative phase variable between the two clusters, $\delta = \beta_1\bar{\beta}_2$, whose dynamics are given by

$$\dot{\delta} = \dot{\beta}_1\bar{\beta}_2 + \beta_1\dot{\bar{\beta}}_2 = \frac{1}{2}(1-\delta)(a\bar{\beta}_2 + \bar{a}\beta_1) = \frac{1}{2}(1-\delta)[\delta(s_1+\bar{s}_2) + (\bar{s}_1 + s_2)]. \quad (4.27)$$

The stability of fixed points is determined by the derivative:

$$\frac{d\dot{\delta}}{d\delta} = -\delta(s_1+\bar{s}_2) + i\mathrm{Im}(s_1+\bar{s}_2). \quad (4.28)$$

There are three cases:

1. $s_1 = -\bar{s}_2$: $\dot{\delta} = 0$ and the flow is neutral.

2. $s_1 + \bar{s}_2 = ic$, $c \neq 0$: There is only one neutral fixed point at $\delta^* = 1$, since $\frac{d\dot{\delta}}{d\delta} = 0$. An example is $\sum_j c_j = s_1 + s_2 = 0$; namely $s_1 + \bar{s}_2 = s_1 - \bar{s}_1 = 2i\mathrm{Im}s_1$. The sync state is the only neutral fixed point. If we use $\delta = e^{i\theta}$ and $\dot{\delta} = i\delta\dot{\theta}$, then $\dot{\delta}$ becomes

$$\dot{\delta} = -i\mathrm{Im}s_1(\delta - 1)^2 = -i\mathrm{Im}s_1(\delta^{\frac{1}{2}} - \delta^{-\frac{1}{2}})^2\delta = 4i\mathrm{Im}s_1(\mathrm{Im}\delta^{\frac{1}{2}})^2\delta \Rightarrow \dot{\theta} = 4\mathrm{Im}s_1 \sin^2\frac{\theta}{2}.$$

   So $\theta^* = 0$ is the only neutral fixed point. The direction of the flow on the unit circle is determined by $\mathrm{Im}s_1$. If we further require c_j being real, then $\mathrm{Im}s_1 = \mathrm{Im}s_2 = 0$, and $s_1 + \bar{s}_2 = 0$. Thus the neutral flow $\dot{\delta} = 0$ does not have any fixed point.

3. $s_1 + \bar{s}_2 \neq ic$: There are two fixed points with opposite stability,

$$\delta_1^* = 1, \qquad \left.\frac{d\dot{\delta}}{d\delta}\right|_{\delta_1^*} = -\mathrm{Re}(s_1 + \bar{s}_2); \tag{4.29}$$

$$\delta_2^* = -\frac{\bar{s}_1 + s_2}{s_1 + \bar{s}_2}, \qquad \left.\frac{d\dot{\delta}}{d\delta}\right|_{\delta_2^*} = \mathrm{Re}(s_1 + \bar{s}_2). \tag{4.30}$$

   An example is $\sum_j c_j = 1$ with $c_j \in \mathbb{R}$. The two fixed points are $\delta_\pm^* = \pm 1$ with opposite stability, $\left.\frac{d\dot{\delta}}{d\delta}\right|_{\delta_\pm^*} = \mp 1$. The sync state is stable while the anti-sync $(N-1, 1)$ state is unstable, which is consistent with what we've found in previous sections.

4.2 Extended $Z_2 Z_{-1}$ model

Similar to the discussion in the previous section, we can generalize the $Z_2 Z_{-1}$ phase model by introducing complex coefficients to the order parameter,

$$a = \sum_{l=1}^{N} c_l z_l^2 \sum_{k=1}^{N} \overline{d_k z_k} = \sum_{l,k} c_l \bar{d}_k z_l^2 z_k^{-1}, \quad \forall c_l,\, d_k \in \mathbb{C}. \tag{4.31}$$

In order to satisfy the gradient condition, $\mathrm{Im}D\mathcal{a} = 0$, we calculate

$$D\mathcal{a} = \sum_j \frac{\partial}{\partial z_j} \sum_{l,k} c_l \bar{d}_k z_l^2 z_k^{-1} = \sum_{l,k} c_l \bar{d}_k \sum_j (2\delta_{jl} z_l z_k^{-1} - \delta_{jk} z_l^2 z_k^{-2}) = \sum_{l,k} c_l \bar{d}_k (2 z_l z_k^{-1} - z_l^2 z_k^{-2})$$

which is real when $d_k = c_k$, $D\mathcal{a} = 2|Z_1|^2 - |Z_2|^2$.

With this condition, the order parameter for weighted $Z_2 Z_{-1}$ model is

$$\mathcal{a} = \sum_{l,k} c_l \bar{c}_k z_l^2 z_k^{-1}, \tag{4.32}$$

and the w flow in the unit disk Δ can be expressed as a gradient of a potential function, $\dot{w} = \frac{1}{2}(1 - |w|^2)^2 \frac{\partial \Phi}{\partial \bar{w}}$. The generic procedure of finding this potential is by integrating the order parameter $\mathcal{a}(M_w p)$ with an argument of a Möbius transformation on a base point $p = (\beta_1, \ldots, \beta_N)$,

$$\frac{\partial \Phi(w, \bar{w})}{\partial \bar{w}} = -\frac{\mathcal{a}(M_w p)}{1 - |w|^2} \Rightarrow \Phi(w, \bar{w}) = -\int d\bar{w} \frac{\mathcal{a}(M_w p)}{1 - w\bar{w}} + f(w) \equiv A(w, \bar{w}) + f(w).$$

The function $f(w)$ can be determined by integrating over w,

$$\begin{aligned} \frac{\partial \Phi(w, \bar{w})}{\partial w} &= \frac{\partial A(w, \bar{w})}{\partial w} + \frac{df}{dw} = -\frac{\overline{\mathcal{a}(M_w p)}}{1 - |w|^2} \Rightarrow \\ f(w) &= -\int dw \frac{\overline{\mathcal{a}(M_w p)}}{1 - |w|^2} - \int dw \frac{\partial A}{\partial w} \equiv A^\dagger(w, \bar{w}) - \int dw \frac{\partial A}{\partial w}. \end{aligned}$$

Therefore, the potential function reads

$$\begin{aligned} \Phi(w, \bar{w}) &= A(w, \bar{w}) + A^\dagger(w, \bar{w}) - \int dw \frac{\partial A}{\partial w}, \\ A(w, \bar{w}) &= -\int d\bar{w} \frac{\mathcal{a}(M_w p)}{1 - w\bar{w}}, \quad A^\dagger(w, \bar{w}) = \int dw \frac{\overline{\mathcal{a}(M_w p)}}{1 - |w|^2}. \end{aligned}$$

As for the weighted Z_2Z_{-1} model, the order parameter upon Möbius transformation is

$$a(M_w p) = \sum_{l,k} c_l \bar{c}_k \Big(\frac{\beta_l - w}{1 - \bar{w}\beta_l}\Big)^2 \frac{\bar{\beta}_k - \bar{w}}{1 - w\bar{\beta}_k} = \sum_{l,k} c_l \bar{c}_k \frac{(\beta_l - w)^2}{1 - w\bar{\beta}_k} \frac{\bar{\beta}_k - \bar{w}}{(1 - \bar{w}\beta_l)^2}.$$

Direct calculations show

$$A(w,\bar{w}) = -\sum_{l,k} c_l \bar{c}_k \frac{(\beta_l - w)^2}{1 - \bar{\beta}_k w} I_{lk} = -\sum_{l,k} c_l \bar{c}_k \Big[\ln\frac{1 - w\bar{w}}{1 - \beta_l \bar{w}} + \frac{(\beta_l - w)(\bar{\beta}_k - \bar{\beta}_l)}{(1 - \bar{\beta}_k w)(1 - \beta_l \bar{w})}\Big],$$

where we have used partial fractions to evaluate the integral

$$I_{lk} = \int d\bar{w} \frac{\bar{\beta}_k - \bar{w}}{(1 - w\bar{w})(1 - \beta_l \bar{w})^2} = \frac{1 - \bar{\beta}_k w}{(w - \beta_l)^2} \ln\frac{1 - w\bar{w}}{1 - \beta_l \bar{w}} + \frac{\bar{\beta}_l - \bar{\beta}_k}{(w - \beta_l)(1 - \beta_l \bar{w})}.$$

Next, let us calculate $A^\dagger(w,\bar{w})$, which amounts to rewriting $\overline{a(M_w p)}$. If we define

$$A_{lk} = \Big(\frac{\beta_l - w}{1 - \bar{w}\beta_l}\Big)^2 \frac{\bar{\beta}_k - \bar{w}}{1 - w\bar{\beta}_k},$$

the order parameter is

$$\begin{aligned} a(M_w p) &= \sum_{l,k} c_l A_{lk} \bar{c}_k = \mathbf{c}\mathbf{A}\bar{\mathbf{c}}, \\ \overline{a(M_w p)} &= \sum_{l,k} \overline{c_l A_{lk} \bar{c}_k} = \sum_{l,k} c_k \overline{A_{lk}} \bar{c}_l \overset{l\leftrightarrow k}{=} \sum_{l,k} c_l \overline{A_{kl}} \bar{c}_k = \mathbf{c}\mathbf{A}^\dagger \bar{\mathbf{c}}. \end{aligned}$$

Therefore $A^\dagger(w,\bar{w})$ is the transposed conjugate of $A(w,\bar{w})$,

$$A^\dagger(w,\bar{w}) = -\sum_{l,k} c_l \bar{c}_k \Big[\ln\frac{1 - w\bar{w}}{1 - \bar{\beta}_k w} + \frac{(\bar{\beta}_k - \bar{w})(\beta_l - \beta_k)}{(1 - \bar{\beta}_k w)(1 - \beta_l \bar{w})}\Big].$$

Furthermore, it is straightforward to show

$$\begin{aligned}\int dw \frac{\partial A(w,\bar{w})}{\partial w} &= \sum_{l,k} c_l \bar{c}_k \int dw \Big[\frac{\bar{w}}{1-w\bar{w}} + \frac{(\bar{\beta}_k - \bar{\beta}_l)(1-\beta_l\bar{\beta}_k)}{(1-\beta_l\bar{w})(1-\bar{\beta}_k w)^2}\Big] \\ &= \sum_{l,k} c_l \bar{c}_k \Big[-\ln(1-w\bar{w}) + \frac{(\bar{\beta}_k - \bar{\beta}_l)(\beta_k - \beta_l)}{(1-\beta_l\bar{w})(1-\bar{\beta}_l w)}\Big].\end{aligned}$$

Then after some simplifications, the potential function becomes

$$\Phi(w,\bar{w}) = -\sum_{l,k} c_l F_{lk}(w,\bar{w}) \bar{c}_k = -\boldsymbol{c}\mathbf{F}(w,\bar{w})\bar{\boldsymbol{c}}, \tag{4.33}$$

$$\begin{aligned}F_{lk}(w,\bar{w}) &= \ln \frac{1-w\bar{w}}{(1-\bar{\beta}_k w)(1-\beta_l\bar{w})} + \\ &\quad \frac{(\beta_l - w)(\bar{\beta}_k - \bar{\beta}_l) + (\bar{\beta}_k - \bar{w})(\beta_l - \beta_k) + (\bar{\beta}_k - \bar{\beta}_l)(\beta_k - \beta_l)}{(1-\bar{\beta}_k w)(1-\beta_l\bar{w})} \\ &= \ln \frac{1-w\bar{w}}{(1-\bar{\beta}_k w)(1-\beta_l\bar{w})} + \frac{(\bar{\beta}_k - \bar{\beta}_l)(\beta_k - w) + (\beta_l - \beta_k)(\bar{\beta}_k - \bar{w})}{(1-\bar{\beta}_k w)(1-\beta_l\bar{w})}.\end{aligned}$$

Notice that $F_{lk} = \overline{F_{kl}}$, namely, $\mathbf{F} = \mathbf{F}^\dagger$, which is a Hermitian matrix. As a result, the potential is guaranteed to be real,

$$\overline{\Phi(w,\bar{w})} = -\sum_{l,k} \overline{c_l F_{lk} \bar{c}_k} = -\sum_{l,k} c_k \overline{F_{lk}} \bar{c}_l = -\sum_{l,k} c_k F_{kl} \bar{c}_l = \Phi(w,\bar{w}).$$

A special case is when all the coefficients add to zero, $\sum_l c_l = 0$. Then the logarithmic part in Φ vanishes, leaving the algebraic part only,

$$\Phi_2(w,\bar{w}) = -\sum_{l,k} c_l \mathcal{F}_{lk}(w,\bar{w}) \bar{c}_k, \quad \mathcal{F}_{lk}(w,\bar{w}) = \frac{(\bar{\beta}_k - \bar{\beta}_l)(\beta_k - w) + (\beta_l - \beta_k)(\bar{\beta}_k - \bar{w})}{(1-\bar{\beta}_k w)(1-\beta_l\bar{w})}.$$

Figure shows the $\dot{w}$ flow and the potential for the $Z_2 Z_{-1}$ model with zero weight sum and $N = 4$. Notice the origin has become a non-hyperbolic fixed point. There are also new fixed points emerging in the unit disk.

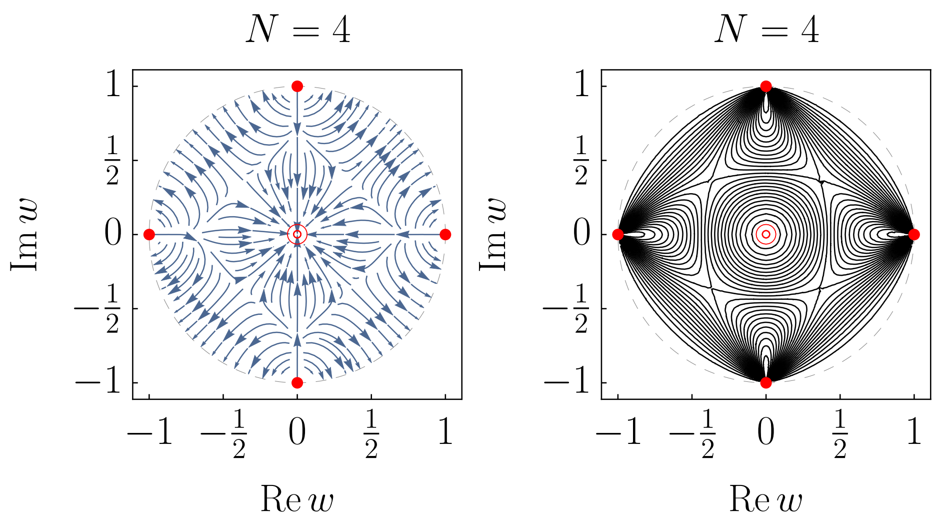

Figure 4.4: The $\dot{w}$ flows (left panel) and the potential Φ (right panel) for the extended Z_2Z_{-1} phase model ($\sum_j c_j = 0$) on the splay base point (red solid circles) $\tilde{p} = (\eta, \eta^2, \ldots, \eta^N)$ with $\eta = e^{2\pi i/N}$. With $N = 4$, the weights are chosen to sum up to zero: $c_j = \left\{-\frac{1}{4}, \frac{1}{4}, -\frac{1}{4}, \frac{1}{4}\right\}$.

4.3 Fixed Points on $(N-1, 1)$ Edges

The order parameter for a two-cluster state of the Z_q moment can be written as

$$s_1 Z_q = \sum_{j=1}^{M} c_j \beta_1^q + \sum_{j=M+1}^{N} c_j \beta_2^q = s_1 \beta_1^q + s_2 \beta_2^q, \quad s_1 = \sum_{j=1}^{M} c_j \in \mathbb{C}, \ s_2 = \sum_{j=M+1}^{N} c_j \in \mathbb{C}.$$

Similar to what we've done for the Z_1 model on the edge, we define a relative phase variable $\delta = \beta_1 \bar{\beta}_2$. For $Z_q Z_{1-q}$ models, the order parameter becomes

$$\begin{aligned} a = Z_q Z_{1-q} &= (s_1 \beta_1^q + s_2 \beta_2^q)(\bar{s}_1 \beta_1^{1-q} + \bar{s}_2 \beta_2^{1-q}) \\ &= |s_1|^2 \beta_1 + |s_2|^2 \beta_2 + s_1 \bar{s}_2 \delta^q \beta_2 + \bar{s}_1 s_2 \bar{\delta}^q \beta_1. \end{aligned} \tag{4.34}$$

The dynamics of δ are govern by

$$\dot{\delta} = \dot{\beta}_1\bar{\beta}_2 + \beta_1\dot{\bar{\beta}}_2 = \frac{1}{2}(1-\delta)(a\bar{\beta}_2 + \bar{a}\beta_1)$$

$$= \frac{1}{2}(1-\delta)[(|s_1|^2 + |s_2|^2)(1+\delta) + 2(s_1\bar{s}_2\delta^q + \bar{s}_1 s_2\delta^{1-q})]$$

$$= -2i\delta\mathrm{Im}\delta^{\frac{1}{2}}[(|s_1|^2 + |s_2|^2)\mathrm{Re}\delta^{\frac{1}{2}} + 2\mathrm{Re}(s_1\bar{s}_2\delta^{q-\frac{1}{2}})]. \tag{4.35}$$

where we've applied the Riccati equation for each cluster, $\dot{\beta}_j = i\omega\beta_j + \frac{1}{2}(a - \bar{a}\beta_j^2)$. Then using $\delta = e^{i\varphi}$ and $\dot{\delta} = i\delta\dot{\varphi}$, the above equation becomes

$$\dot{\varphi} = -2\sin\frac{\varphi}{2}\big[(|s_1|^2 + |s_2|^2)\cos\frac{\varphi}{2} + 2\mathrm{Re}(s_1\bar{s}_2 e^{i(q-\frac{1}{2})\varphi})\big]. \tag{4.36}$$

Let's consider two special cases.

Case I: $\sum_{j=1}^{N} c_j = 1,\ \forall c_j \in \mathbb{R}$**.**

This is the ordinary $Z_q Z_{1-q}$ model. If we denote $s_1 = \sum_{j=1}^{M} c_j \equiv s$, then $s_2 = \sum_{j=M+1}^{N} c_j = 1 - s$. Therefore the dynamics of δ are

$$\dot{\delta} = \frac{1}{2}(1-\delta)[(s^2 + (1-s)^2)(1+\delta) + 2s(1-s)(\delta^q + \delta^{1-q})],$$
$$\dot{\varphi} = -2\sin\frac{\varphi}{2}\Big[(s^2 + (1-s)^2)\cos\frac{\varphi}{2} + 2s(1-s)\cos\frac{(2q-1)\varphi}{2}\Big].$$

This recovers calculations in previous sections, where we've shown that there are new fixed points on the $(N-1,1)$ edge other than the sync and equal $(N-1,1)$ states when the number of oscillators is smaller than a critical value N_{max} for a given rank q. For example, when $q = 2$, $N_{max} = 6$.

Case II: $\sum_{j=1}^{N} c_j = 0, \ \forall c_j \in \mathbb{R}$**.**

This is the neutral case with $s_1 = s = -s_2$. Then flows on the edge are governed by

$$\dot{\delta} = s^2(1-s)[(1+\delta) - (\delta^q + \delta^{1-q})],$$
$$\dot{\varphi} = -4s^2 \sin\frac{\varphi}{2}\Big(\cos\frac{\varphi}{2} - \cos\frac{2q-1}{2}\varphi\Big) = -8s^2 \sin\frac{\varphi}{2}\sin\frac{q}{2}\varphi\sin\frac{q-1}{2}\varphi.$$

Clearly, the sync ($\varphi = 0$) and the equal $(N-1,1)$ state ($\varphi = \pm\pi$) are always fixed points. And there are multiple fixed points $\dot{\varphi}^* = 0$ for higher rank q. Their stabilities depend on q,

$$\frac{d\dot{\varphi}}{d\varphi} = -4s^2\Big(\cos\frac{\varphi}{2}\sin\frac{q}{2}\varphi\sin\frac{q-1}{2}\varphi +$$
$$q\sin\frac{\varphi}{2}\cos\frac{q}{2}\varphi\sin\frac{q-1}{2}\varphi + (q-1)\sin\frac{\varphi}{2}\sin\frac{q}{2}\varphi\cos\frac{q-1}{2}\varphi\Big).$$

But the sync state is neutral, since $\frac{d\dot{\varphi}}{d\varphi}\Big|_{\varphi^*=0} = 0$.

4.4 Summary

In this chapter, we generalized our discussions on phase models to include unequal weights in the order parameter. When the sum of all weights is real, the system satisfies the gradient condition and can be described by a real potential function. We make a $2D$ electrostatic analog for the extended Z_1 model when all the weights sum up to zero. A base point correspond to N charges living on the unit circle. The weight c_j is the value of the charge. Flows are field lines which are circles emitting from “positive” charges to “negative” charges. There are no nodes in the unit disks. Saddle points can exist both in the disk and on the unit circle. This implies neutral stability of the sync state.

CHAPTER V

Conclusions

This dissertation concerns N identical Kuramoto oscillators whose state space is an N-dim torus T^N. Due to the form of sinusoidal coupling, the system is described by complex Riccati equation. Time evolution of N oscillators is then constrained to lie on $3D$ orbits of unit-disk-preserving Möbius transformations acting on T^N. We derive explicit ODEs for group parameters w and ζ, and show they lead to the implicit transformation and variables found by Watanabe and Strogatz.

For phase models which are invariant under a global phase shift, the dynamics are reduced to $2D$ invariant manifolds which have a natural geometry equivalent to the Poincaré disk Δ with hyperbolic metric. The classic Kuramoto model (the Z_1 model) is a gradient flow with a unique fixed point at the hyperbolic barycenter of N oscillators.

The gradient flow condition allows us to identify new families of Kuramoto phase models that can be described by potentials or Hamiltonians and exhibit low-dimensional dynamics. The new models also have rich structures of fixed points and bifurcations.

We extend this group-theory-based formalism to Kuramoto oscillator systems with non-identical couplings, namely, oscillators contribute unequally to the order parameter. When the net contribution is zero (with equal amounts of excitations and inhibitions), the system is simultaneously gradient and Hamiltonian, which is analogous to a $2D$ electrostatic system with equal numbers of positive and negative charges.

Future directions include 1) a complete classification of phase models that satisfy the gradient condition; 2) applying this formalism to multiple populations of identical Kuramoto oscillators which may exhibit chimera states.

Finally, we would like to conclude with the following key points:

- Dimensional reduction due to Möbius transformations
- Equivalent $2D$ flows in the Poincaré disk of hyperbolic geometry
- Gradient/Hamiltonian duality for extended phase models
- Rich structure of fixed points and bifurcations in reduced G-orbits

BIBLIOGRAPHY

BIBLIOGRAPHY

Acebrón, J. A., L. L. Bonilla, C. J. P. Vicente, F. Ritort, and R. Spigler (2005), The kuramoto model: A simple paradigm for synchronization phenomena, *Reviews of modern physics*, *77*(1), 137.

Braun, W., A. Pikovsky, M. A. Matias, and P. Colet (2012), Global dynamics of oscillator populations under common noise, *EPL (Europhysics Letters)*, *99*(2), 20,006.

Chen, B., J. R. Engelbrecht, and R. Mirollo (2017), Hyperbolic geometry of kuramoto oscillator networks, *arXiv preprint arXiv:1707.00713*.

Engelbrecht, J. R., and R. Mirollo (2014), Classification of attractors for systems of identical coupled kuramoto oscillators, *Chaos: An Interdisciplinary Journal of Nonlinear Science*, *24*(1), 013,114.

Goebel, C. J. (1995), Comment on constants of motion for superconductor arrays, *Physica D: Nonlinear Phenomena*, *80*(1-2), 18–20.

Kuramoto, Y. (1975), Self-entrainment of a population of coupled non-linear oscillators, in *International symposium on mathematical problems in theoretical physics*, pp. 420–422, Springer.

Marvel, S. A., R. E. Mirollo, and S. H. Strogatz (2009), Identical phase oscillators with global sinusoidal coupling evolve by möbius group action, *Chaos: An Interdisciplinary Journal of Nonlinear Science*, *19*(4), 043,104.

Mirollo, R. E. (1994), Splay-phase orbits for equivariant flows on tori, *SIAM Journal on Mathematical Analysis*, *25*(4), 1176–1180.

Mirollo, R. E. (2012), The asymptotic behavior of the order parameter for the infinite-n kuramoto model, *Chaos: An Interdisciplinary Journal of Nonlinear Science*, *22*(4), 043,118.

Nichols, S., and K. Wiesenfeld (1992), Ubiquitous neutral stability of splay-phase states, *Physical Review A*, *45*(12), 8430.

Ott, E., and T. M. Antonsen (2008), Low dimensional behavior of large systems of globally coupled oscillators, *Chaos: An Interdisciplinary Journal of Nonlinear Science*, *18*(3), 037,113.

Ott, E., and T. M. Antonsen (2009), Long time evolution of phase oscillator systems, *Chaos: An interdisciplinary journal of nonlinear science*, *19*(2), 023,117.

Ott, E., B. R. Hunt, and T. M. A. Jr. (2011), Comment on long time evolution of phase oscillator systems [chaos 19, 023117 (2009)], *Chaos: An Interdisciplinary Journal of Nonlinear Science*, *21*(2), 025,112.

Pikovsky, A., and M. Rosenblum (2008), Partially integrable dynamics of hierarchical populations of coupled oscillators, *Physical review letters*, *101*(26), 264,103.

Pikovsky, A., and M. Rosenblum (2009), Self-organized partially synchronous dynamics in populations of nonlinearly coupled oscillators, *Physica D: Nonlinear Phenomena*, *238*(1), 27–37.

Pikovsky, A., and M. Rosenblum (2015), Dynamics of globally coupled oscillators: Progress and perspectives, *Chaos: An Interdisciplinary Journal of Nonlinear Science*, *25*(9), 097,616.

Pikovsky, A., M. Rosenblum, and J. Kurths (2003), *Synchronization: A Universal Concept in Nonlinear Sciences*, Cambridge Nonlinear Science Series, Cambridge University Press.

Stewart, I. (2011), Phase oscillators with sinusoidal coupling interpreted in terms of projective geometry, *International Journal of Bifurcation and Chaos*, *21*(06), 1795–1804.

Strogatz, S. (2004), *Sync: The emerging science of spontaneous order*, Penguin UK.

Strogatz, S. H. (2000), From kuramoto to crawford: exploring the onset of synchronization in populations of coupled oscillators, *Physica D: Nonlinear Phenomena*, *143*(1), 1–20.

Strogatz, S. H., and R. E. Mirollo (1991), Stability of incoherence in a population of coupled oscillators, *Journal of Statistical Physics*, *63*(3), 613–635.

Tsang, K. Y., R. E. Mirollo, S. H. Strogatz, and K. Wiesenfeld (1991), Dynamics of a globally coupled oscillator array, *Physica D: Nonlinear Phenomena*, *48*(1), 102–112.

Vlasov, V., M. Rosenblum, and A. Pikovsky (2016), Dynamics of weakly inhomogeneous oscillator populations: perturbation theory on top of watanabe–strogatz integrability, *Journal of Physics A: Mathematical and Theoretical*, *49*(31), 31LT02.

Watanabe, S., and S. H. Strogatz (1993), Integrability of a globally coupled oscillator array, *Physical review letters*, *70*(16), 2391.

Watanabe, S., and S. H. Strogatz (1994), Constants of motion for superconducting josephson arrays, *Physica D: Nonlinear Phenomena*, *74*(3-4), 197–253.

Weltin, K., and L. Hua (2012), *Starting with the Unit Circle: Background to Higher Analysis*, Springer New York.

Winfree, A. T. (1967), Biological rhythms and the behavior of populations of coupled oscillators, *Journal of theoretical biology*, *16*(1), 15–42.